UNCLASSIFIED

AD 278 535

Reproduced by the

ARMED SERVICES TECHNICAL INFORMATION AGENCY
ARLINGTON HALL STATION
ARLINGTON 12, VIRGINIA

UNCLASSIFIED

NOTICE: When government or other drawings, specifications or other data are used for any purpose other than in connection with a definitely related government procurement operation, the U. S. Government thereby incurs no responsibility, nor any obligation whatsoever; and the fact that the Government may have formulated, furnished, or in any way supplied the said drawings, specifications, or other data is not to be regarded by implication or otherwise as in any manner licensing the holder or any other person or corporation, or conveying any rights or permission to manufacture, use or sell any patented invention that may in any way be related thereto.

DISCLAIMER NOTICE

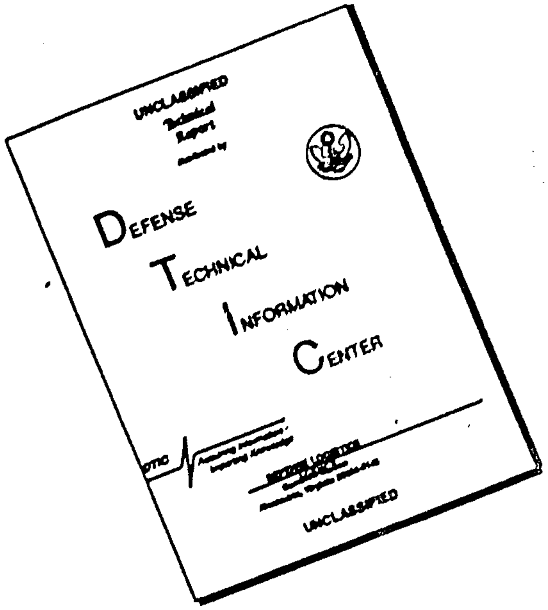

THIS DOCUMENT IS BEST QUALITY AVAILABLE. THE COPY FURNISHED TO DTIC CONTAINED A SIGNIFICANT NUMBER OF PAGES WHICH DO NOT REPRODUCE LEGIBLY.

DIVISION OF
HILLER AIRCRAFT CORP

278 535

ADVANCED RESEARCH

REPORT NO.
ARD-300

CATALOGED BY ASTIA
AS AD No. 278535

ARD-300

SUMMARY REPORT - PHASE III PROGRAM

ANNULAR NOZZLE EJECTOR

Nonr 2840(00)
CO:JFM:idm
Ser 1031
19 July 1962

FIRST ENDORSEMENT on HILLER AIRCRAFT CORP. ltr ARD-62-M29 ERS:hg of 18 July 1962

From: Bureau of Naval Weapons Representative, Palo Alto, California
To: Distribution List

Subj: Distribution of Summary Report - Phase III Program - Annular Nozzle Ejector - Contract Nonr 2840(00), Hiller Report No. ARD-300

1. Forwarded.

John F. Murdock
JOHN F. MURDOCK
By direction

HILLER
AIRCRAFT CORP

In Reply Please Refer to:
ARD-62-M29 ERS:hg

July 18, 1962

To: Distribution List

Via: Bureau of Naval Weapons Representative,
Palo Alto, California

Subject: Distribution of Summary Report - Phase III
Program - Annular Nozzle Ejector -
Contract Nonr 2840(00), Hiller Report
No. ARD-300

Encl.: (1) Subject Report
(2) Distribution List for Subject Report

1. Subject report is, hereby, transmitted to the addressees listed in enclosure (2), per instructions of the Office of Naval Research, Code 461.

2. We would like to hear from you, if this report raises any questions or comments.

HILLER AIRCRAFT CORP.

E R Sargent

E. R. Sargent
Manager, Propulsion Dept.
Advanced Research Division

[illegible]EM DISTRIBUTION LIST

Chief, Bureau of Naval Weapons
Department of the Navy
Washington 25, D. C.
ATTN: Code RAAD-3
Code RR-25
Code R-[illegible]

Chief of Naval Operations
Department of the Navy
Washington 25, D. C.
ATTN: OP-[illegible]T
OP-[illegible]

Chief of Naval Research
Department of the Navy
Washington 25, D. C.
ATTN: Code [illegible]1 (1[illegible] copies)
Code [illegible]

Commanding Officer
[illegible] Branch Office
[illegible] Library Building
[illegible] Street
[illegible], Illinois

Commanding Officer
[illegible] Branch Office
[illegible]
[illegible] Street
[illegible], New York
ATTN: [illegible] ([illegible] copies)

Commanding Officer
[illegible] Branch Office
[illegible] Navy
[illegible], New York

Commanding Officer
[illegible] Branch Office
[illegible]
San Francisco [illegible], California

Commanding Officer
[illegible] Branch Office
[illegible] East Green Street
Pasadena 1, California

Commanding Officer & Director
[illegible] Laboratory
[illegible], California

Contract Administrator
Southeastern Area
Office of Naval Research
2110 G Street, N. W.
Washington 7, D. C.

Director
Naval Research Laboratory
Technical Information Office
Washington 25, D. C. ([illegible] copies)

Chief, Bureau of Ships
Department of the Navy
Washington 25, D. C.
ATTN: Code [illegible]21
Code [illegible]20

Commanding Officer & Director
David Taylor Model Basin
Aerodynamics Laboratory
Washington 7, D. C.
ATTN: Mr. [illegible] ([illegible] copies)

Commanding Officer & Director
David Taylor Model Basin
Hydromechanics Laboratory
Carderock, Maryland
ATTN: Mr. A. [illegible]

Commandant of the Marine Corps
Arlington Annex
Washington 25, D. C.
ATTN: Code AO[illegible]E
Code AO[illegible]H

Marine Corps Development Center
Marine Corps Schools
Quantico, Virginia
ATTN: Air Section

Maritime Administration
[illegible] Street, N.W.
General Accounting Office Building
Washington, D. C.
ATTN: Mr. [illegible] Taylor [illegible]

Office of Chief of Transportation
Department of the Army
Washington 25, D. C.
ATTN: TAFI-R[illegible]

Commanding Officer
U.S. Army Transportation Research Command
Ft. Eustis, Virginia
ATTN: TCREC-TRG, Mr. W. Sickles (2 copies)

Chief, U.S. Army R&D Liaison Group
9851 D. U.
APO #757
New York, New York
ATTN: Mr. Robert Piser (2 copies)

Senior Standardization Representative
U. S. Army Standardization Group (U.K.)
Box #65, U.S. Navy #100, F.P.O.
New York, New York
ATTN: LCOL M. Lynch (2 copies)

Human Engineering Laboratory
Aberdeen Proving Ground
Maryland
ATTN: Dr. Leon T. Katchmar

Human Resources Research Office
P. O. Box 3596
Washington, D. C.
ATTN: Dr. T. McKnight

Armed Services Technical Information
Agency
Document Service Center
Arlington Hall Station
Arlington 12, Virginia 10 copies

National Aeronautics & Space Administration
[illegible]
Washington [illegible]
ATTN: [illegible]

NASA
Langley Research Center
Langley AFB, Virginia
ATTN: [illegible]

Transportation Intelligence Agency
Arlington Hall Station
Arlington [illegible], Virginia
ATTN: [illegible]

Office, Director of Defense
(Research & Engineering)
Washington 25, D.C.
ATTN: Director of Aeronautics

Office of Technical Services
Department of Commerce
Washington 25, D.C.

University of Maryland
Institute of Fluid Dynamics &
Applied Mathematics
College Park, Maryland
ATTN: Professor Weske

Princeton University
Aeronautical Engineering Dept.
The James Forrestal Research
Center
Princeton, New Jersey
ATTN: Mr. T. Sweeney

Stevens Institute of Technology
Fluid Dynamics Laboratory
Hoboken, New Jersey
ATTN: Mr. Peter I. Brown

University of California
Institute of Engineering Research
Berkeley [illegible], California
ATTN: Professor [illegible]

Aeronutronic
A Division of Ford Motor Co.
Ford Road
Newport Beach, California
ATTN: [illegible]

AiResearch Manufacturing Co.
of Arizona
[illegible] South [illegible] Street
Phoenix, Arizona
ATTN: Mr. L. M. [illegible]

Bell Aerosystems Company
P. O. Box #1
Buffalo 5, New York
ATTN: Mr. F. [illegible]

Bell Helicopter Corporation
P. O. Box 482
Fort Worth 1, Texas
ATTN: Mr. R. Lynn

Booz-Allen Applied Research Inc.
4921 Auburn Avenue
Bethesda 14, Maryland
ATTN: Mr. P. [illegible] Fielding

Convair
Division of General Dynamics Corp.
Mail Zone 6-109
P. O. Box 1950
San Diego 12, California
ATTN: Mr. J. E. Loos

Cornell Aeronautical Laboratory, Inc.
4455 Genesee Street
Buffalo 21, New York
ATTN: Mr. A. Millikin

Curtiss-Wright Corporation
Advanced Systems Center
Dallas, Texas
ATTN: Mr. W. F. Freeman

Douglas Aircraft Company
El Segundo Division
El Segundo, California
ATTN: Mr. R. W. Pratt

General Motors Corporation
12 Mile and Mound Roads
Warren, Michigan
ATTN: Mr. [illegible] Price

Grumman Aircraft Engineering Corp.
Bethpage, L. I., New York
ATTN: Mr. [illegible]

Hiller Aircraft Corp.
[illegible] Willow Road
Palo Alto, California
ATTN: Mr. [illegible] Gates

Mr. W. K. Walker
7240 Wisconsin Avenue
Bethesda 14, Maryland

Hydronautics, Inc.
200 Monroe Street
Rockville, Maryland
ATTN: Mr. M. P. Tulin

Library
Institute of the Aeronautical
Sciences
2 East 64th Street
New York 21, New York

Kellett Aircraft Corporation
Research & Development
P. O. Box 35
Willow Grove, Pennsylvania
ATTN: Mr. Leonard Goland

California Division
Lockheed Aircraft Corporation
Burbank, California
ATTN: Mr. E. Stout

Martin Company
Mail Zone A2[illegible]
Denver, Colorado
ATTN: Mr. R. L. Green

Martin Company
Advanced Systems Requirements
Orlando, Florida
ATTN: Mr. K. Co[illegible]sairt

National Research Associates
P. O. Box #11[illegible]
College Park, Maryland
ATTN: Mr. E. J. Knight

North American Aviation, Inc.
Space & Information Systems
Division
12214 Lakewood Boulevard
Downey, California
ATTN: Mr. L. M. Foster
(CDR #62-11)

Pneumodynamics Division
Cleveland Pneumatic Industries
4936 Fairmont Avenue
Bethesda 14, Maryland

Ryan Aeronautical Company
Lindbergh Field
San Diego 12, California
ATTN: Mr. D. L. Marlin

United Aircraft Corporation
Research Laboratories
East Hartford, Connecticut
ATTN: Mr. L. . Hillman

Vehicle Research Corporation
1661 Lombardy Road
Pasadena, California
ATTN: Dr. S. Rethorst

Vertol Aircraft Corporation
Woodland Avenue
Morton, Pennsylvania
ATTN: Mr. Stepniewski

Report No. ARD-300

December 1961

SUMMARY REPORT - PHASE III PROGRAM
ANNULAR NOZZLE EJECTOR

M. F. Gates
Principal Investigator

J. W. Fairbanks
Research Assistant

Reproduction in Whole or in
Part is Permitted for Any
Purpose of the United States
Government

ADVANCED RESEARCH
DIVISION OF HILLER AIRCRAFT CORP.

Conducted for the Office of Naval Research and the U.S
Army Transportation Corps under ONR Contract Nonr-2[illegible]

1. SUMMARY

This report discusses the results of the Phase III program of Contract Nonr 2840(00) - ANNULAR NOZZLE EJECTOR. The report also reviews the Phase I and II programs and the over-all program precepts.

The Phase III program was a study of the annular ejector to determine a configuration that accomplishes the following: (a) equals or improves out of ground effect performance; (b) gives superior performance in ground effect; and (c) overcomes the performance loss during ground effect transition encountered in the Phase II work. To achieve these goals, this contractor investigated the combined possibilities of a conically divergent annular primary jet, wide angle augmenter tube, and flow control vanes.

The particular primary nozzle geometry chosen (jet aspect ratio, jet divergence angle and area ratio) did not combine effectively with wide angle augmenters to achieve an ejector with out of ground effect performance superior to that of Phase I and II. However, equivalent performance was achieved. The investigations were performed with small 2-D and 3-D model ejectors with a primary jet thrust of approximately 5 lbs. supplied at approximately 21" Hg gage total pressure (1.7 pressure ratio).

The investigation also included the use of vanes at the bellmouth and augmenter inlets and at the augmenter exit. Proper use of the vanes reduced the augmentation loss in ground effect transition to approximately 1/3 the loss without vanes. The maximum resulting loss in augmentation was approximately 8% of out of ground effect augmentation.

Limited tests with the full-scale ejector indicated that bellmouth losses chargeable to lip separation could be eliminated essentially by a flat lip extension simulating the original Phase I model geometry. The loss due to separation was on the order of 1% of the primary jet thrust.

TABLE OF CONTENTS

Page No.

TABLE OF CONTENTS (CON'T)

ACKNOWLEDGMENTS

This program phase was sponsored by the U. S. Army through the Office of Naval Research, United States Navy. The authors wish to acknowledge the guidance given this program by Mr. E. R. Sargent, Manager Propulsion Department, Advanced Research Division of Hiller Aircraft Corp. Others who have contributed significantly to this program are D. A. Graber in the laboratory, H. Wichers with his photographic coverage and W. Churchill with his editorial assistance.

LIST OF FIGURES

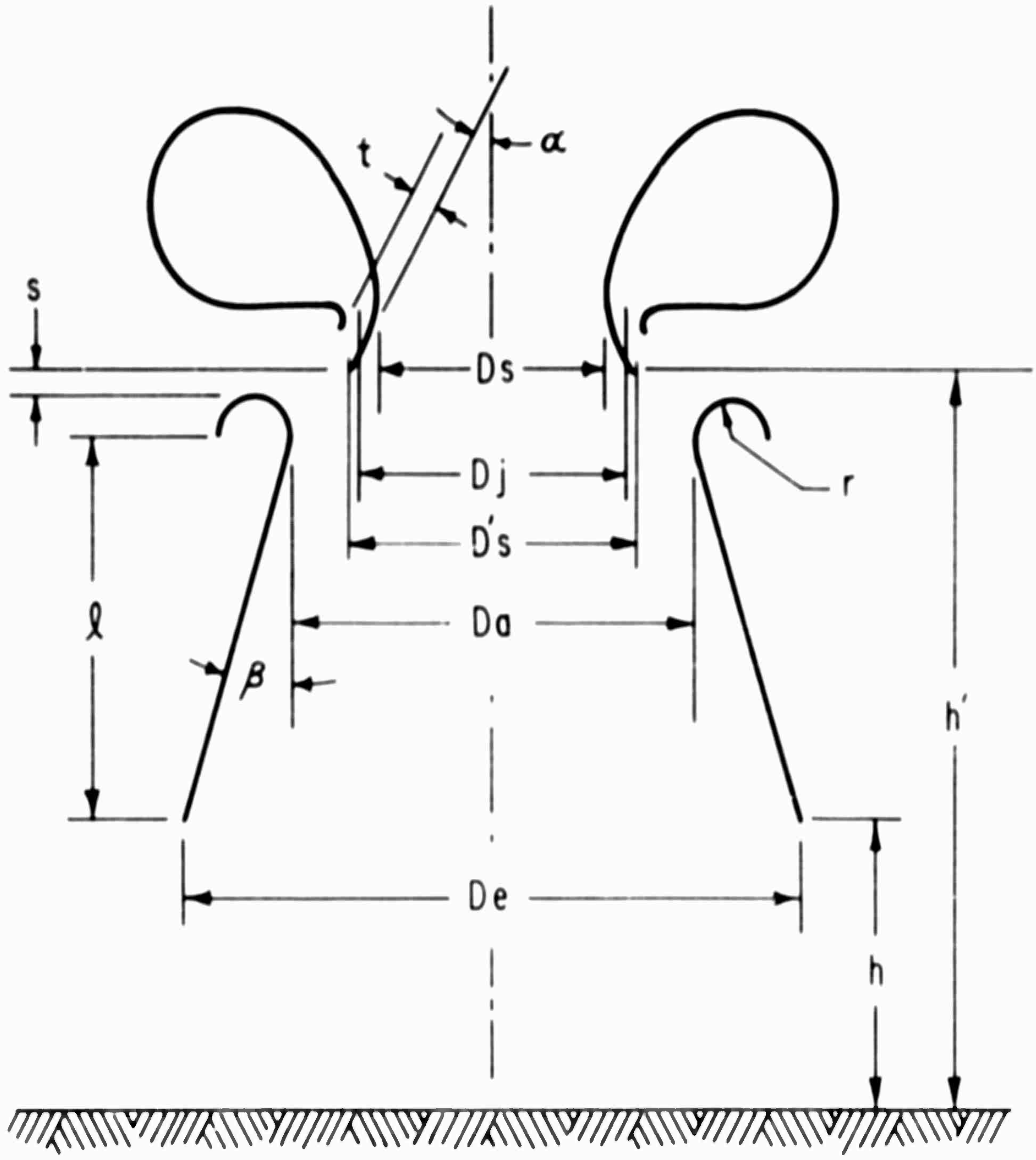

ANNULAR EJECTOR GEOMETRICAL PARAMETERS

SYMBOL LIST

Consistent units are used where required or are otherwise noted.

A	= Proportionality constant representing slope of ϕ vs log $(\sigma_c \sigma_d)$ at constant σ_d
C_p	= specific heat
2-D	= two-dimensional
3-D	= three-dimensional
D_a	= augmenter throat diameter (or width in 2-D)
D_e	= augmenter exit diameter (or width in 2-D)
D_j	= mean primary nozzle jet diameter (or width in 2-D)
D_s	= primary bellmouth eye throat (or width in 2-D)
D'_s	= primary bellmouth eye diameter-exit (or width in 2-D)
F_j	= total measured thrust of primary nozzle assembly with side plates
F'_j	= thrust of primary nozzle with side plates, without bellmouth thrust
F_{jsp}	= thrust of primary nozzle without side plates
F'_{jsp}	= thrust of primary nozzle - one element - alone jet centerline, without side plates
F_m	= total measured thrust, lbs.
g	= local acceleration of gravity
h	= ground clearance from augmenter exit plane
h'	= ground clearance from primary nozzle exit plane
J	$= 778 \dfrac{\text{ft lb}_f}{\text{BTU}}$
k	$= \dfrac{C_p}{C_v}$
ℓ	= length of augmenter measured from center of lip radius to exit plane

SYMBOL LIST (CON'T)

P	=	pressure, total
p	=	pressure, static
r	=	augmenter lip radius for 2-D = .44; for 3-D = $\frac{D_a}{10}$
s	=	gap between nozzle exit plane and augmenter inlet
$S = \frac{s}{t}$	=	nozzle-augmenter spacing parameter
t	=	initial primary jet thickness
T	=	temperature
V	=	velocity
$\dot{w}_m$	=	measured primary weight flow rate
2α	=	total angle of primary jet divergence
2β	=	total angle of augmenter divergence
σ_b	=	primary area ratio = $\frac{\text{bellmouth eye area}}{\text{primary area jet}}$
σ_c	=	secondary area ratio = $\frac{\text{augmenter inlet area}}{\text{primary jet area}}$
σ_d	=	augmenter area ratio = $\frac{\text{augmenter exit area}}{\text{augmenter inlet area}}$
$\sigma_c\sigma_d$	=	total area ratio = $\frac{\text{augmenter exit area}}{\text{primary jet area}}$
θ	=	$\frac{T_j}{520}$
ϕ'	=	augmentation ratio, uncorrected
ϕ	=	augmentation ratio, corrected
ϵ	=	jet aspect ratio = $\frac{\text{mean primary nozzle circumference}}{t}$
η_h	=	primary nozzle efficiency, $\frac{F'_{jsp}}{\text{ideal thrust}}$
Y	=	jet-wall spacing parameter

2. INTRODUCTION

2.1 Program Background

Study of the annular ejector concept and its application was initiated by this contractor in 1956. This ejector is shown schematically in Fig. 1. Since 1959 the government has participated in this program through the Office of Naval Research with funds provided by the Office of Naval Research, the U. S. Marine Corps and the U. S. Army. The first phase program* confirmed and extended the early rudimentary model tests within a set, narrow range of critical geometric parameters which include ℓ/D and σ_c. The basic model geometry is shown in Figures 1 and 2 of Appendix I. The range of parameters investigated was predicted on aircraft installation requirements. Data from these tests (Fig. 7, Appendix I) permitted the design of an "Optimum" annular ejector configuration in Phase I for full-scale testing in the Phase II program.

Phase I also included a study to determine the effect of axial rotation or swirl of the primary jet on the ejector performance. Figures 10 and 11 of Appendix I illustrate the model. These tests indicated that while introduction of such rotation resulted in considerable increase in flow augmentation for the same physical ejector, there was no increase in thrust augmentation. Lack of increase in augmentation was attributed to a cosine thrust loss and additional extraneous losses caused by turning the primary jet away from its axial direction to produce the axial rotation.

The addition of the "Coanda" ejector primary jet nozzle (Fig. 8, Appendix I) to the annular ejector system was also investigated. This modification did not improve the basic performance of the annular nozzle configuration.

The Phase I model tests used a primary jet of approximately 12 pounds

---

*The Appendix of Reference 1, which covers the model work conducted under Phase I, is appended to this report as Appendix I for the convenience of the reader.

thrust utilizing an air supply of approximately 21 inches of mercury at 200°F.

The augmentation performance achieved with the basic model geometry that was chosen for full-scale testing was 1.53.*

The geometric parameters of this model were:

$\sigma_c = 9.77$ $\quad S = 0$ $\quad 2\beta = 8^\circ$

$\sigma_c\ \sigma_d = 19.8$ $\quad 2_c = 0^\circ$ $\quad$ primary nozzle aspect ratio = 100

$\ell/D_a = 3$

This basic model (Fig. 2, Appendix I) incorporated a primary nozzle and plenum system of very high efficiency. The efficiency of this model primary nozzle and plenum expressed as augmentation ratio, ϕ, was .98 to .99. The large volume of this plenum chamber was not commensurate with aircraft installation requirements. Nor was the fabrication cost commensurate with the budget for the full-scale test hardware. Since efficient plenum design was of minor importance to that phase of the annular ejector program, the design of the full-scale ejector incorporated a rather modest plenum to reduce hardware costs. To compare the model and full-scale data intelligently, it was necessary to modify the model plenum to reflect the geometry of the full-scale design. Tests of this revised model configuration indicated an augmentation ratio penalty of 5 to 7 points from the use of such a plenum design.

In the Phase II program** (1960), the full-scale annular ejector assembly and associated test hardware were constructed and tested. This installation is shown in Figs. 1 and 2 of Appendix II. A J-34 turbo-jet engine was used to supply the primary gas for these tests. One-third of

*referred to the isentropic thrust resulting from expansion of the measured weight flow rate at the supply pressure to ambient pressure. Also, see paragraph 3.5.1.

**Pertinent data from Phase II summary report is appended to this report as Appendix II for the convenience of the reader.

the gas generated by the turbo-jet was used in the annular ejector; the remainder was discharged into the atmosphere without influencing the validity of basic data. The actual weight flow rate of gas supplied to the ejector assembly was determined accurately with a sharp-edged orifice flow meter immediately upstream of the ejector assembly. The entire ejector assembly and turbo-jet, together with the connecting ducting, were installed on a platform that was free to move in the horizontal plane except as restrained by appropriate load cells. The load cells, installed on two axes of the thrust table, provided the thrust measurements required for ejector evaluation.

The data obtained from tests of this hardware indicated an augmentation ratio* of 1.48, approximately 5 points less than the Phase I model tests. This 5-point discrepancy was attributed to manufacturing variations in the primary nozzle exit at the time of writing the Phase II summary report. It is now believed that bellmouth separation is also partially responsible for the discrepancy.

The net results of the Phase II full-scale tests were as follows: (1) The establishment of the feasibility of the annular ejector concept and (2) Indication that ejector size (Reynolds Number) and elevated primary jet temperature had a minor effect on ejector performance. Fig. 3 of Appendix II presents a comparison of full-scale and model performance.

The results of ejector wake survey conducted in Phase II are shown in Fig. 4 of Appendix III. Note the magnitude of the reduction in wake velocity (indicated by wake total pressure) and temperature. The primary jet temperature and pressure were 1200°F and 17 in. Hg. respectively.

Other Phase II tests using the scale model of the full-size ejector determined the augmentation performance as a function of ground clearance.

---

*adjusted for correctable supply plenum losses

These tests showed that augmentation performance was affected adversely by ground proximity at clearances below approximately 1.3 to 1.4 augmenter inlet diameters, (Fig. 5, Appendix II). This decrease in augmentation ratio continued until a ground clearance of approximately 0.3 to 0.4 diameters was achieved, and then improved as ground clearance was further reduced. Below a ground clearance of approximately 0.15 diameters the thrust augmentation increased above that achieved out of ground effect. These same tests illustrated that below 0.1 diameters ground clearance even greater improvement in thrust augmentation could be achieved by blocking all secondary flow passages. At ground clearances above 0.1 diameters, blockage of the secondary flow passages resulted in a reduction of thrust augmentation.

2.2 Overall Program Precepts

Preliminary design studies conducted by the contractor covering GEM, VTOL and STOL applications of the annular ejector and other ejector systems have shown that the space required to house the lift-propulsion system is a vital concern. This can be expressed in parametric form by the ratio of thrust (or lift) per unit system volume. The need to minimize volume or to maximize the thrust per unit volume parameter for an efficient end application is relatively obvious considering that skin friction drag is essentially proportional to the 2/3 power of the total enclosed volume of a given vehicle. The importance of this parameter is also clear if the designer must exchange cargo volume for lift-propulsion system volume. When the designer considers supersonic VTOL and STOL aircraft, the frontal area of the lift-propulsion system increases in importance. The allowable thrust per unit volume for a given system can vary with the detail requirements of a particular application.

Exit wake velocity is also important in view of the operational characteristics and problems of GEM, VTOL and STOL craft. The magnitude of the exit wake velocity determines the severity of the exit wake - ground impingement hazards other variables, such as type of ground surface, being constant).

The first of the two parameters discussed, thrust per unit volume, has been the primary precept of the annular ejector program. The second, exit wake velocity, is sufficiently reduced in most cases by the ejector's inherent "diluting" characteristics. Geometric factors influencing the volume of a given ejector system are length-diameter ratio of the augmenter tube, the ratio of augmenter inlet area to primary jet area, the diffuser area ratio, and in the case of the annular ejector, the primary nozzle aspect ratio. In general, ejector technology indicates that superior thrust augmentation results from the use of maximum values of these geometric factors, as limited by the natural phenomena existing in the ejector flow system (augmenter separation and stall, critical Mach Number at the augmenter inlet, mixing efficiency, and augmenter internal friction losses). However, such a configuration is not necessarily optimum on the basis of the thrust-volume parameter.

It is also generally known from previous experience and ejector theory that configurations optimized on the basis of the volume loading parameter have total area ratios in the range from 10 to 100 rather than 100 to 1,000. Moreover, the more conventional applications best utilize total area ratios below 50. Consequently, the range of the total area ratio parameter considered to date by Hiller has been between 10 and 100.

2.3 Phase III Program

The basic intent of the Phase III program is a detailed investigation of the annular ejector concept in ground effect. Complete understanding of the flow system in ground effect is essential to successful application of the annular ejector to VTOL, STOL or GEM vehicles. The annular ejector must have excellent ground effect characteristics to satisfy the terminal phases of the VTOL and STOL mission and permit its application to the pure GEM vehicle. The Phase III program was to continue model tests initiated at the close of Phase II, to determine an annular ejector configuration which had, 1) equal or improved out of ground effect performance as compared with the Phase II work, (2) negligible performance penalty in transition (h/D = 1 to .1) and, (3) conventional GEM performance in ground effect (h/D < .3). The details of this program are discussed in paragraph 3 below.

2.4 Brief Review of Ejector Theory

Over the years, many investigators have analyzed the ejector cycle both as a pumping device and as a thrust augmenter. The interest at Hiller has been primarily in the thrust augmentation characteristics of the annular ejector. Morrisson (Reference 2) and McClintock and Hood (Reference 3) are perhaps the more notable of the earlier thrust augmentation works. Recently, Bertin and Le Nabour (Reference 4) and Weber (Reference 5) have published papers most pertinent to the annular ejector. Bertin's work deals directly with the annular ejector, and pre-dates that done by this contractor. Bertin's analysis of the ejector considers the compressible case, and is presented to show the theoretical effects of pressure and temperature ratio, as well as diffuser efficiency. As in most analyses of the ejector, Bertin assumes that the mixing process is completed prior to diffusion. Weber's analysis of the divergent shroud ejector is of particular interest because he assumes that mixing of the two streams is incomplete at the ejector exit, namely that it continues through the diffusion process. This analysis is closely analogous to the flow system that exists in the annular ejector. Weber, however, considers only low area ratio ejectors, and computes a nozzle thrust coefficient that evaluates the actual thrust of the nozzle-shroud configuration on the basis of the ideal, combined, total exit momentum (secondary and primary). Consequently, his results are not directly applicable, but his analytical treatment does apply. The works specifically referenced here are based on constant area mixing with the exception of Weber. Other analyses have considered constant pressure mixing (a convergent mixing tube) to arrive at a theoretical prediction of ejector thrust augmentation performance. These analyses have shown little advantage from such complication.

Figure 2 compares the theories of several investigators. Thrust augmentation is plotted as a function of total area ratio. Note that these theories are represented by straight lines on the semi-log plot for a constant value of diffuser area ratio, σ_d. This fact indicates that the performance expressions can be expressed in the form

$$\phi = A \log (\sigma_c \sigma_d) + B \Big|_{\sigma_d \text{ constant}}$$

This relationship justifies presenting ejector test data in terms of these dimensionless ratios. Test points are also shown representing Hiller and Bertin full scale ejectors. Note that the slope of a line through the two full scale data points would give a value of A equal to that indicated for the theoretical curves.

2-D test values of ϕ at $\sigma_c = 2$ are also plotted on this theoretical curve for comparison. The 2-D curve does not follow this generalization. This is because the curve represents a fixed primary nozzle configuration optimized for a single value of σ_c rather than a "rubber" nozzle configuration which is optimum for the particular value of σ_c.

3. DISCUSSION

3.1 Conduct of Phase III Program

Paragraph 2.3 above presents the precepts for the Phase III work. To achieve the goals outlined, it was decided to investigate the possibility of performance gains through use of a conically divergent annular primary jet ($2\alpha > 0^{\circ}$). Bertin's work (Reference 4) had indicated that considerable improvement in ejector performance out of ground effect could be obtained at the higher values of $\sigma_c \sigma_d$ through use of a divergent primary jet. Reference (4) indicates successful use of values of 2α as large as 60° with an augmenter divergence angle (2β) of 15°. The higher diffusion angles of the augmenter are possible because of the proximity of the primary jet to the augmenter wall. The primary jet energizes the augmenter boundary layer and delays separation. Since a greater value of 2β would give a larger augmenter exit area (ground effect base area), it was hypothesized that improved ground effect performance would result. It was further hypothesized on the basis of the contractor's Phase II ground effect investigations that appropriate control of the flow system through valving of the bellmouth, secondary (or augmenter) inlet and the augmenter outlet would result in improved transition performance.

The experimental investigation started with two-dimensional (2-D) models because of their simple construction and adaptability to flow visualization techniques. Three basic models were constructed for both flow visualization and quantitative tests to establish the effect of the various parameters, in and out of ground effect, and to determine a configuration suitable for scaling to a three-dimensional (3-D) configuration. The optimum 2-D augmenter determined by these tests for a $2\alpha = 60^{\circ}$ primary nozzle had 2β equal to 17° and σ_c equal 23. This augmenter was then scaled to a 3-D configuration matching the 3-D primary nozzle available from Phase II work. This nozzle had been previously modified to incorporate a nominal jet divergence angle (2α) of 60°. Tests with this 3-D configuration revealed a flow system with little similarity to the

2-D model system. In other words, the 3-D model was ineffective as a thrust-producing device. Subsequently, the 2-D tests were broadened in an effort to eliminate the difficulty in scaling between 2 and 3-D models. Additional 3-D tests were also performed with other augmenter geometries in an attempt to solve the scaling problem. The 3-D model finally obtained with 2α equal to 60° required a 2β of approximately 8° to 10° to achieve a stable flow regime and effective ejector operation. The augmentation performance of this configuration out of ground effect was roughly equivalent to that of the $2\alpha = 0^{\circ}$, $2\beta = 8^{\circ}$ configuration, which was investigated in both model and full-scale tests in Phases I and II of this program.

While performing the required turbo-jet maintenance runs, further investigations were made of the discrepancy between the model and full-scale thrust augmentation performance originally encountered in the Phase II work.

3.2 2-D Model Tests

The purpose of the 2-D tests was threefold: to determine an ejector configuration for scaling to 3-D geometry meeting the Phase III precepts; to gain preliminary data on the performance possibilities of a 2-D annular ejector configuration; to increase the basic understanding of the annular ejector flow system. To achieve these goals, flow visualization and performance tests were conducted using models with a primary jet thrust of approximately 5 pounds at a supply pressure ratio of 1.7. Toledo scale was used for thrust measurement, and a sharp-edged orifice flow meter per ASME Standards was used for flow measurement. Schlieren, smoke, and tuft techniques were used for flow visualization.

The three models were constructed with nominal primary jet divergence angles (2α) of 0°, 30° and 60°. The distance between the side plates was 1.5 inches. The $2\alpha = 30^{\circ}$ model is shown in Fig. 3.

Dimensional inspection of these models indicated that the desired jet divergence angle of 0°, 30°, and 60° would be obtained. Upon completion of the tests with these models, the side plates were cut off at the nozzle exit plane to permit individual testing of the nozzle elements without the unsymmetrical forces caused by ejector pumping through the bellmouth in the presence of the extended side plates. Schlieren studies of these truncated models indicated that the true jet divergent angles (2α) were approximately 0°, 22° and 61°, respectively. Where appropriate, the data has been presented in this report as a function of the actual value of α rather than the nominal value of α.

Fig. 4 presents a summary curve of "Uncorrected"* thrust augmentation as a function of $\sigma_c \sigma_d$ for the nominal values of 2α of 0°, 30° and 60°. The figure shows that no advantage in thrust augmentation is gained through use of $2\alpha > 0^\circ$ when side plate losses are present. The 2-D models are of such proportions that an essentially "square" flow cross section results at the eye. That is to say, the length (or span) of the 2-D jet-slots forming the 2-D simulated annular jet is equal to the width of the eye, D_s, (distance between the jet-slots). Thus, the models have relatively high losses, which can be attributed to side wall friction. In other words, the side wall wetted area is large with respect to the free or unbounded jet area.

Supplementary side plate evaluation tests were conducted using the three truncated models. From these tests a side plate correction factor was obtained as described in paragraph 3.5.2.

Fig. 5 presents a summary curve similar to Fig. 4, but incorporates the correction for side plate frictional losses. It will be noted from this figure that improved performance would be anticipated from use of a 2α value of approximately 30° in a high jet aspect ratio 2-D configuration that would reduce side wall friction, or in a 3-D configuration that would eliminate side plate friction.

---

*Measured thrust values are not corrected for side plate frictional losses. (All of the 2-D thrust augmentation data has been presented on an uncorrected basis with the exception of figure 5).

Both Figs. 4 and 5 represent the optimum performance obtained for a given value of $\sigma_c\sigma_d$ and 2α, with variable σ_c, β and S. A total of approximately 200 ejector configurations was tested utilizing the variable geometry augmenter. A configuration is shown under test in Fig. 3 (Note augmenter separation). The data is plotted in figures 9 through 12.

These 2-D tests have shown that it is possible to use values of 2β as large as 20° without incurring diffuser separation. However, it has been found that the maximum thrust augmentation occurs considerably before diffuser separation, that is, at lower values of 2β. In fact, using primary nozzles of 2α equal to either 30° or 60°, the optimum value of 2β was roughly 16°, which may indicate that β is essentially independent of α in this range. However, the optimum value of σ_c was found to be a strong function of α. These parameters are presented in Fig. 6.

To present β as a function of α alone is an over-simplification. The optimum value of 2β is also an involved function of the jet-wall spacing parameter, γ, the ratio of augmenter inlet area to primary jet area (σ_c), and the axial location or spacing (S) of the augmenter downstream of the primary jet outlet. γ and S probably extert the greatest influence on optimum β, σ_c being involved through interrelation of the system parameters. Low values of γ give increased boundary layer energization and greater augmenter friction losses. Consequently, appropriate trade-offs must be made. Changes in γ in these 2-D tests were accomplished by altering σ_c. Consequently, it is not possible to support these hypotheses unequivocably from this data.

In the annular ejector system, matching the proper augmenter inlet geometry to the primary nozzle is believed to depend on two prime factors, namely, the secondary area ratio σ_c and the jet-wall spacing parameter, γ. The choice of 2-D primary nozzle parameters made for this series of models maintains the similarity simultaneously between current 2-D and Phase II 3-D for σ_c and γ.

3.2.1 Reference Test, $2\alpha = 0^{\circ}$ Model

The purpose of this model was to provide a reference to the previous

3-D, $2\alpha = 0^{\circ}$ work done in Phases I and II. However, in providing a direct reference in scaling from 2-D to 3-D configurations, it is not possible to keep constant all the dimensionless ratios and other parameters. It is impossible to maintain equal values of the jet aspect ratio, Θ, primary area ratio, σ_b, secondary area ratio, σ_c, and the jet-to-wall spacing parameter, γ, between a 3-D and 2-D configuration. However, the 2-D case does allow greater independence of the parameters. For instance, in the 2-D case jet aspect ratio, Θ is independent of σ_b, while in the 3-D case they are mutually dependent.

In the design of the basic 2-D model, $2\alpha = 0^{\circ}$, it was decided to sacrifice similarity of the jet aspect ratio between 2 and 3-D in favor of maintaining σ_c and γ, and also to simplify the model construction by shortening its span, i.e., nozzle length. It was realized that jet aspect ratio (30 in 2-D, 100 in Phase II, 3-D) was of importance and would require consideration in comparison of 2-D and 3-D results. Primary area ratio σ_b of the 3-D models was preserved at $\sigma_b = 1.65$ in the 2-D models.

3.2.1.1 Performance Comparison 2-D: 3-D @ $2\alpha = 0^{\circ}$

It will be noted that the 2-D $2\alpha = 0^{\circ}$ tests indicate a maximum corrected augmentation ratio of 1.37 (Fig. 4). This augmenter geometry ($2\alpha = 0^{\circ}$, $2\beta = 8^{\circ}$, $\sigma_c = 9.75$, $\sigma_c \sigma_d = 15.42$) essentially duplicates the 3-D model geometry ($2\alpha = 0^{\circ}$, $2\beta = 8^{\circ}$, $\sigma_c = 9.77$, $\sigma_c \sigma_d = 19.8$). The prime geometric difference between the models is in the jet aspect ratio: in the 2-D case it equals 30; in the 3-D case it equals 100. Phase I indicated an augmentation ratio $\psi = 1.53$ for this 3-D model. The large discrepancy between the 2-D and 3-D performance - 16 points - can be attributed largely to the decrease in jet aspect ratio, and to "eye" aspect ratio of the 2-D model. The side plates, which are unenergized, or unblown surfaces in the 2-D model (as compared to a 3-D annular configuration where all the surfaces are energized) compose a large portion of the bounding surfaces in these square, low eye aspect ratio 2-D models. The difference in σ_d between the 2-D and 3-D tests can also explain the difference in performance.

3.2.1.2 Performance 2-D @ $2\alpha = 0^\circ$

Analysis of the $2\alpha = 0^\circ$ primary jet test data, (Fig. 7) indicated the optimum performance with an augmenter divergence angle $2\beta = 8^\circ$, positioned with the augmenter inlet at the plane of the nozzle exit ($S = 0$). Little variation in thrust augmentation was found by varying σ_c from 9.5 to 10.5. The only result was to increase $\sigma_c\sigma_d$ required to obtain a given value of ϕ. Flow visualization studies at $\sigma_c = 10$ indicated the primary jet would remain attached to the augmenter walls through a 2β variation from 0° to 14°. Lower 2β values showed a relatively unmixed primary jet clinging closely to the augmenter wall. At 2β equal 6° to 10°, the primary jet appeared dispersed over a larger area indicating improved mixing and obviously greater diffusion. The studies are depicted graphically in Fig. 8.

Bellmouth eye static pressure, which is a direct measure of the eye velocity, is an accurate measure of bellmouth thrust and indicative to some degree of overall ejector performance. Consequently, its behavior as a function of 2β (or σ_d) is of interest. The static pressure measured at the center of the $2\alpha = 0^\circ$ bellmouth eye decreased with increasing β and total area ratio ($\sigma_c\sigma_d$) until just prior to the appearance of separation in the augmenter at $2\beta = 14^\circ$, -30" H_2O was measured. With the optimum configuration ($2\beta = 8^\circ$), -2-" H_2O was measured. The continuing decrease of eye static pressure below that which exists with $2\beta = 8^\circ$ indicates continuing increase in secondary pumping, and consequently gross thrust beyond that which occurs at the maximum overall performance point. This continued increase in secondary thrust is offset by increased augmenter diffusion losses, and consequent increased internal augmenter drag.

The flow regime at $2\beta = 14^\circ$ was unstable, and occasionally reverted to the unseparated or fully attached state. At $2\beta = 15^\circ$ separation occurred over approximately 1/4 of the augmenter wall, while flow remained attached to the opposite wall, (Fig. 8). However, the stalled region could be easily diverted to either augmenter wall by momentarily inserting a flat vane at a slight angle of attack near the augmenter centerline. This fact indicated the stall was not an augmenter-primary jet misalignment problem. The augmenter separation was accompanied by an abrupt increase of about 10" H_2O in eye static pressure (to -20" H_2O), indicating a sudden decrease of secondary pumping and an accompanying loss of performance.

Maintaining all parameters constant, while increasing 2β to 18^o, moved the point of separation upstream to the augmenter throat where the flow on one side was attached over a very short length of the throat, (Fig. 8) while the eye pressure increased further. The stalled region at this configuration was quite stable, although it could still be diverted by a vane to either wall. Almost 3/4 of the total augmenter exit area was occupied by this separated region.

3.2.2 2-D @ $2\epsilon = 30^o$

Maximum 2-D out of ground effect performance was obtained with the $2\epsilon = 30^o$ primary jet, which produced an uncorrected thrust augmentation of 1.29. The augmenter configuration required to achieve this performance has a secondary area ratio (σ_c) of 14, an augmenter divergence angle (2β) of 15^o, and a nozzle-augmenter spacing parameter (S) of 10. The data is presented in Figs. 9 and 10 for S equal to 0 and 10 respectively, showing thrust augmentation as a function of total area ratio ($\sigma_c\sigma_d$) for several values of σ_c between 10 and 20. Cross plots for constant diffuser area ratio (σ_d) are over-printed in red on these figures. As augmenter wall length was maintained constant in these tests, the line of constant σ_d also represents constant β (indicated by data symbols). The solid red curves show thrust augmentation at a constant σ_d, while the broken red curves through the constant σ_c curves permit separation of σ_c and σ_d effects to a limited degree. Lower and higher values of σ_c were not investigated due to the nature of the resulting flow regime.

The optimum configuration for the $2\alpha = 30^{\circ}$ model resulted in a slight angle of incidence between the primary jets and the augmenter walls (α-β = 4°). In the case of $2\alpha = 0^{\circ}$, the angle of incidence was also 4°. The configuration was conducive to a stable flow pattern with an augmenter boundary layer sufficiently energized to prevent augmenter separation at the large 2β angles, and with maximum effective secondary pumping (Fig. 8).

Maximum augmentation, ϕ, occurs at a value of 2β a few degrees less than that at which augmenter wall separation initially occurs, a characteristic common to clinging flow phenomenon. Separation occurred at diminishing values of 2β (or σ_d) as σ_c was increased, which, in effect, increases the jet-wall spacing parameter, and consequently decreases boundary layer energization. Reduction of the nozzle-augmenter spacing parameter (S) below 10 to reduce the installed volume causes a small performance loss (2 pts). This trend reverses that observed in 3-D tests, and is attributed to the restrictive nature of the two dimensionality in the 2-D secondary flow passage. The influence of S is demonstrated further by a comparison of maximum augmentation performance in Figs. 9 and 10. At S = 0 (Fig. 9), optimization requires a larger σ_c (16) than the S = 10 case ($\sigma_c = 14$), while the best 2β is reduced. The maximum performance, as indicated by Fig. 10 occurred at $2\beta = 15^{\circ}$, $\sigma_c = 14$ and $\sigma_c\sigma_d = 25$. At this point the eye static pressure was -20" H_2O. Further testing, holding $\sigma_c = 14$ constant and increasing 2β (i.e. σ_d), resulted in a reduction in augmentation with eye pressure increasing only slightly. This indicates pumping and diffuser action have reached a maximum and wall friction losses have increased to reduce augmentation. Separation was first detected at 2β of approximately 20°. This initial stall condition was similar to that observed with the $2\alpha = 0^{\circ}$ model with an unstable point of separation on the lower section of one augmenter wall. Increasing 2β by approximately 5° with σ_c still held constant at 14, moved the point of separation upstream to a fixed position downstream of the augmenter throat, and resulted in a region of stable, fully developed stall which covered essentially half of the augmenter exit area. At larger values of σ_c separation occurred with smaller 2β angles. Initial stall is illustrated in Fig. 3 where the tuft is carried upstream by the recirculating flow in the stalled region. The tuft behavior in this configuration indicated an unstable flow regime.

Performance under the stall conditions is obviously poor. Several detrimental factors are involved in this undesirable performance region including a sharp decline in secondary pumping and diffuser action, and a large increase in shearing forces between the main flow and the stalled region.

3.2.3 <u>2-D @ $2\alpha = 60^{\circ}$</u>

Maximum augmentation performance with $2\alpha = 60^{\circ}$ was achieved with an augmenter having $2\beta = 17^{\circ}$, $\sigma_c\sigma_d = 36$, and $S = 10$. The performance curves are given in Figs. 11 and 12 for $S = 0$ and 10 respectively as a function of $\sigma_c\sigma_d$ for constant values of σ_c. Again, σ_d is cross-plotted as in the previous $2\alpha = 30^{\circ}$ case. The family of curves (Fig. 12) presenting the optimum configuration ($S = 10$) indicates that performance improves gradually with increasing $\sigma_c\sigma_d$ for a constant value of σ_c, which is actually an increase in diffuser area ratio. Since the augmenter wall length was constant in all these 2-D tests, an increase in $\sigma_c\sigma_d$ entails increases in 2β (i.e. σ_d) as noted by the coding of the data points. This interdependence of the parameters does not permit selection of the parameter most critical to optimum performance on the basis of data obtained in this study alone.

With $S = 0$ (Fig. 11) little change in optimum performance was seen between $\sigma_d = 1.2$ and 1.5 (2β of 5° to 20°) for all values of σ_c investigated. The thrust augmentation was slightly less than that obtained with S = 10 as in the $2\alpha = 30^{\circ}$ case. Stall was not experienced with the $2\alpha = 60^{\circ}$, although 2β was increased up to 42° and σ_c to 28. In all configurations tested, the partially mixed primary jet adhered to the augmenter walls maintaining an essentially "plane jet" flow throughout the length of the augmenter. As previously noted in the discussion of the $2\alpha = 0^{\circ}$ model (paragraph [illegible].1.2), improved performance required diffusion and mixing of the primary flow with the induced flow. It is seen in Fig. [illegible] that this type flow regime was not achieved in this case.

The $2\alpha = 60^{\circ}$ bellmouth eye static pressure behaved similarly to that observed with $2\alpha = 30^{\circ}$ with similar changes in geometry except that, in general, the pressure at the eye was not as low as in the $2\alpha = 30^{\circ}$ case. This observation implies reduced bellmouth pumping and inferior augmenter performance. The latter is noted also by reviewing the performance curves (Figs. [illegible] and [illegible]).

The angle of incidence between the undeflected primary jet and the augmenter wall ($\alpha - \beta$) was of the order of 24° in the best $2\alpha = 60^{\circ}$ configuration. This value is much greater (by 20°) than that encountered with $2\alpha = 0^{\circ}$ or $2\alpha = 30^{\circ}$, and undoubtedly causes greater fluid shear stress at the wall with consequent higher losses.

Fig. 12 shows that optimum performance occurs at σ_d of 1.5 for $2\alpha = 60^{\circ}$, while at $2\alpha = 0^{\circ}$ and 30° the best σ_d was on the order of 1.5 (Fig. [illegible]) and 1.[illegible] (Fig. 10), respectively. It is believed that optimum σ_d should increase continuously with 2α on the basis of Bertin's work (Ref. 4) which implies σ_d in the order of 2 for $2\alpha = 60^{\circ}$. It is obvious that this trend has not occurred in this work, nor is the $2\alpha = 60^{\circ}$ performance exemplary.

The cause of the over-all poor performance obtained with $2\alpha = 60^{\circ}$ is not completely understood, but is believed to be largely attributable to selection of the primary nozzle parameters, σ_b and jet aspect ratio. In other words, the choice of σ_b and jet aspect ratio for the 2-D primary nozzle precludes the use of a sufficiently large value of σ_c (with adequate boundary layer energization-low γ) to take full advantage of the larger values of 2β that were indicated possible. Further work in this particular area should reveal significant increases in thrust augmentation.

3.2.4 2-D Primary Nozzle Performance

Each of the three primary nozzles was tested with the side plates cut off downstream of the nozzle exit plane to determine basic nozzle efficiency.

Each nozzle of the primary assemblies was individually tested to determine the actual thrust vector along the jet axis (not the axis of symmetry of the assembly). Comparison of this measured thrust with ideal thrust, in the same manner as ϕ is determined, defines the combined nozzle and turning efficiency. The efficiency of each 2-D nozzle is presented in Fig. 13 along with other pertinent primary nozzle characteristics. Truncating the nozzle assemblies was required to achieve accurate jet thrust readings. Truncating the side plates eliminates the augmentation due to bellmouth pumping by destroying the eye suction with unrestricted access of ambient air.

When 2α is greater than zero, the thrust performance of the primary nozzle assembly along its axis of symmetry is of considerable interest. Such information would evaluate the "aerodynamic turning "efficiency of the system in converting the initially divergent primary jets to a parallel (or cylindrical in 3-D) jet wake, thus eliminating any cosine loss due to initial jet divergence. To determine such an efficiency, jet thrust, bellmouth thrust, and side plate thrust loss must be separated. These components are interdependent. In the 2-D case side plates are necessary to maintain the sink. The sink is caused by the bellmouth flow mixing with the primary jet and simultaneously sweeping away the flow. The sink provides the pressure differential that produces aerodynamic turning of the divergent jet, and is inter-related with the pumping that produces bellmouth thrust. It is difficult to determine wall friction loss with sufficient precision to give reasonable accuracy to the computed aerodynamic turning efficiency. Determination of the net bellmouth thrust is equally difficult, but preliminary data indicates good aerodynamic turning efficiency.

3.2.5 Ground Effect 2-D

A series of adjustable vanes were installed on the optimum $2\alpha = 60^{\circ}$ 2-D model with the ejector configuration ($\sigma_c = 24$, $2\beta = 15^{\circ}$, $S = 10$, $\sigma_c \sigma_d = 34.6$) in an attempt to improve performance in the transition regime ($h = 0.1"$ to $8.0"$). Two curved vanes were installed at the bellmouth to control the bellmouth flow as desired. Single flat vanes were similarly installed in each secondary flow passage between the augmenter inlet lip and the nozzle plenum. Four short, flat vanes were installed on equidistant centers slightly above the augmenter exit plane to control the combined flow. The modified model is shown in Fig. 14. For purposes of comparison this ejector was initially investigated in ground effect without vanes installed. Fig. 15 shows a loss in performance (up to 30 points) for this configuration which is very similar to that observed in the Phase II tests with the 3-D, $2\alpha = 0$ model (see Fig. 5, Appendix II). The model was observed over a ground-effect range of $h = 0.1"$ to $8.0"$*. The latter limit was imposed by the length of the model side plates. The performance is normalized with respect to out of ground effect performance. The vaned performance is normalized to out of ground effect performance with the optimum vane setting, to remove the effect of vane losses from the data, which were not designed for aerodynamic cleanliness, but rather for test expediency. For the record, the loss imposed by the vanes on the ejector system was on the order of eleven per cent of the unvaned performance. The curve, which describes the vaned ejector performance, was obtained by adjusting the vane systems for optimum performance at each value of ground clearance investigated.

---

*The ground clearance has not been normalized in this report because of lack of a sufficiently characteristic reference dimension. The exit diameter D_e, of this 2-D augmenter was 6.9".

Performance, from h = 5" to 0.3" inclusive, was controlled primarily by the vanes installed near the augmenter exit in a configuration as seen in Figs. 14 and 15. Optimum vane alignment had the inboard vanes forming a closed "V" shape, which created a vortex pair system in the central portion of the augmenter, and largely reduced the amount of reverse flow up the center of the augmenter. The base pressure acted on the closed vanes to give a vertical thrust component. Optimum outboard vane positioning began with these two vanes approximately parallel to the augmenter wall out of ground effect. Then, the leading edge was rotated toward the augmenter wall as the ground clearance was reduced until the vanes at h = 0.1" were inclined 30° to the ground plane, (see Fig. 15). Flow observations indicate the outboard vanes act to turn the jet inboard thus creating a higher base pressure.

The bellmouth vanes were found to be effective only at h < 0.3" after the bellmouth pumping was destroyed by the build-up of static pressure in the augmenter. Closing the curved bellmouth vanes so that they effectively blocked the bellmouth provided additional surface on which the base pressure could act. These vanes contributed in a large part to the approximate 50 point increase in performance, (see Fig. 15). With h > 0.3" the eye vanes were aligned to conform with the least disturbance to the eye flow field, utilizing the maximum thrust measurement as the alignment criteria.

Augmenter inlet vane positioning was not critical to performance at the ground clearance investigated except when the bellmouth vanes were closed. This regime is demonstrated by tuft in Fig. 16. Beyond the 20° limit, a thrust decrease was observable as the vanes were moved closer to the blocked position. The thrust loss in ground effect with closed augmenter inlet vanes varied with h and was approximately 10% to 15% of the open vane position performance.

3.3 3-D Model Program

It is not possible to maintain all geometric parameters constant when scaling from two-dimensional to three-dimensional geometry. This conversion or scaling is difficult, even when ejector phenomena are not included in the flow system (for instance, the correlation of 2-D and 3-D diffuser data without the influence of ejector phenomenon). Scaling 2-D to 3-D geometry increases in difficulty as the 2-D configuration deviates on either axis from a square configuration. When the ejector phenomena are also included in the scaling problem, the additional parameters of the ratio of primary jet area to augmenter inlet area, and the jet-wall spacing parameter, etc. make it extremely difficult, if not impossible, to scale effectively from 2-D to 3-D configuration.

3.3.1 Matching of Augmenter Configuration to Primary Nozzle

The initial 3-D augmenters designed for use with the $2\alpha = 54^{\circ}$ nozzle were based on the preliminary results of the 2-D tests. These tests indicated that a value of $2\beta = 15^{\circ}$ and σ_c between 22 and 26 would operate successfully with the $2\alpha = 54^{\circ}$, 3-D nozzle. 3-D tests using these augmenters failed to duplicate the flow regime obtained in the 2-D tests. Specifically, it was not possible to achieve attached flow throughout the augmenter tube. The length of these $2\beta = 15^{\circ}$ augmenters was varied over a range of $\ell/D_a = 4$ to less than 1.0 which in turn reduced σ_d from 3.2 to 1.5. Tests of such configurations also failed to give an acceptable flow regime, indicating over-expansion was not the cause of the difficulty. The observed eye pressure also indicates that inlet Mach Number was not critical. The observed stall area encompassed between 1/8 and 1/2 of the circumference of the augmenter exit, and the larger stalled region occurred with the larger σ_d. Decreasing ℓ/D_a, at the same value of 2β, improved flow stability and increased thrust augmentation slightly in this case by reducing the length of stalled augmenter (lower drag). Accurate thrust measurements were difficult to obtain due to turbulence involved in the unstable flow regime, which caused large, uneven fluctuations in thrust scale readings. The general performance level did not warrant further investigation at this value of 2β. Other testing with $2\beta = 15^{\circ}$ used available augmenters with σ_c as low as 19 to increase boundary layer energization. At σ_c = 19 the jet-wall spacing, γ, was essentially zero. This reduced γ, or increased boundary layer energization, did not produce a stable flow regime at $2\beta = 15^\circ$.

3.3.1.1 Scaling Difficulties

The scaling difficulties encountered with the $2\beta = 15^\circ$ augmenters indicated a basic difference between the flow mechanics of the 2-D and 3-D models. In the 2-D, $2c = 60^\circ$ model, the primary jet clings to the augmenter wall in essentially one-dimensional or plane jet flow with little or no diffusion action. Also, there the jet has no tendency to spread or diffuse peripherally across the side plate. The behavior of the flow is essentially that which occurs when a jet is turned by clinging to an adjacent curved surface. In the case of the 3-D model, the jet is a continuous fluid sheet which clings to the periphery of the augmenter's circular cross section. As this flow continues through the augmenter, it is required to expand circumferentially as well as laterally to maintain attachment to the augmenter wall. Consequently, at the same value of β, it can be expected that considerably greater diffusion is required of the primary jet to maintain attached flow in the 3-D case. This basic difference is believed to explain the scaling difficulties encountered between 2-D and 3-D configurations of the type investigated in this program.

The static pressure measured at the bellmouth eye in the 2-D and 3-D cases lends interesting support to this contention. The 3-D, $2\alpha = 54^\circ$ eye static pressure depression was of the order of 2 to 2.5 times that in the 2-D, $2c = 60^\circ$ case. This difference in eye pressure indicates considerable discrepancy in the bellmouth pumping and augmenter performance. The reasons for poor performance of the 2-D, $2c = 60^\circ$ model were discussed in paragraph 3.2.3.

3.3.1.2 Optimum Augmenter Configuration

At this point a second series of augmenters available from parallel programs were tested with $2\beta = 8^\circ$, 10°, and 12° and a σ_c range of 21 to 28. A maximum performance of $\phi = 1.49$ was obtained at $S = 0$ with a $2\beta = 8^\circ$, $\sigma_c = 21.8$ and $\sigma_c\sigma_d = 42.3$ augmenter geometry. A typical 3-D test set-up with the $2\alpha = 54^\circ$ primary nozzle and a $2\beta = 10^\circ$ augmenter at $S = 0$ is shown in Fig. 17. Fig. 18 shows the details of the primary nozzle outlet. Fig. 19 presents the thrust augmentation of these two augmenters ($2\beta = 8^\circ$ and 10°) as a function of $\sigma_c\sigma_d$. The variation in $\sigma_c\sigma_d$ is obtained by reducing the length of the augmenter. Lines of constant ℓ/D_a are cross-plotted. It was found that high augmentation depended upon careful alignment of the primary nozzle and augmenter centerlines. This augmenter alignment was made on the basis of maximum thrust readings. With $2\beta = 10^\circ$, $\sigma_c = 22$ augmenter, a slight lateral misalignment (1% D_a) resulted in augmenter separation. The $2\beta = 8^\circ$, $\sigma_c = 21$ augmenter was less sensitive to alignment than the previous case, but flow could also be detached by a misalignment of only 5% D_a.

3.3.1...1 Effect of S on Ejector Performance

A series of tests was conducted with the $2\beta = 8^\circ$, $\sigma_c = 21$ augmenter to determine the effect of the nozzle-augmenter spacing parameter on ejector thrust augmentation. This test indicated $S = 0$ for maximum thrust performance (see Fig. 20). Values of S above and below this point caused a marked performance decline. As was observed in the 2-D case, ($2\alpha = 0^\circ$ and $2\alpha = 30^\circ$ model) maximum performance was similarly achieved in 3-D with the 2β value a few degrees less than that which produced separation. At $2\beta = 8^\circ$ and $\sigma_c = 28$ completely attached flow was not obtained. Further investigation of σ_c between 21 and 28 ($2\beta = 8^\circ$) would quite probably uncover a configuration of superior performance. At $2\beta = 1.^\circ$ the same problem of diffuser separation occurred as at $2\beta = 15^\circ$.

3.3.2 Ground Effect Evaluation - 3-D

While a configuration was not achieved with augmentation superior to that of Phase II, it was believed of interest to evaluate the greater values of 2β and 2α in ground effect with 3-D configurations.

3.3.2.1 Primary Nozzle Alone

Ground-effect tests were first conducted with the $2\alpha = 54^{\circ}$ primary nozzle alone to provide a comparison for later work with augmenters. Ground clearance was found to affect adversely thrust augmentation of the primary nozzle alone up to a clearance of 13" or $5D_s$ as shown in Fig. 21. Ordinarily, ground effect on conventional propeller jet lift systems influences performance only between 1.5 to 2.0 diameters clearance. The divergent primary jet had a characteristic unstable bellmouth pumping with occasional flow reversal in the 2" < h' < 13" region. Below h' = 2" thrust fell off at a much higher rate as the nozzle bellmouth eye flow alternated in and out of the eye at a regular, increasing frequency. This frequency reached a maximum of approximately 1,000 cps at h' = 1.0". At h' = 1.0" negligible secondary pumping occurs over the bellmouth surfaces, while the flow was completely reversed in the eye proper. In proximity (h' < 2") with the ground plane, a low pressure region of approximately -0.6" H_2O is created under the nozzle plenum assembly by the circulation of ambient air caused by the pumping of the primary jet as it flows outwardly along the ground plane. This low pressure acting on the lower side of the nozzle naturally contributes to the loss in thrust augmentation. Consequently, at h' = 0.3" the thrust augmentation is only .34 compared to the out-of-ground effect performance of 1.02.

3.3.2.2 Complete Ejector Assembly

Testing was conducted with the two augmenters exhibiting the best out of ground effect performance ($2\beta = 8^{\circ}$, $\sigma_c = 21.7$, and $2\beta = 10^{\circ}$, $\sigma_c = 22.1$) to determine their in ground effect and transition performance characteristics. This data is presented in Figs. 21 and 22 for these augmenters at several values of P/T_a. It is interesting to note that the augmenter length had little effect on the elevation (h') of the nozzle exit plane at which ground proximity effected ejector performance. This elevation (h') was approximately 21" or $8D_s$ for both augmenters. This suggests that the flow system is dependent on a characteristic length downstream of the primary nozzle which is greater than the length of the augmenter.

Figs. 21 and 22 also show performance increasing sharply with $h < 1"$ for each ℓ/D_a after a gradual decrease from the out of ground effect performance test.

As has been discussed previously, it was believed that increased augmenter exit area, in effect, increased "base-area", would give improved thrust augmentation close to the ground. Such increased exit area can be achieved through variable augmenter geometry or operation at large β's. Fig. 23 presents the thrust augmentation characteristics and as a function of augmenter exit diameter at low values of h ($h < .3$). As 2β was constant at 8^o and 10^o, the change in area is achieved by a change in ℓ/D_a. In proximity ($h < 0.3"$) to the ground plane, a large back pressure builds up at the augmenter exit since the augmenter is essentially stalled. Ejector action is negligible. Bellmouth flow pumping action ceases, followed by a reversal of the primary jet out the secondary flow inlet. This flow regime is characterized by increased static pressure along the augmenter walls which provides the increased thrust augmentation. The performance is not significantly different from that encountered in Phase II program with $2\alpha = 0^o$, $\sigma_c = 10$, $\ell/D_a = 3$. This is shown in Fig. 5 of Appendix II.

On the basis of 2-D testing, the installation of vanes in the primary 3-D nozzle bellmouth and the augmenter exit would produce impressive performance gains in ground effect.

3.4 Full Scale Ejector

The full scale ejector is shown in Fig. 2 of Appendix II. In conjunction with the required maintenance runs of the J-34, which is the primary gas generator for the full scale ejector, a minimum program was undertaken to investigate the bellmouth secondary flow characteristics. The initial objective of this program was to investigate further the discrepancy between full-scale and 3-D model performance encountered in Phase II. Preliminary smoke visualization survey indicated separation at the bellmouth lip. The bellmouth lip was instrumented with three total pressure rakes (Fig. 24), each consisting of four variable height probes to aid in the evaluation of lip losses and subsequent lip modifications. These total pressure probes were radially aligned, parallel to the lip surface, thus enabling pressure measurements at desired intervals up to 4" above the surface. Static pressure taps were located at each rake station.

Due to the discontinuity presented to the inlet potential flow by the original sharp-edged bellmouth lip, the angle of attack at the outboard rake, which overhangs the lip by 0.5 inches, was of the order of 45° based on flow visualization studies. Consequently, error of large magnitude can be expected in the data from these probes prior to lip modification. The sharp bellmouth lip caused a separation bubble to begin at that point. This bubble reached maximum size in the region of the middle rake as indicated by both total pressure profile and flow visualization studies.

The data obtained in this survey prior to lip modification (Fig. 25), is of a qualitative nature due to the general problem of probe alignment with the streamlines. The total pressure profile over the unmodified lip surface indicates the total head losses are very small above 2" from the lip surface. This general profile is at the outboard rake and continues with little deviation along the instrumented section of the bellmouth contour. Following the reference tests, the bellmouth lip was modified. The bellmouth lip modification (Fig. 26) consisted of extending the lip radially 42" with a flat surface, thereby essentially duplicating the original model configuration*. While this modification also had a sharp edge, the flow field area at that point was sufficient to result in negligible velocity at the same point. Consequently, separation vanished. The lip pressure data obtained following this modification (Fig. 25) indicates the inlet losses are essentially eliminated

*The intent of the flat surface in the original model was to simulate a wing installation.

by the extension. Flow visualization and lip pressure data indicate attached flow over the bellmouth as would be expected. Smoke flow visualization illustrates (Fig. 27) the secondary flow patterns over the bellmouth lip before and after modification.

The bellmouth eye was traversed at the nozzle exit plane before and after the lip modification to determine the static and total pressure profile that would permit evaluation of the losses due to lip separation. Four probes, two static and two total pressure, were located 1/4" and 1/2" above the bellmouth surface in the nozzle exit plane as shown in Fig. 28. Adjustable probes were used to survey the remainder of the eye. The pressure profiles obtained with these probes are also shown in Fig. 28 both before and after the extended lip modification. The lip extension eliminated approximately 85% of the bellmouth thrust loss that was indicated by the initial eye pressure survey.

The magnitude of the thrust loss prior to lip modification as determined from the pressure surveys was on the order of 1% of the primary jet thrust.

3.5 Data Reduction

3.5.1 Thrust Augmentation

Thrust augmentation is defined as the ratio of the total measured thrust divided by the thrust produced by the isentropic expansion of the measured flow rate of air from the supplied total pressure to ambient pressure. Expressed in equation form as follows:

$$\phi = \frac{Fm}{\frac{\dot{w}}{g} V_{theo}}$$

$$\text{where } V_{theo} = \left\{ \frac{1}{2} gJC_p T_t \left[1 - \left(\frac{P_o}{P_t} \right)^{\frac{k-1}{k}} \right] \right\}^{1/2}_{\Delta s = 0}$$

to simplify data reduction

$$\text{let } \theta = \frac{T_t}{520}$$

and then multiplying and dividing the right hand side by T_{os1} and substituting

$$V_{theo} = \sqrt{\theta}\left\{\frac{1}{2}\, gJC_p\, T_{os1}\left[1 - \left(\frac{P_o}{P_j}\right)^{\frac{k-1}{k}}\right]\right\}^{1/2}$$

which, when appropriate gas properties are used for the gas temperature involved, reduces to

$$V_{theo} = f\left(\frac{P_o}{P_j},\ \sqrt{\theta}\right)$$

or, for gas properties at a 300°F (C_p = .24, k = 1.4 for model tests) and a pressure ratio $\frac{P_o}{P_j}$ of 1.7 gives

$$V_{theo} = 29.1\sqrt{\theta}$$

which gives for data reduction purposes, the expression

$$\phi = \frac{F_m}{\dot{w}\sqrt{\theta}}\ \frac{1}{29.1}$$

3.5.2 Side Plate Corrections

The side plate correction was derived and determined as follows:

$$\frac{F_{jsp}}{\dot{w}\sqrt{\theta}} - \frac{F_j^*}{\dot{w}\sqrt{\theta}} = \text{Specific primary jet thrust loss due to side plate friction}$$

$$1 + \frac{\dfrac{F_{jsp}}{\dot{w}\sqrt{\theta}} - \dfrac{F_j^*}{\dot{w}\sqrt{\theta}}}{\dfrac{F_j^*}{\dot{w}\sqrt{\theta}}} = \text{Side plate correction factor}$$

ϕ = (ϕ') (side plate correction factor)

$\frac{F_{jsp}}{\dot{w}\sqrt{\theta}}$, determined directly from tests of truncated primary nozzles.

$$\frac{F_j^*}{\dot{w}\sqrt{\theta}} = \frac{F_j - \text{External pressure forces acting on bellmouth}}{\dot{w}\sqrt{\theta}}$$

External pressure forces can be expressed in terms of the net thrust due to the secondary flow at the bellmouth exit (D'_s)

Considering only first order effects

$$F_{Bellmouth} = \frac{V'_s \dot{w}_s}{g} + (p'_s - p_o) D'_s (1.5)$$

where 1.5 is the distance between side plate, the prime indicates conditions at bellmouth exit, and the subscript s indicates bellmouth system

$$V'_s = \sqrt{\frac{2}{\rho}}\sqrt{q_s}$$

where $q'_s = p_o \ p'_s$

and $\dot{w}_s = V'_s D'_s \rho \times 1.5$

or

$$F_{Bellmouth} = \left[V'^2_s + (p'_s - p_o)\right] D_s \times 1.5$$

substituting for V'_s

$$F = D'_s (p_o - p'_s)$$

assuming one dimensional diffuser flow in bellmouth exit

by Bernoulli and continuity

$$(p_o - p'_s) = \left(\frac{D_s}{D'_s}\right)^2 (p_o - p_s)$$

substituting

$$F_{bellmouth} = D'_s (1.5) \left(\frac{D_s}{D'_s}\right)^2 (p_o - p_s)$$

4. CONCLUSIONS

4.1 The basis of the 2-D tests (jet aspect ratio, $\theta = 30$, $\sigma_b = 7.65$) the additional complexity of using $2\alpha > 0^\circ$ is unwarranted. On the basis of data corrected for side plate losses, it was concluded that larger values of θ or (eye aspect ratio) which would minimize side plate losses, would result in optimum performance at 2α in the neighborhood of 30°.

4.2 From augmentation performance determined in 3-D tests (with jet aspect ratio, $\theta = 100$ and $\sigma_b = 7.65$) the complexity of $2\alpha > 0^\circ$ is unwarranted. It is hypothesized on the basis of 2-D data that superior performance would be obtained at large values of jet aspect ratio by use of $2\alpha > 0^\circ$.

4.3 The addition of flow control vanes to the ejector system can substantially improve ground effect performance. The use of vanes reduces the maximum loss of augmentation in ground effect to 8% of out of ground effect performance.

4.4 While bellmouth lip separation is undesirable, the magnitude of the loss was not of significant magnitude when referred to total performance.

5. REFERENCES

1. Spiegelberg, C. H.: "Summary Report - Phase I Program Annular Nozzle Ejector" - Contract Nonr 2840(00), Hiller Aircraft Corp., Advanced Research Division Report No. 243, November 1959.
   Appendix:
   Ciolkosz, Z. M., Gates, M. F., and Cochran, C. L.: "Summary Report - Model Test Program - Annular Nozzle Ejector" - Contract Nonr 2840(00), Hiller Aircraft Corp., Advanced Research Division Report No. 242, September 1959. (Not Available Separately, but appended to this report for the reader's convenience).

2. Morrisson, Reaves, Jet Ejector and Augmentation, NACA Advanced Report, September 1942.

3. McClintock, F. and Hood, J. H.: "Aircraft Ejector Performance", Journal of Aeronautical Sciences, Vol. 13, No. 7, November 1946.

4. Bertin, J., and Le Nabour, M.: "Contribution Au Developpement Des Trompes et Ejecteurs", De La Societe Bertin and C[ie], Technique et Science Aeronautiques, Tome 3, 1959.

5. Weber, H. E.: "Ejector-Nozzle Flow and Thrust" ASME paper Number 59-Hyd-5.

6. Sargent, E. R., "Theoretical Performance of a Static Thrust Augmenter", Curtiss Wright Corporation, Airplane Division, Report No. R-150, dated 1944.
   Sargent, E. R.,"Theoretical Performance of a Dynamic Thrust Augmenter", Curtiss Wright Corporation, Airplane Division, Report No. R-158, dated December 1944.

7. Sutton, J. F. et al: "Steady Flow Ejector Research Program", Lockheed Aircraft Corporation, Georgia Division, Report No. E.R.-4708, dated December 1960.

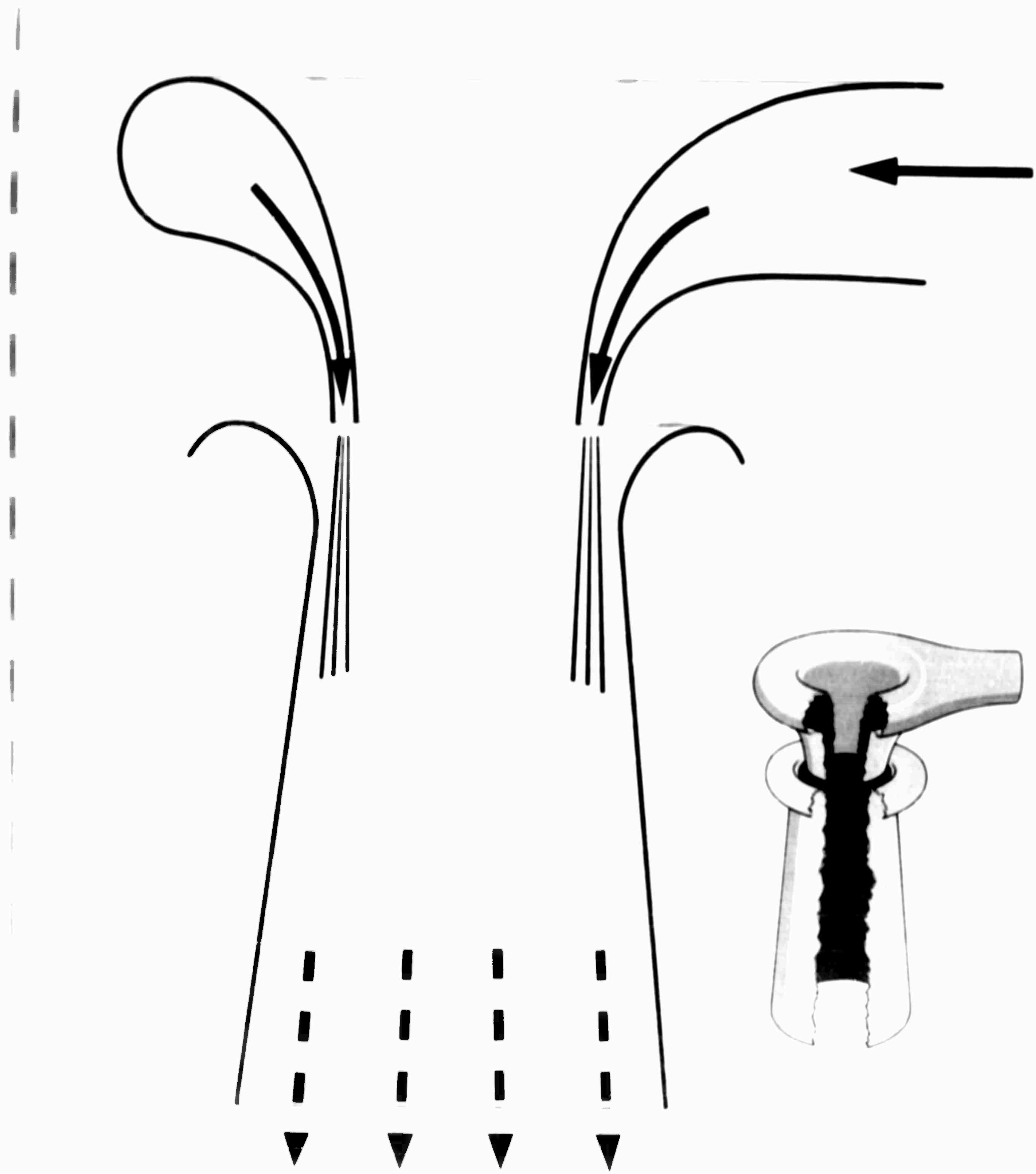

FIGURE 1

BASIC ANNULAR EJECTOR

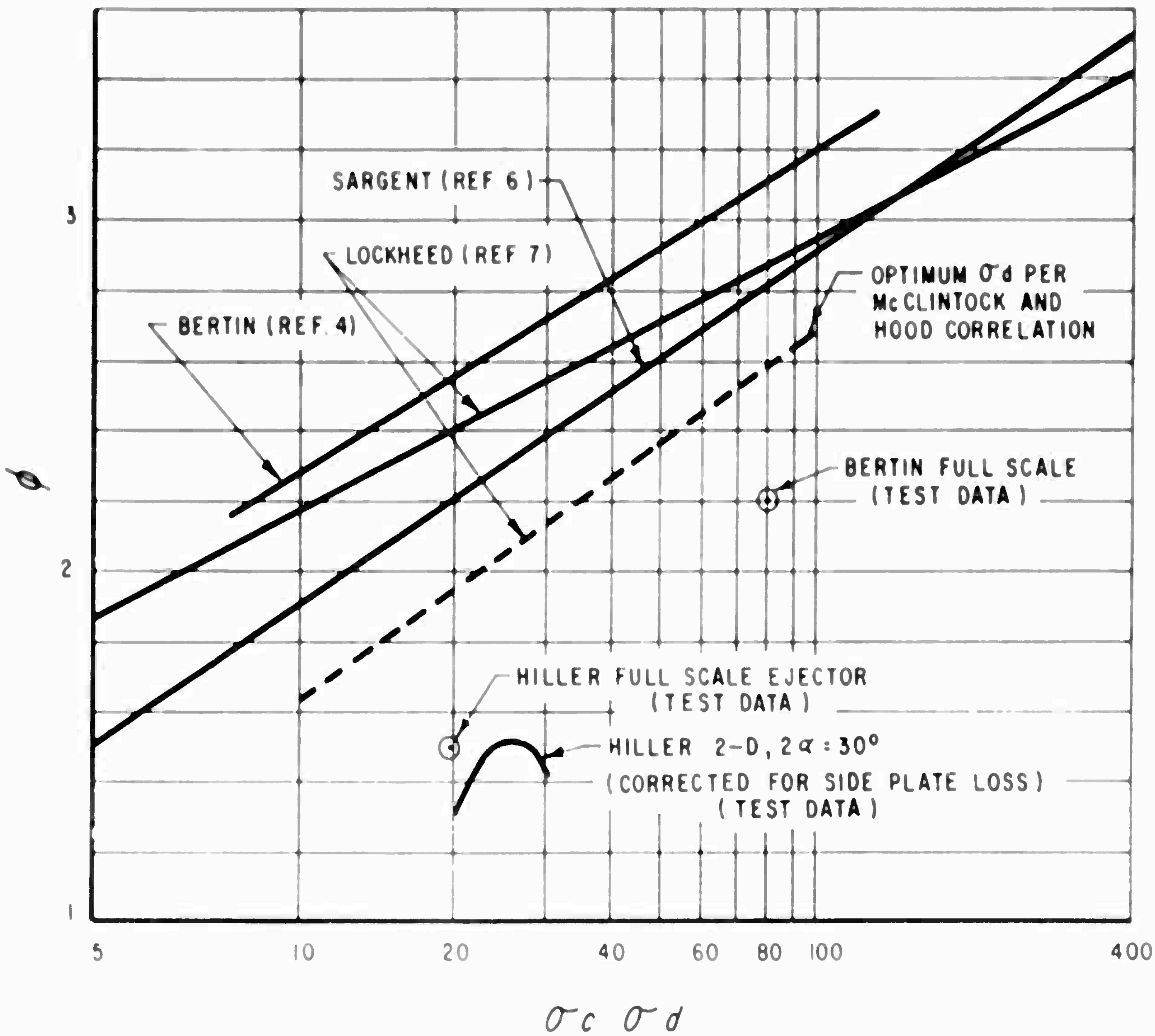

FIGURE 7: THEORETICAL [illegible] PERFORMANCE, $\sigma_1 = 2$

FIGURE 3: 2-D ANNULAR EJECTOR MODEL ($2\alpha = 30^{\circ}$, $2\beta = 15^{\circ}$, $\sigma_c = 22.5$)

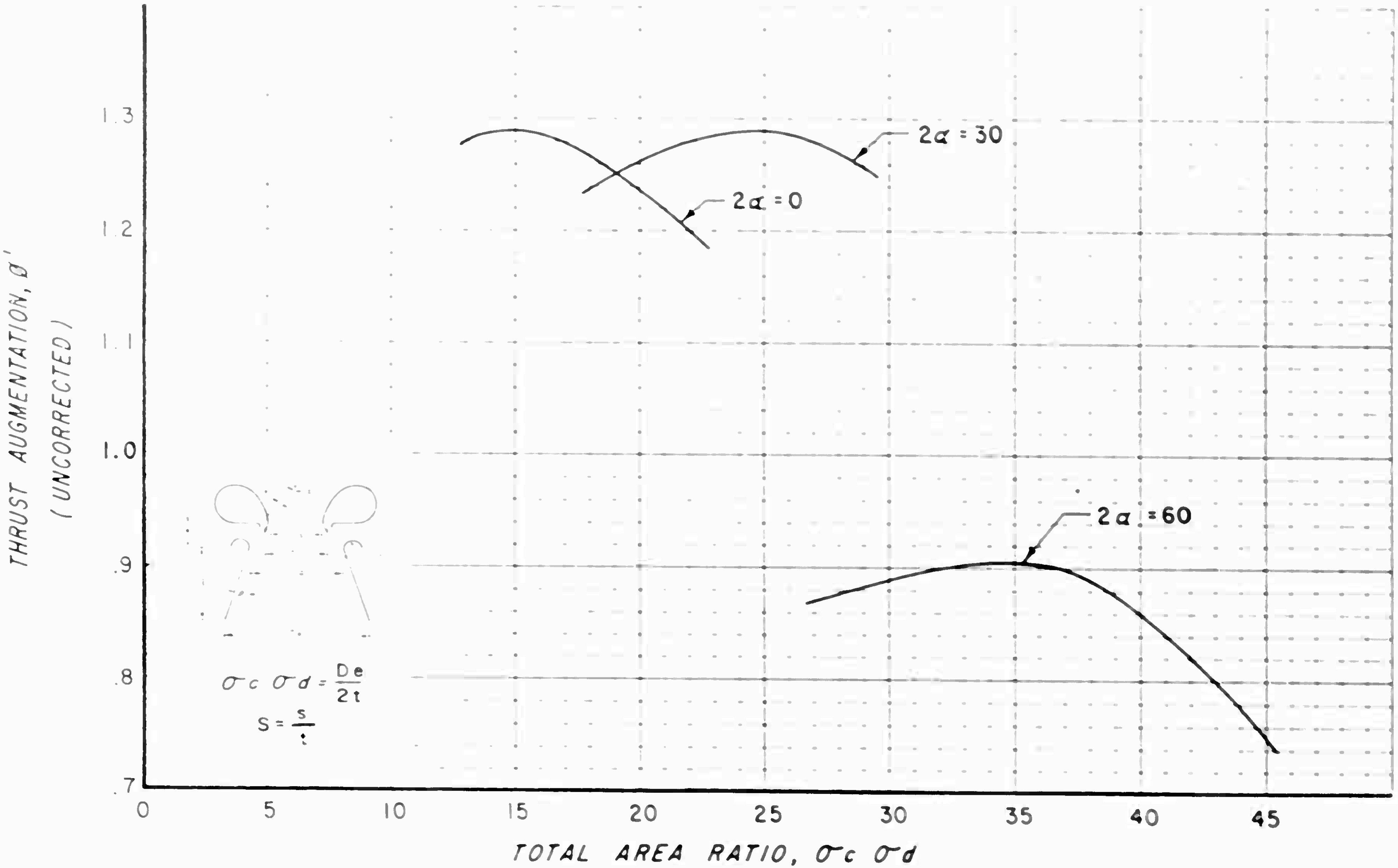

FIGURE 4t. 2-D ANNULAR EJECTOR PERFORMANCE SUMMARY AS A FUNCTION OF TOTAL AREA RATIO (UNCORRECTED FOR SIDE PLATE LOSS)

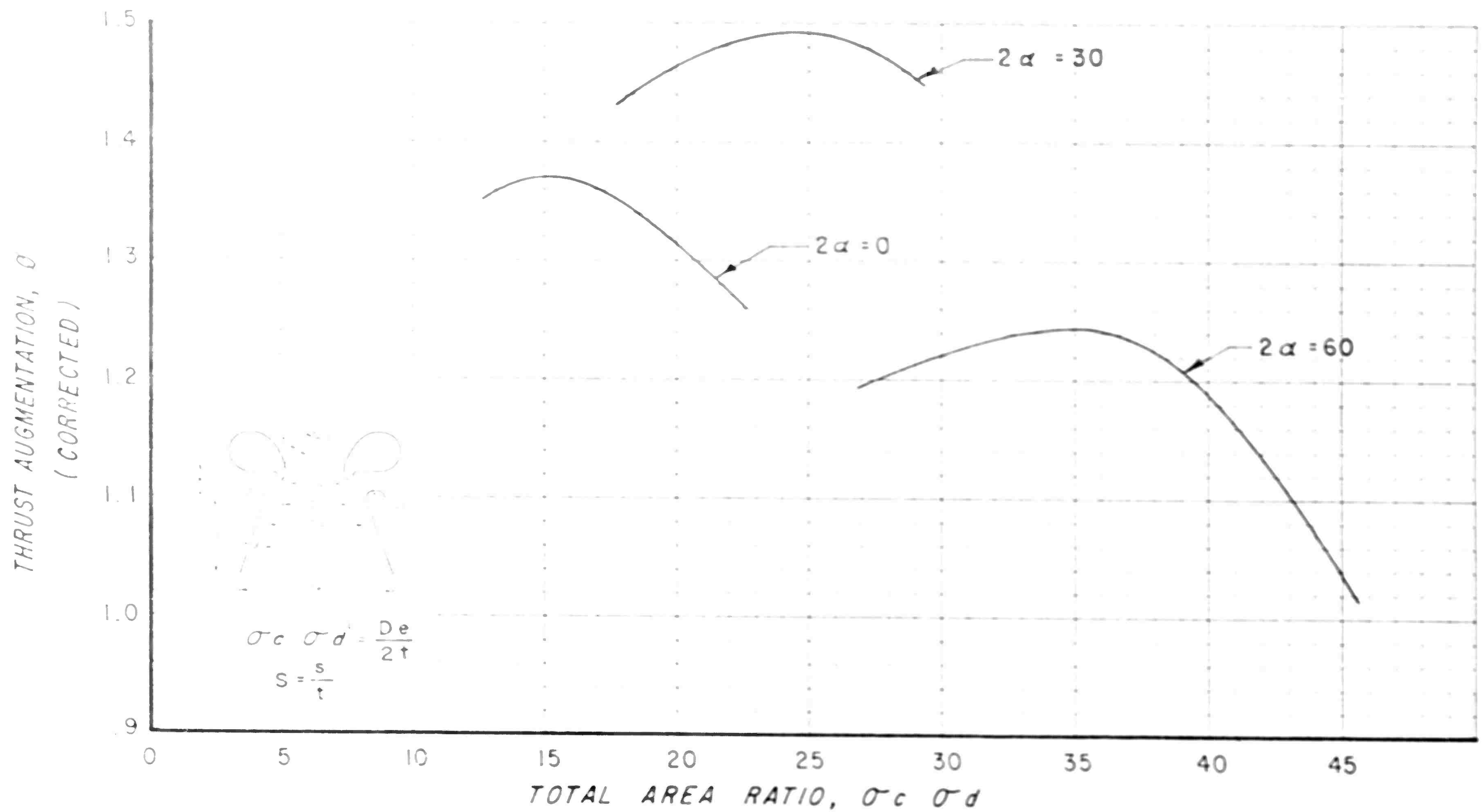

FIGURE 5. 2-D ANNULAR EJECTOR PERFORMANCE SUMMARY AS A FUNCTION OF TOTAL AREA RATIO (CORRECTED FOR SIDE PLATE LOSS)

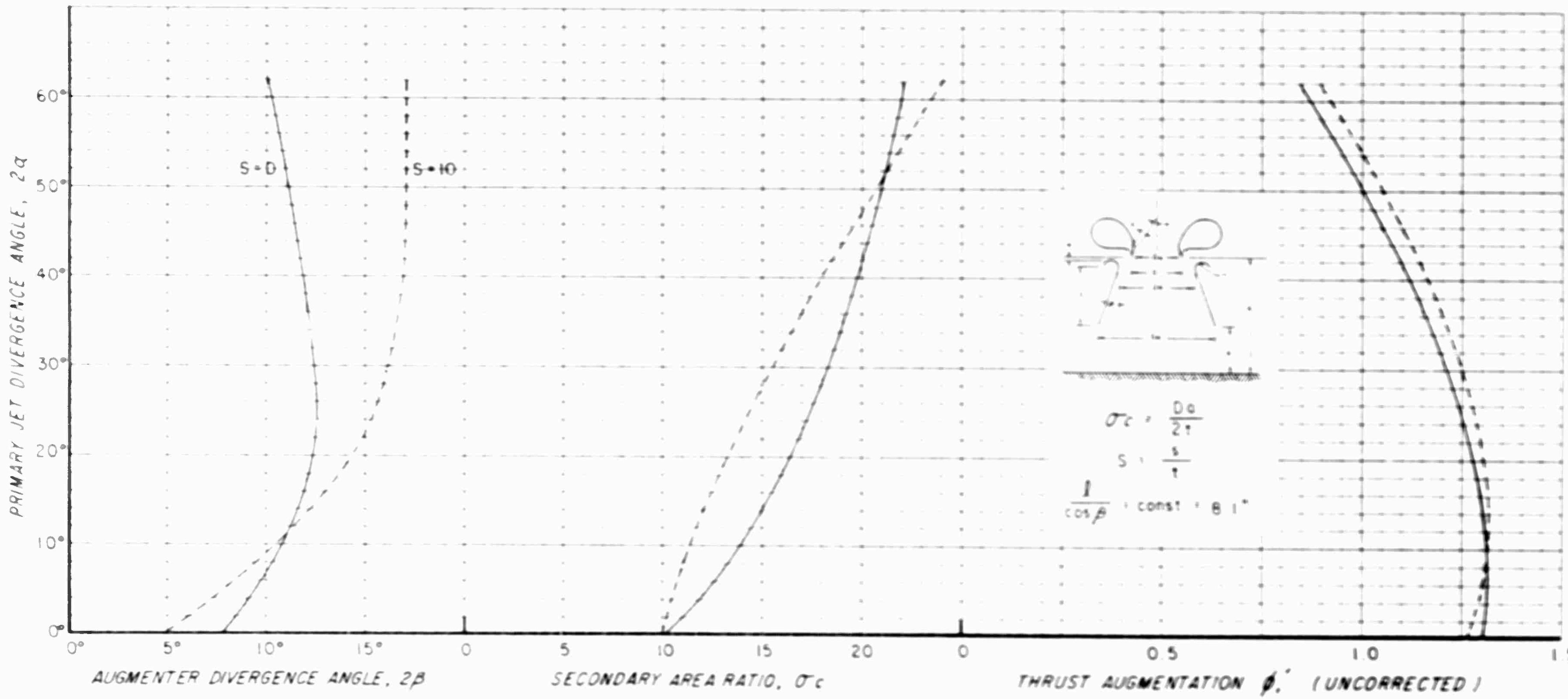

FIGURE 6: OPTIMUM 2-D AUGMENTER PARAMETERS AS A FUNCTION OF 2α (AUGMENTER WALL LENGTH CONST.)

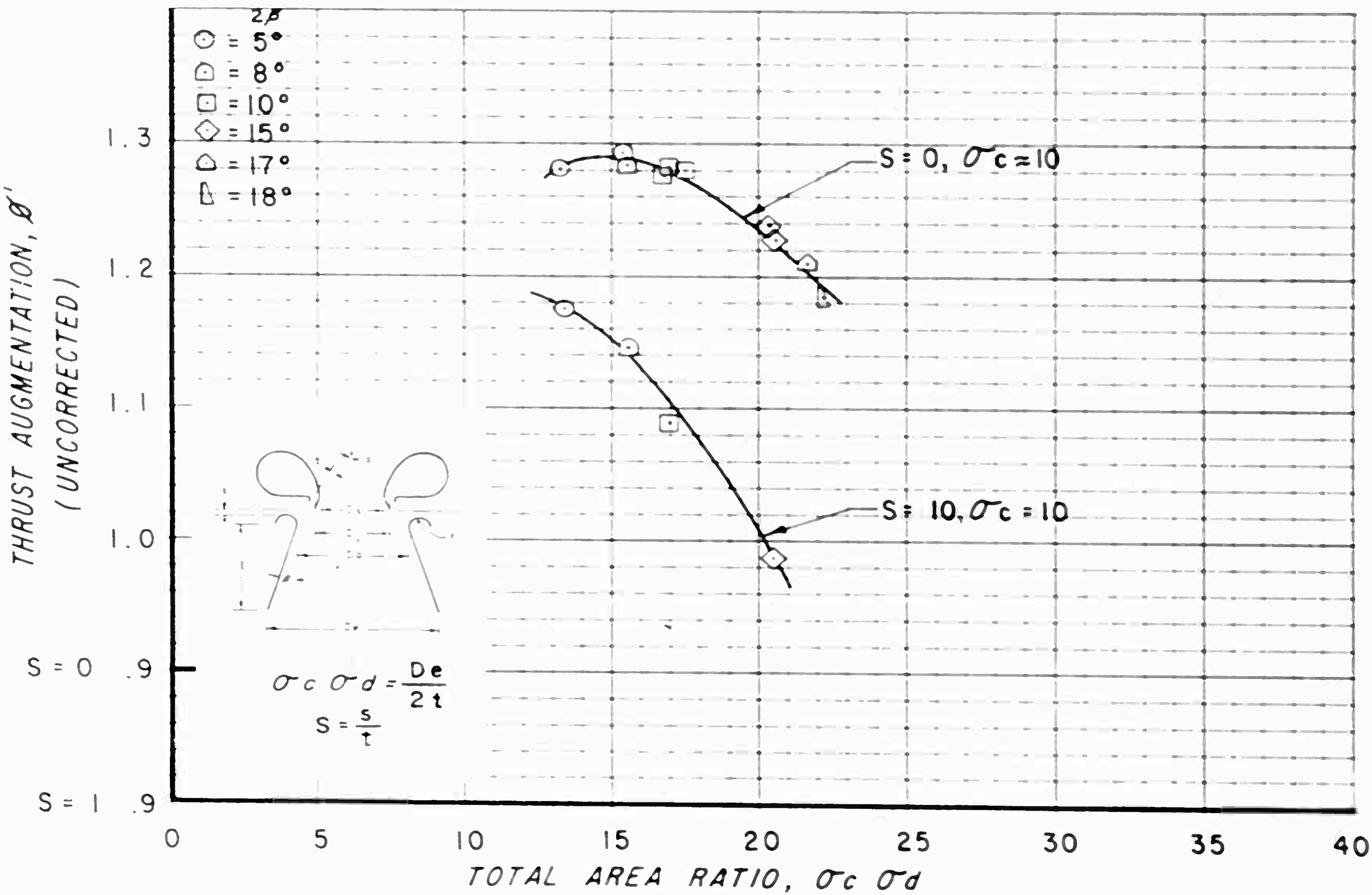

FIGURE 7: 2-D PERFORMANCE AS A FUNCTION OF TOTAL AREA RATIO, 2α = 0° (UNCORRECTED FOR SIDE PLATE LOSS)

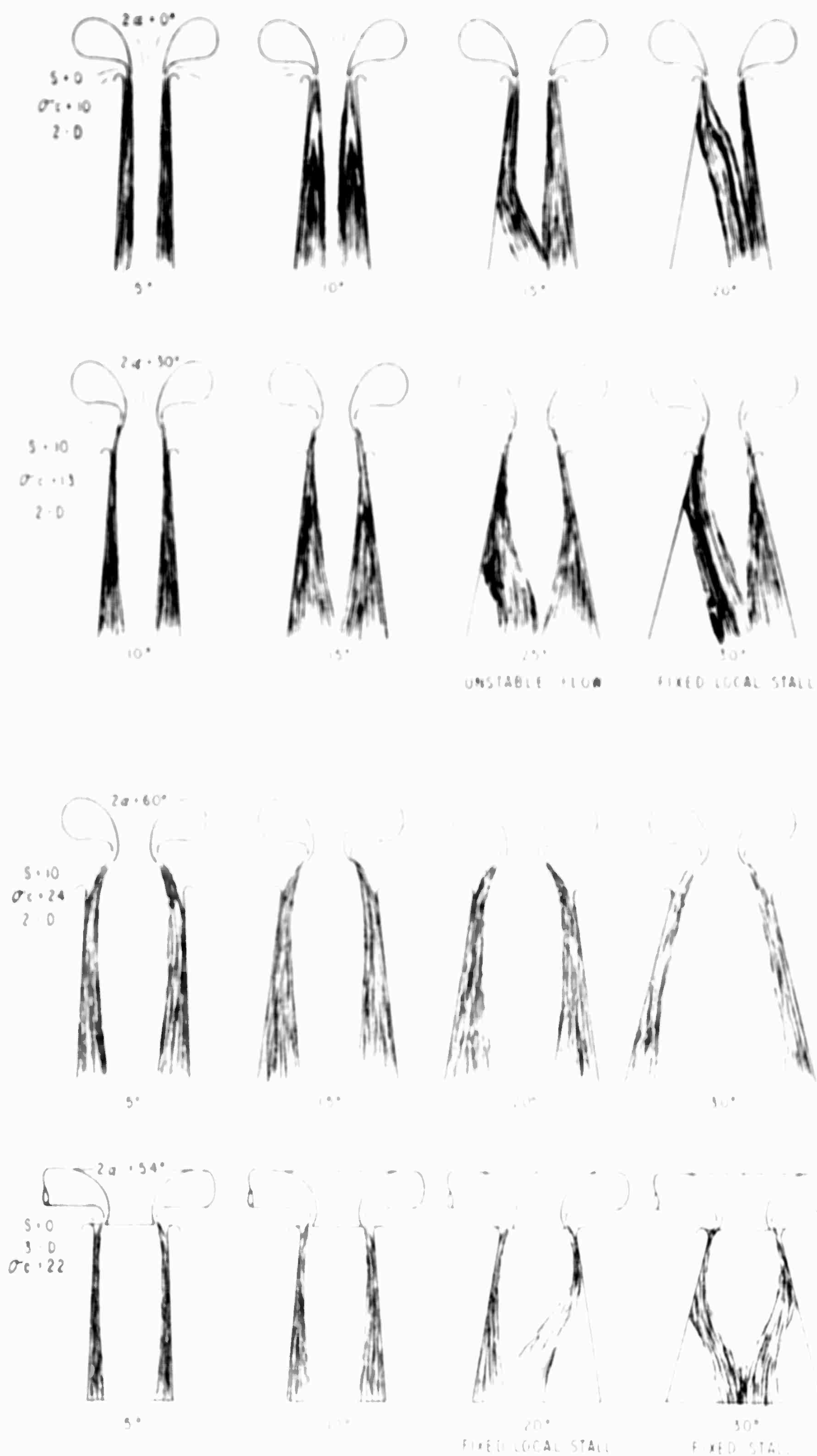

FIGURE 8: FLOW REGIMES OBSERVED IN 2-D & 3-D ANNULAR EJECTOR MODELS

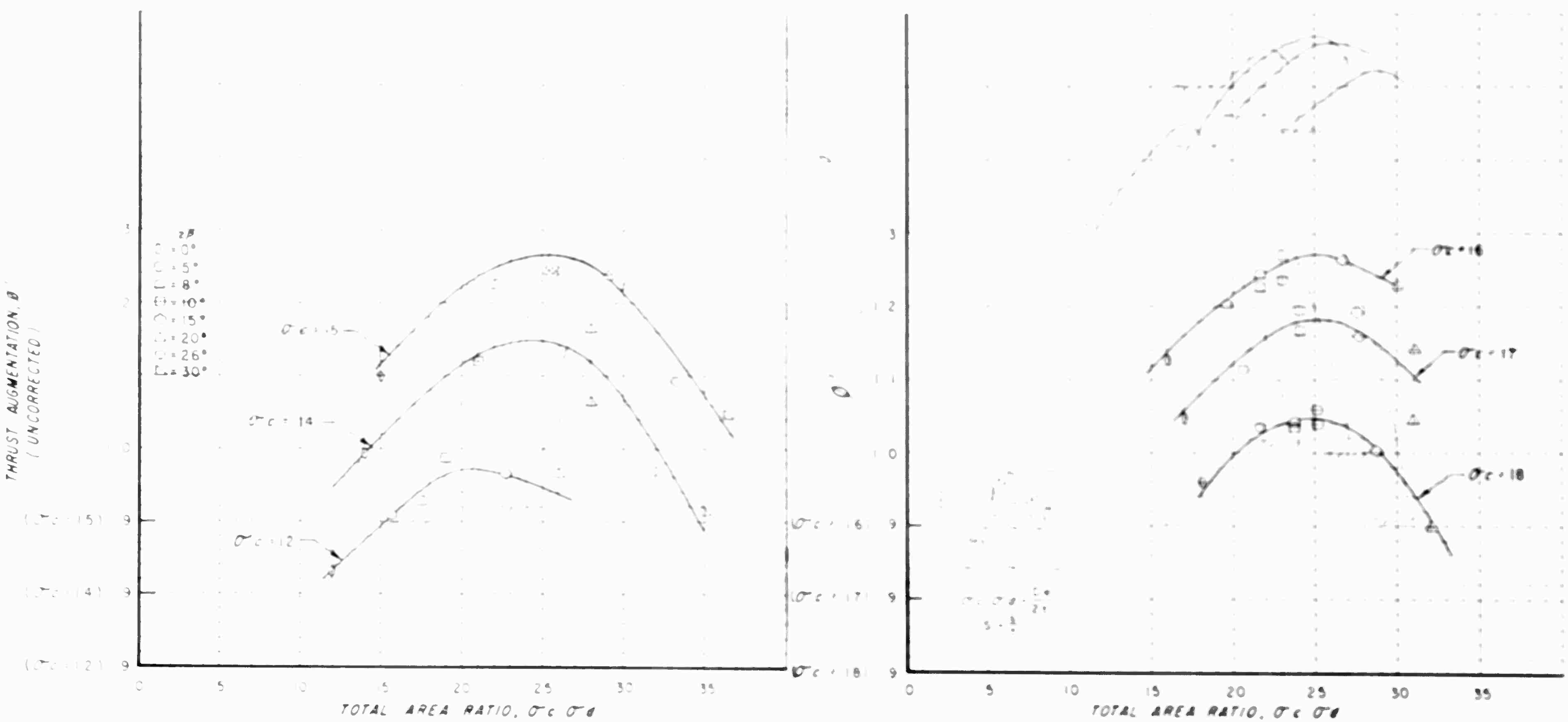

FIGURE 9: 2-D PERFORMANCE AS A FUNCTION OF TOTAL AREA RATIO, $2\alpha = 30^{\circ}$, S = 0 (UNCORRECTED FOR SIDE PLATE LOSS)

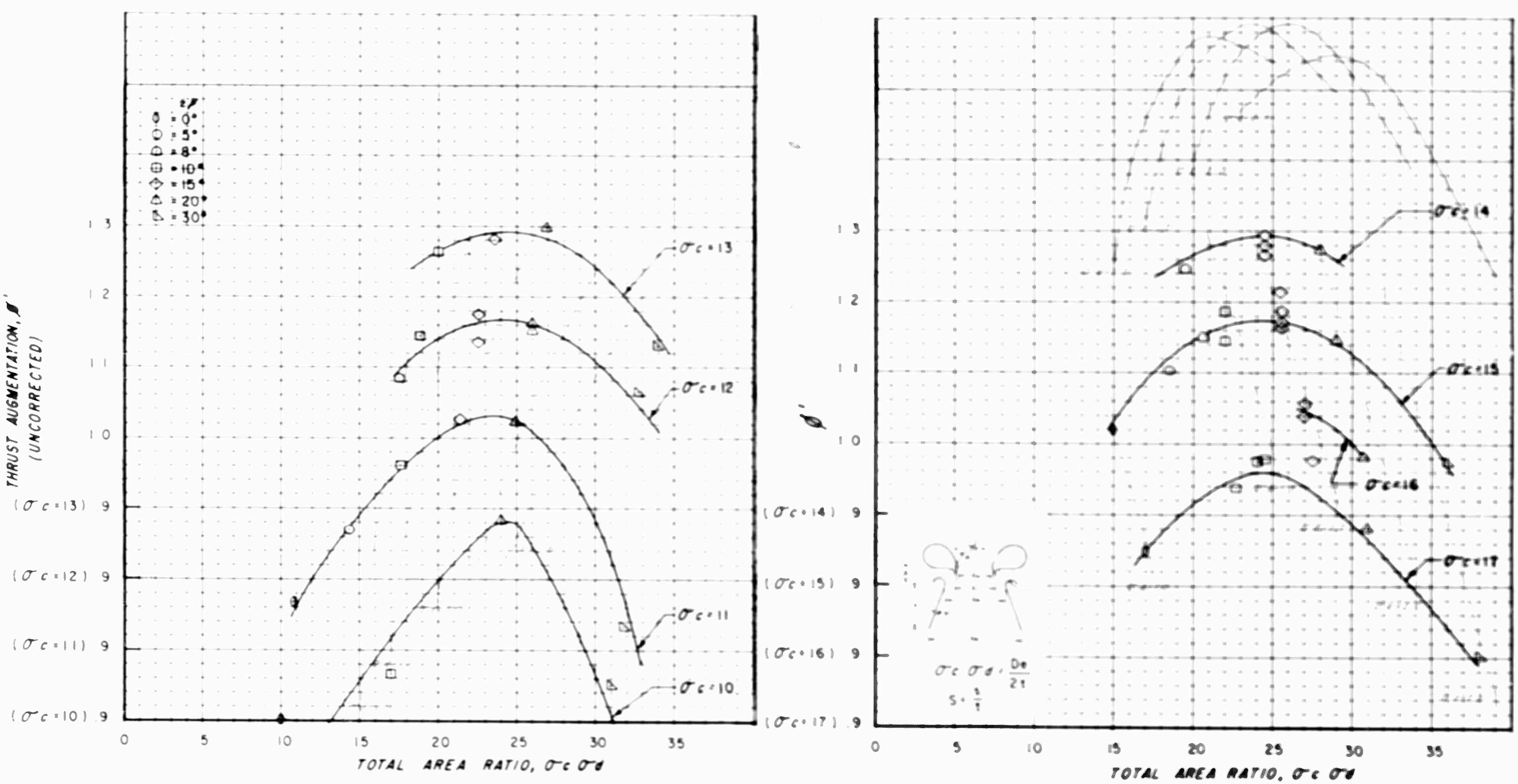

FIGURE 10. 2-D PERFORMANCE AS A FUNCTION OF TOTAL AREA RATIO $2\alpha = 30^{\circ}$, S = 10 (UNCORRECTED FOR SIDE PLATE LOSS)

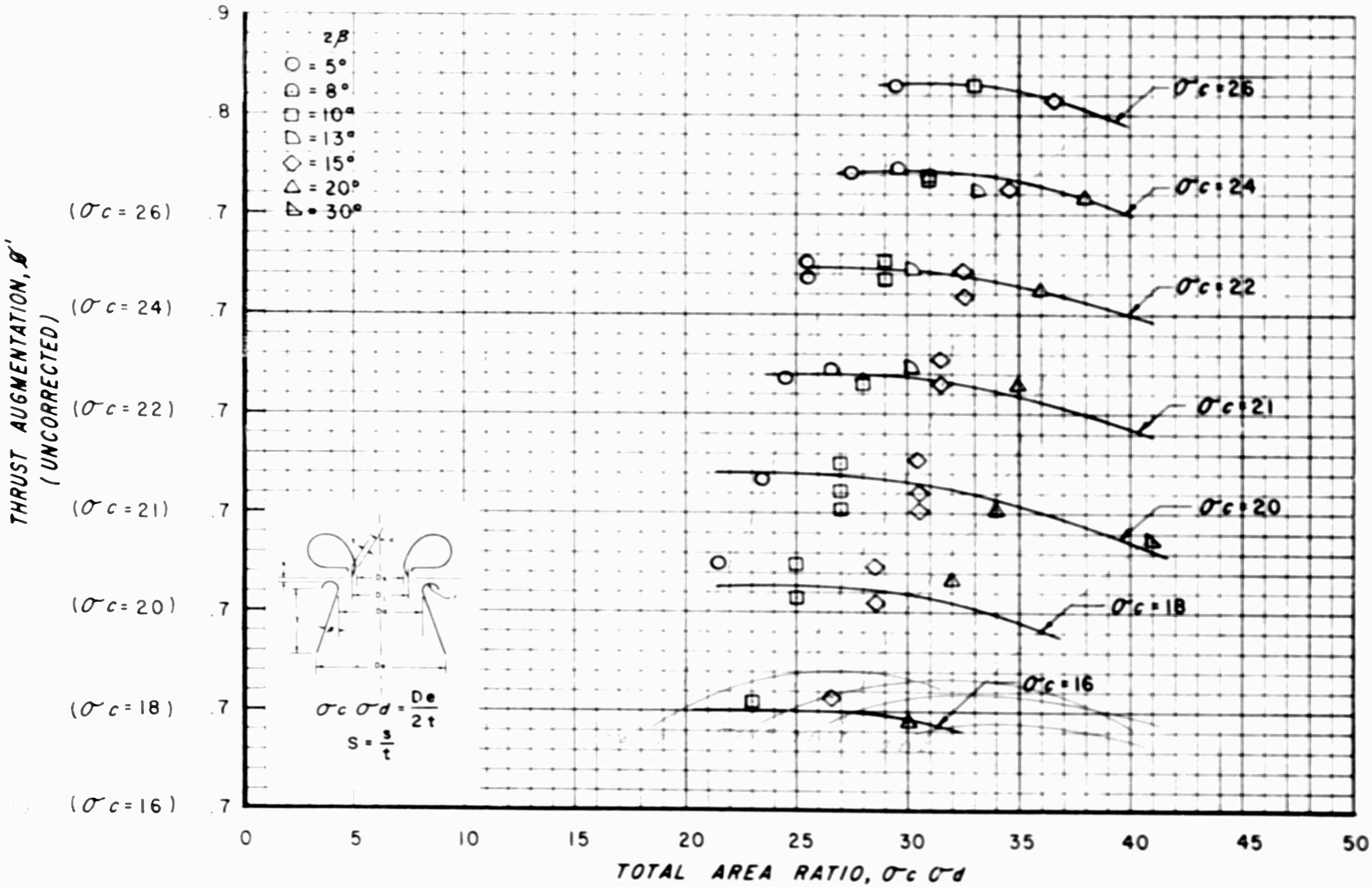

FIGURE [illegible] PERFORMANCE AS A FUNCTION OF TOTAL AREA RATIO, [illegible] (UNCORRECTED FOR SIDE PLATE LOSS)

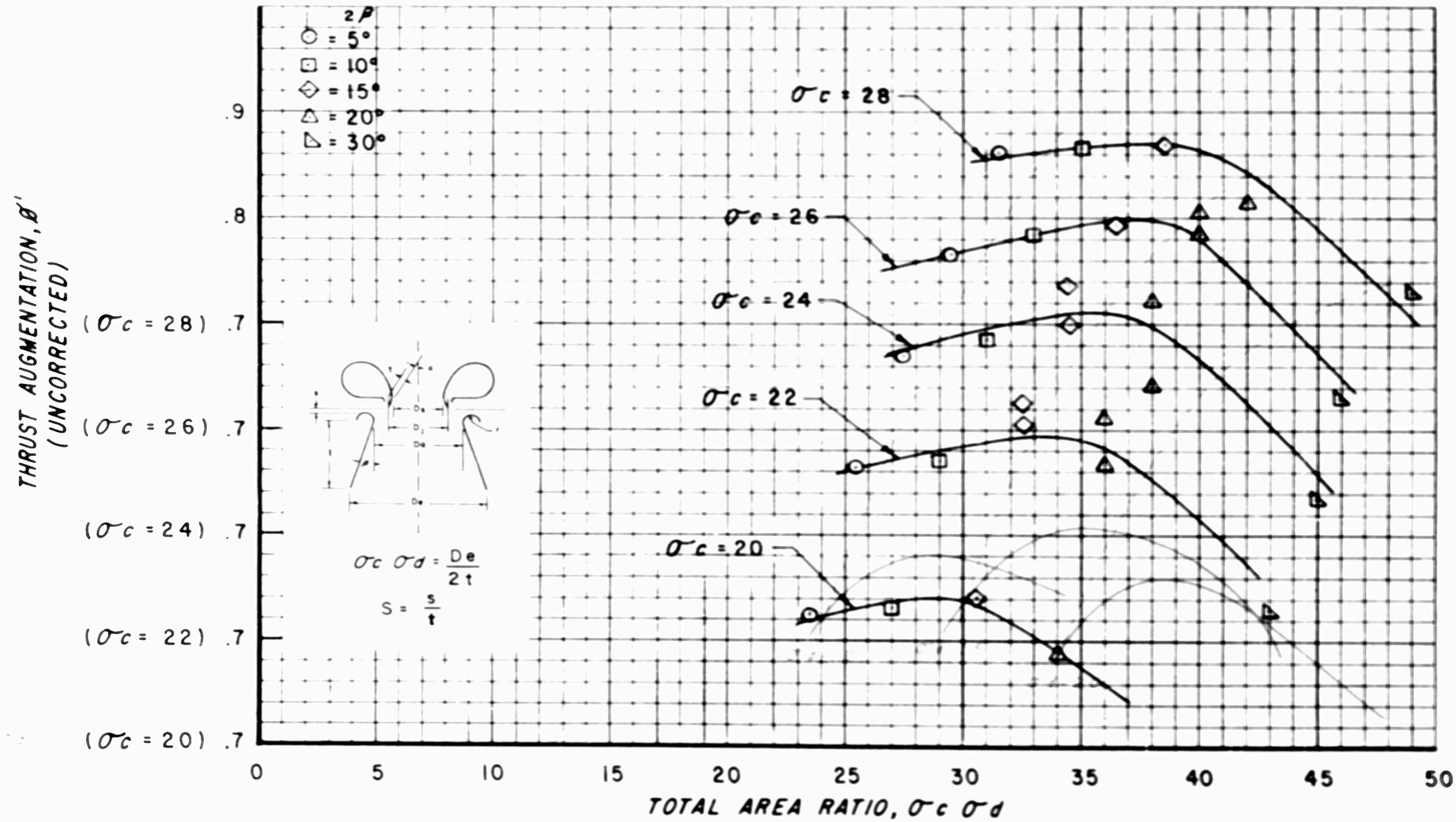

FIGURE 12 2-D PERFORMANCE AS A FUNCTION OF TOTAL AREA RATIO, $2\alpha = 60°$, $S = 10$ (UNCORRECTED FOR SIDE PLATE LOSS)

Configuration	2D	2D	2D	3D
Nominal 2α, degrees	0	30	60	60
Actual 2α, degrees	0	22	$\approx$ 61	54
Nozzle efficiency, %	98	96	95	--
Jet aspect ratio	30	30	30	100
$\sigma_b = \frac{D_s}{2t}$	7.65	7.65	7.65	7.65
Jet thickness, in.	.1	.1	.1	$\approx$ .076

FIGURE 13: MODEL PRIMARY NOZZLE CHARACTERISTICS

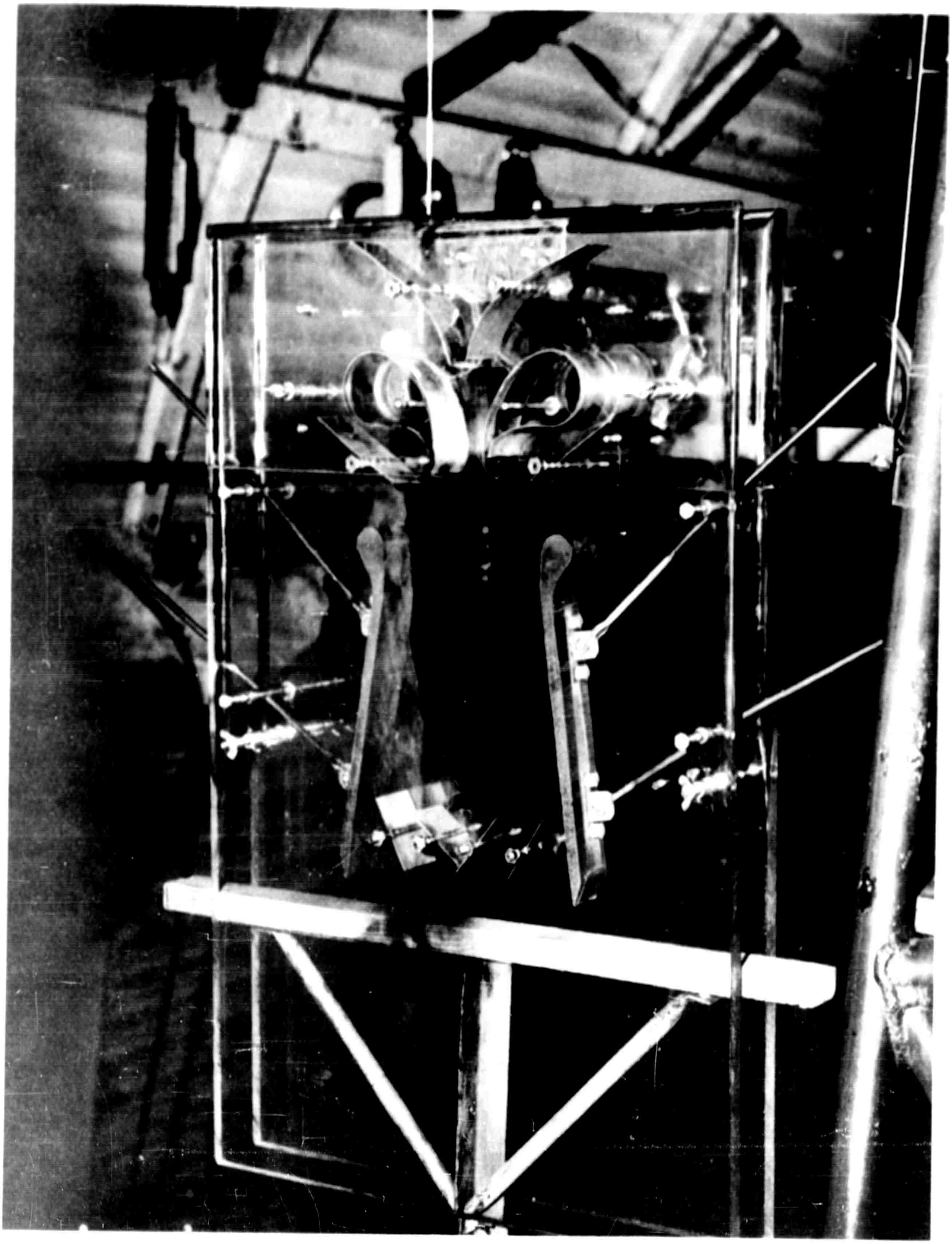

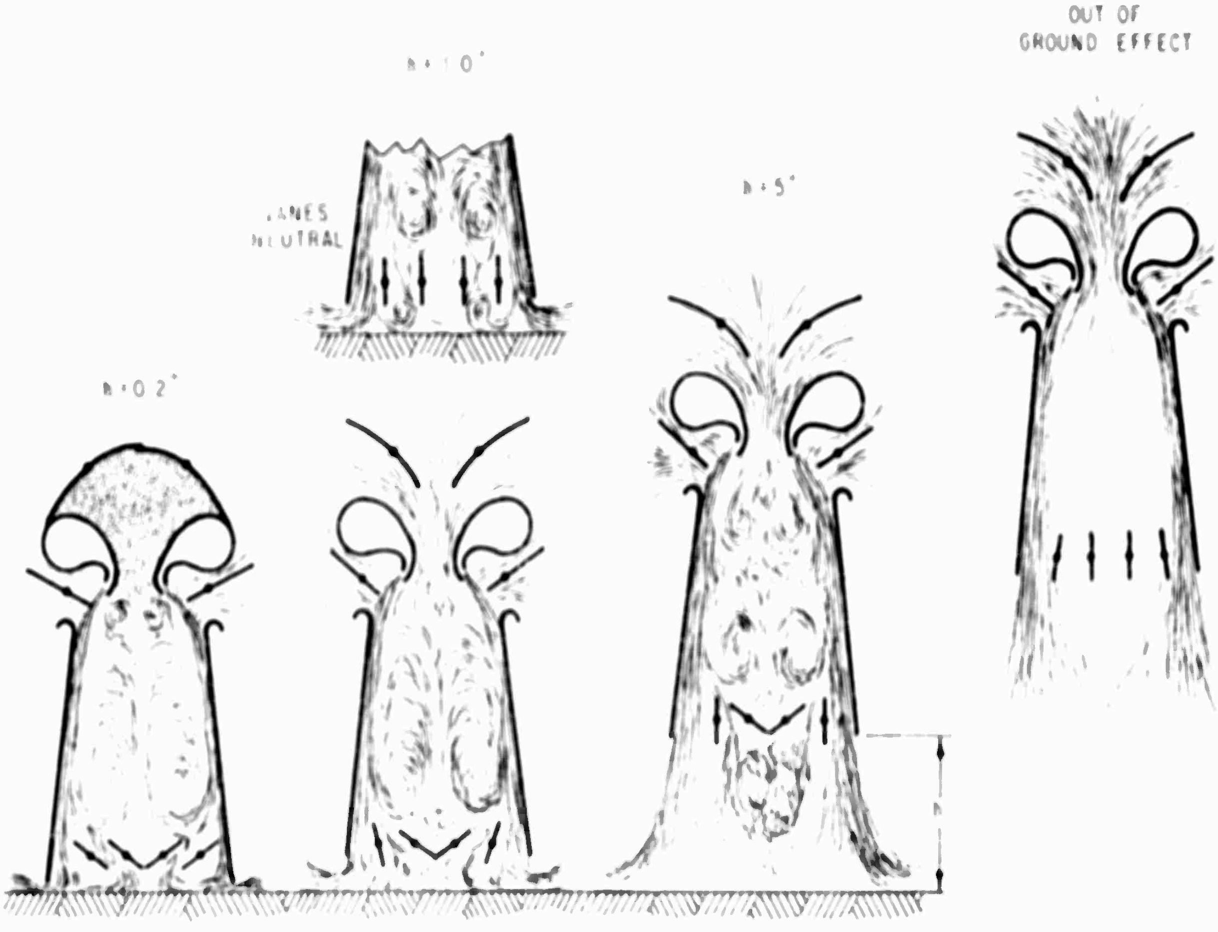

OBSERVED FLOW REGIMES

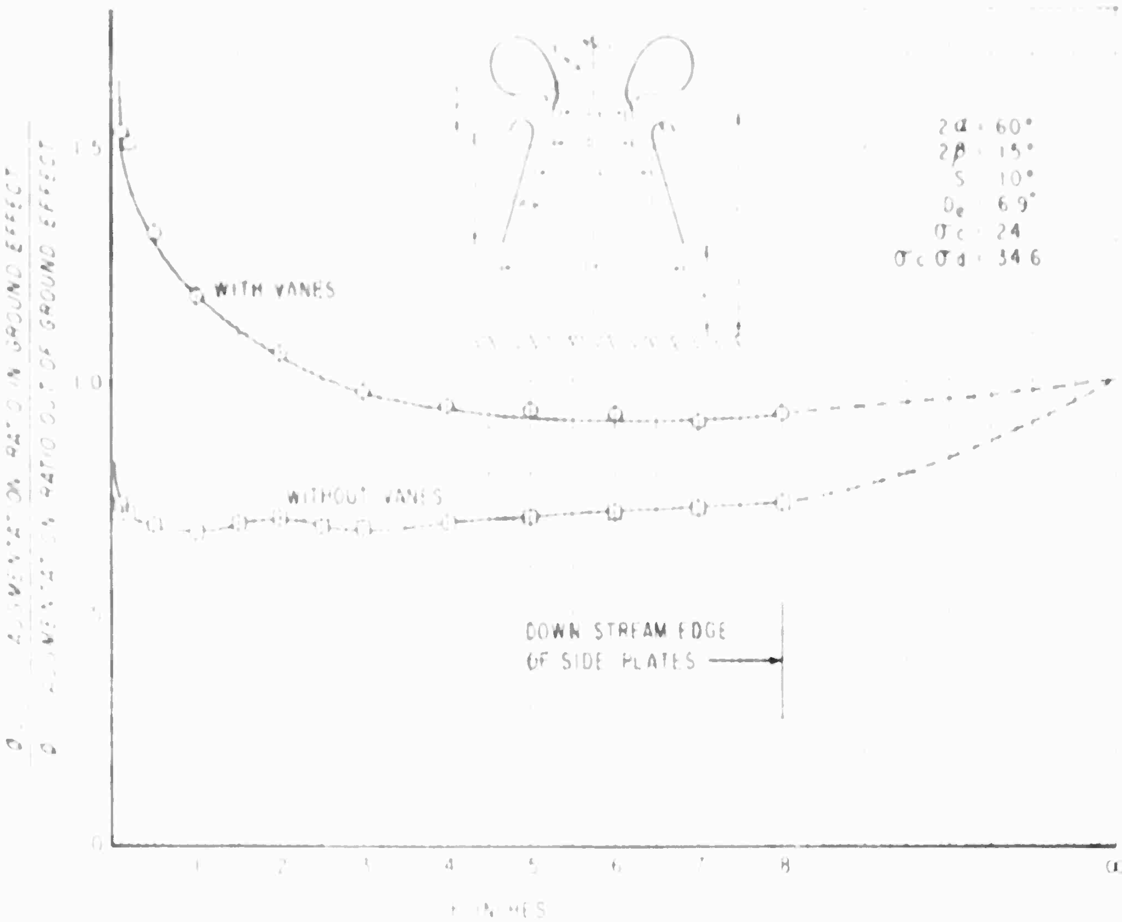

FIGURE [illegible] IN GR[illegible]UN[illegible] EFFECT, VANED AND UNVANED

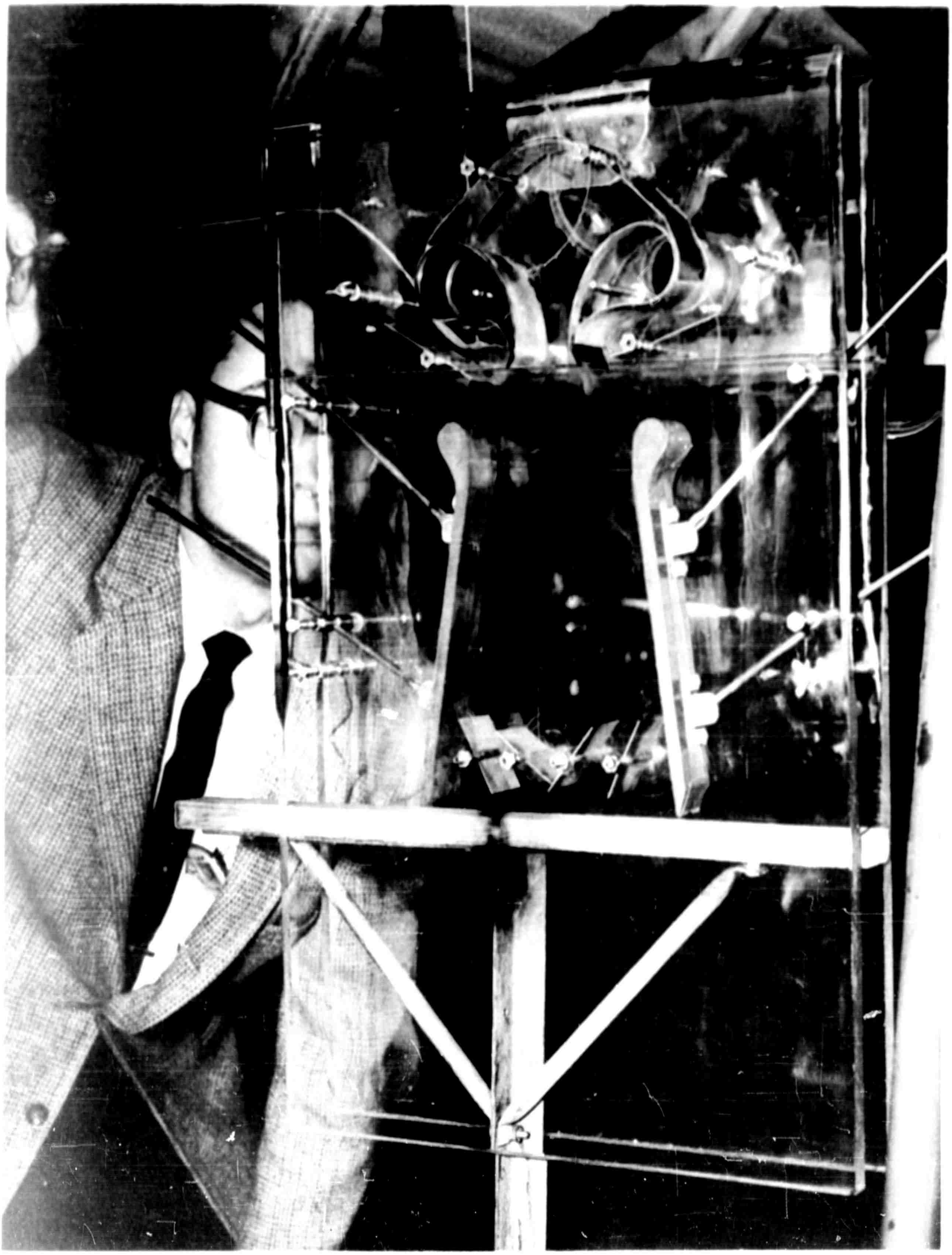

[illegible]: [illegible] -D VANED MODEL IN-GROUND-EFFECT ([illegible] WITH VANES CLOSED).

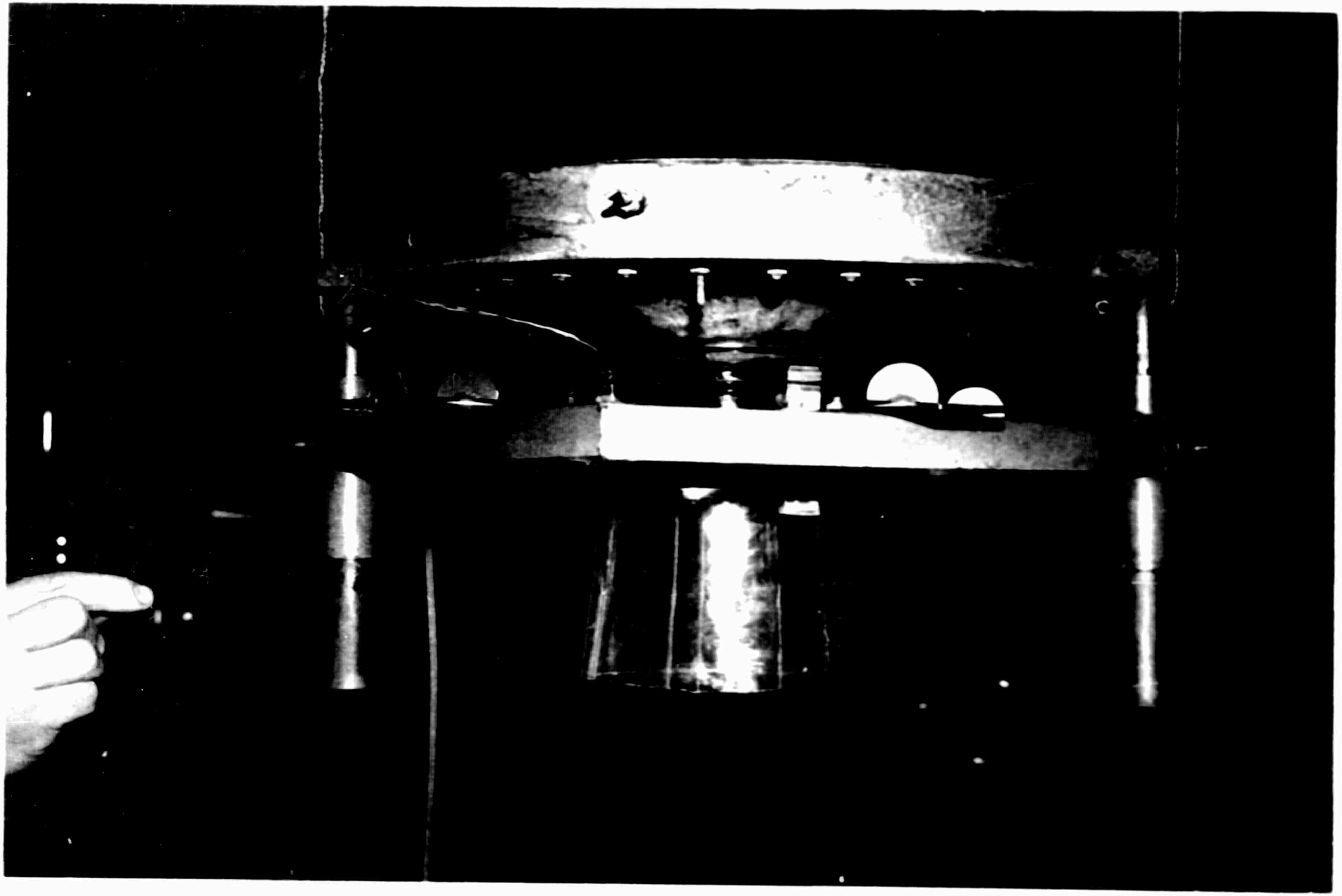

FIGURE 17: 3-D MODEL WITH $2\beta = 10^{\circ}$, $\sigma_c = 23$ AUGMENTER IN PLACE NOTE TUFT IN SECONDARY FLOW

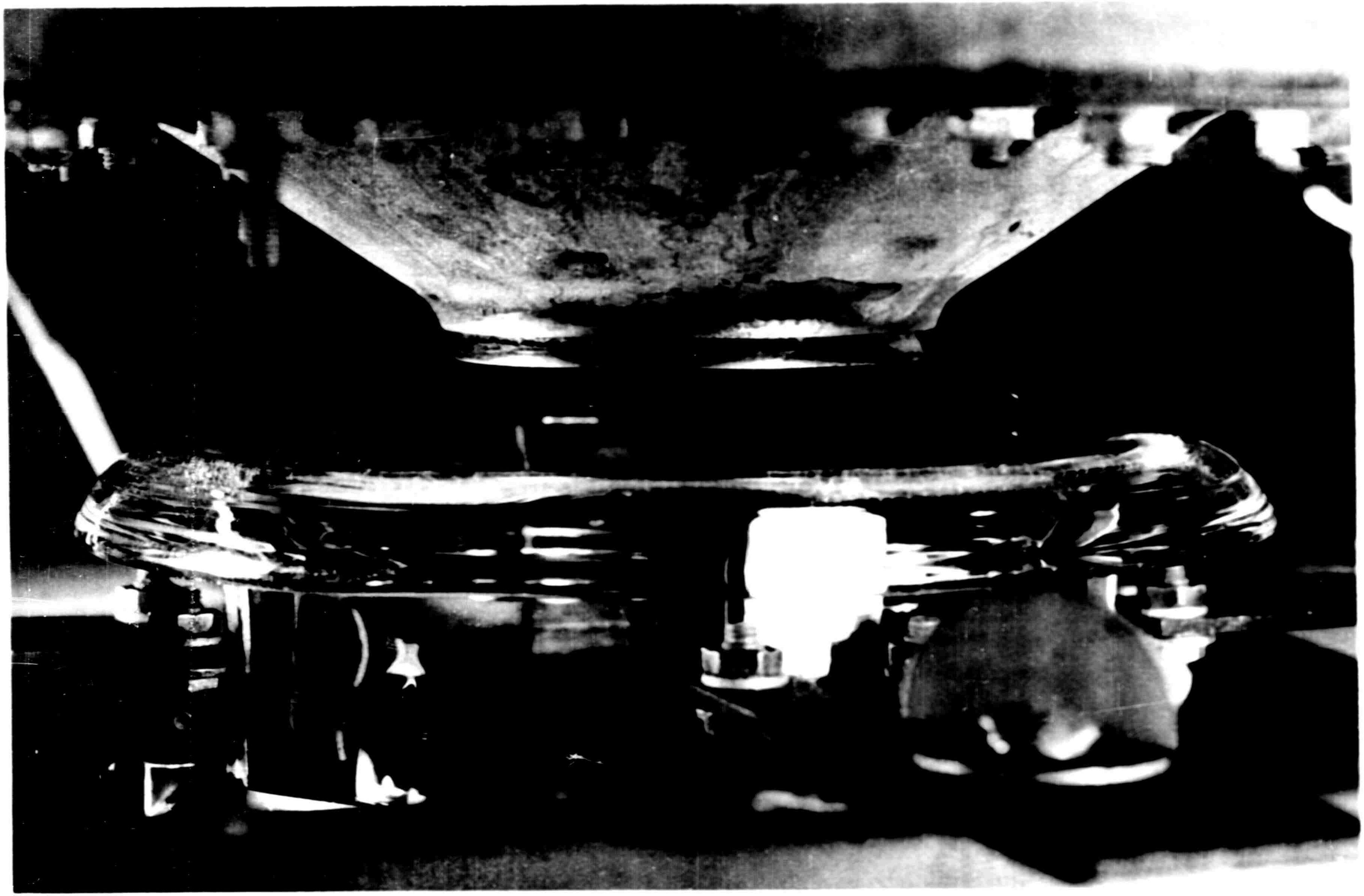

FIGURE 18: 3-D PRIMARY NOZZLE DETAILS ($2\alpha = 54^{\circ}$).

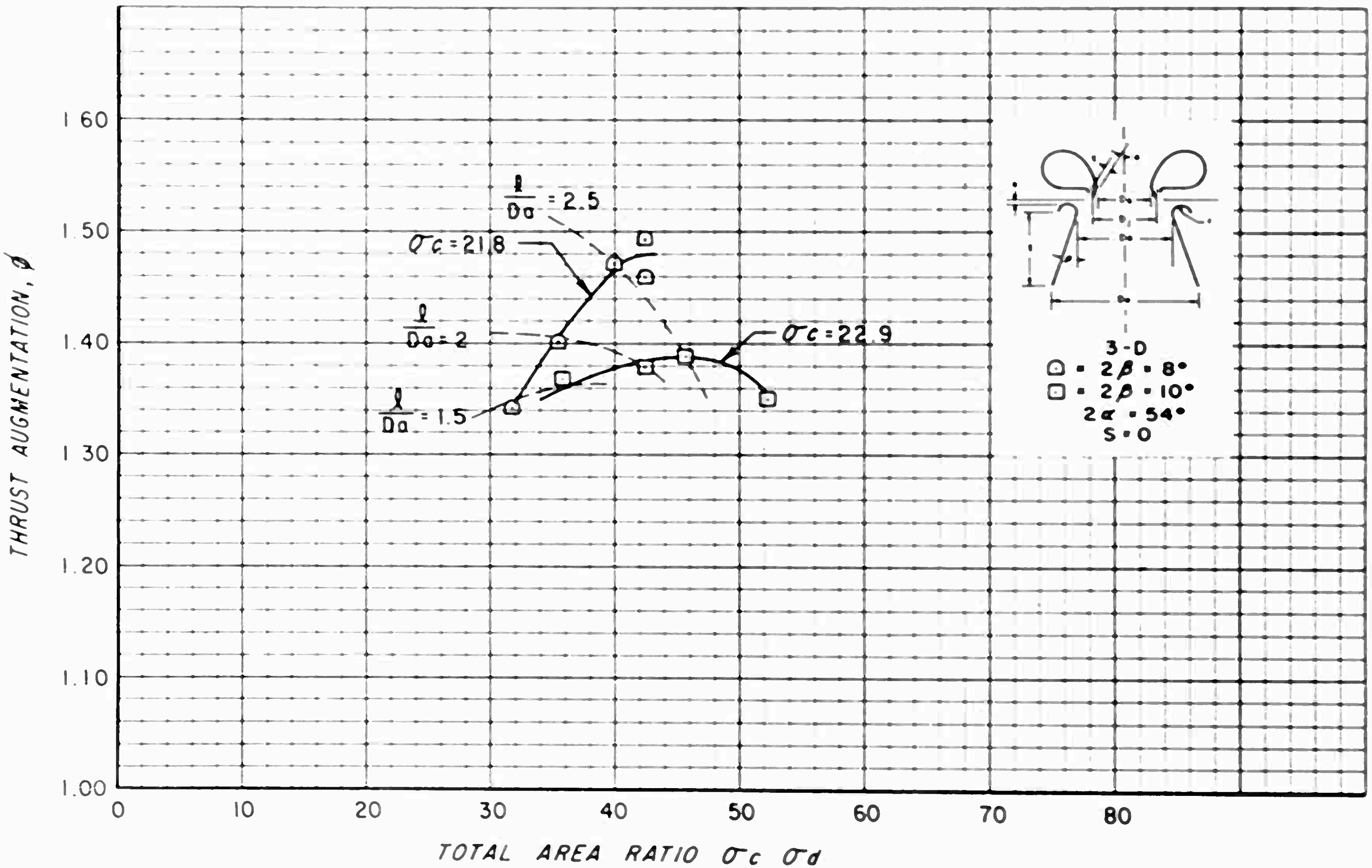

FIGURE 19: THRUST AUGMENTATION AS A FUNCTION OF TOTAL AREA RATIO (2α = 54°)

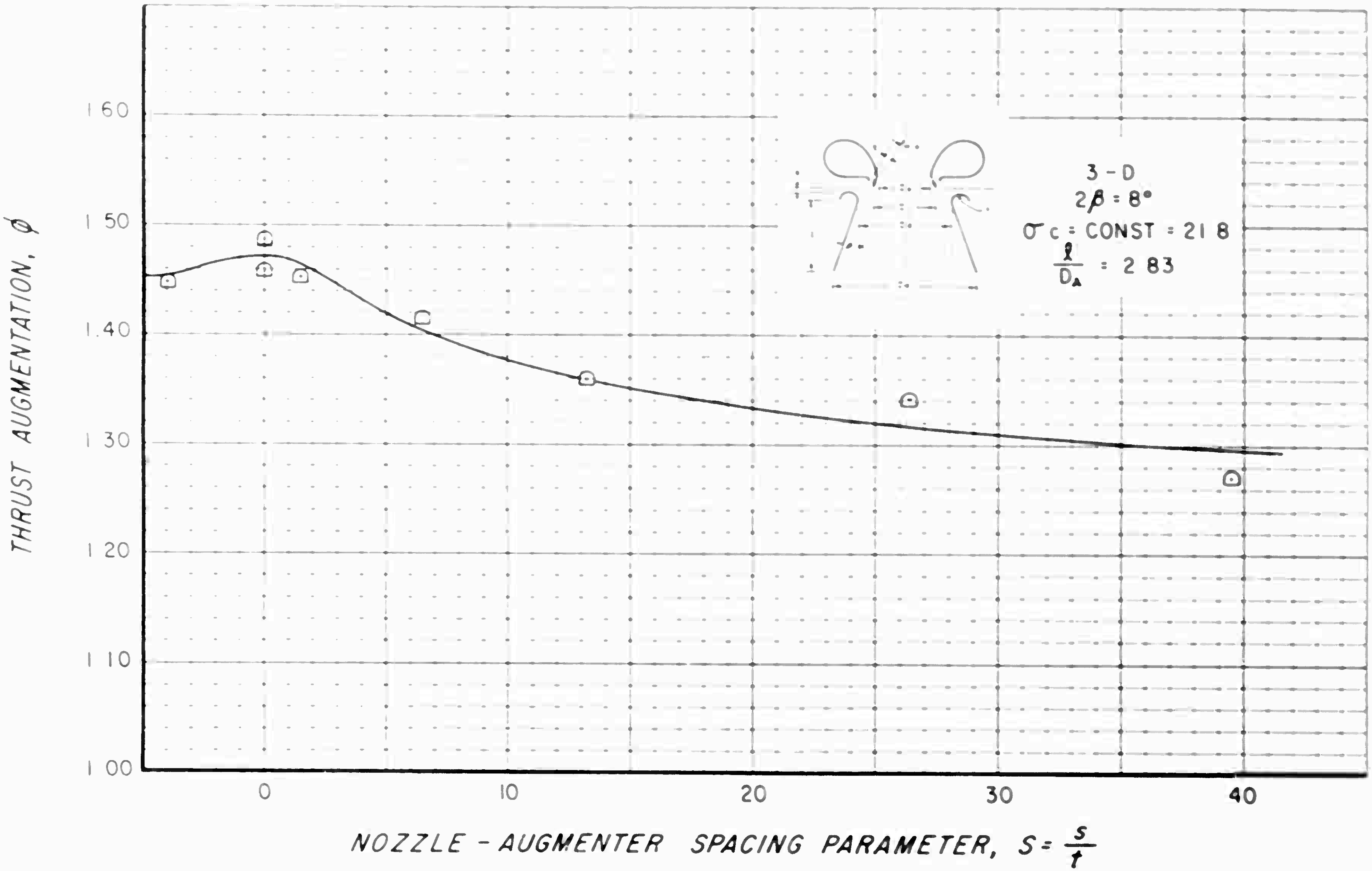

FIGURE 20. THRUST AUGMENTATION AS A FUNCTION OF NOZZLE AUGMENTER SPACING PARAMETER

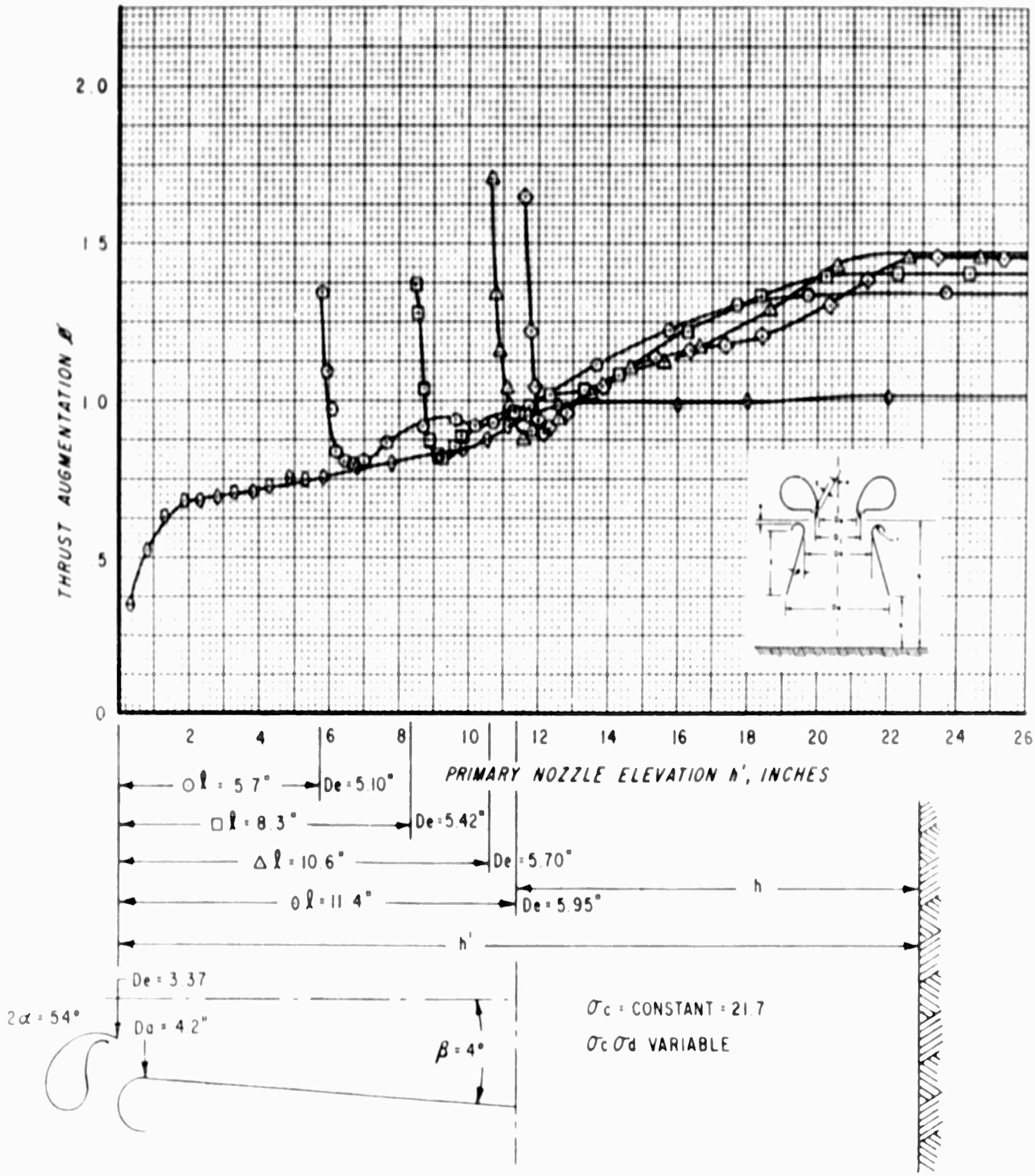

FIGURE 21: THRUST AUGMENTATION IN GROUND EFFECT AS A FUNCTION OF PRIMARY NOZZLE ELEVATION, 2β = 8°, 3-D

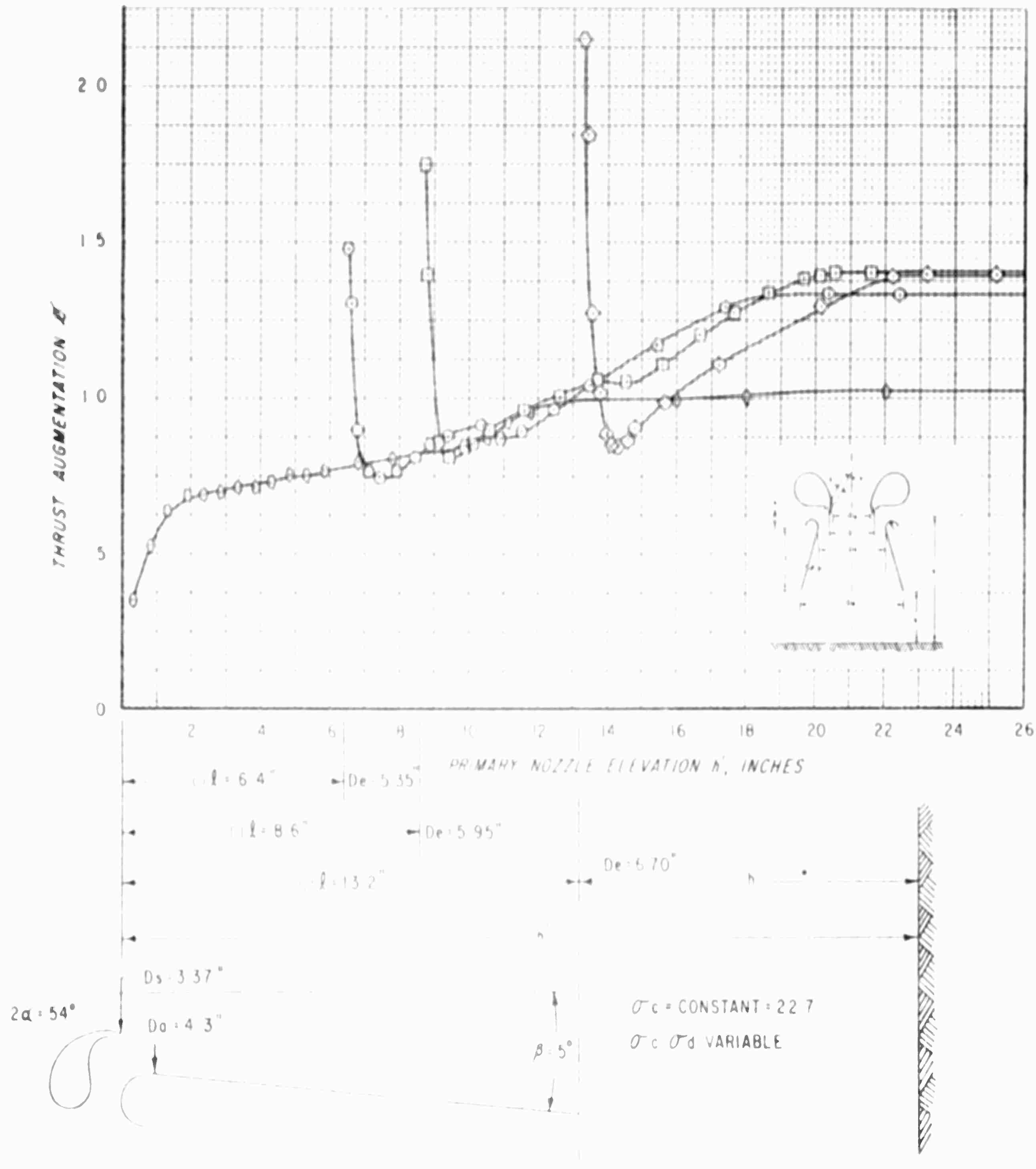
THRUST AUGMENTATION
2 0
1 5
1 0
5
0
2
4
6
8
10
12
14
16
18
20
22
24
26
PRIMARY NOZZLE ELEVATION h, INCHES
De 5 35"
De 5 95"
De 6 70"
Ds 3 37"
2α = 54°
Da 4 3"
β 5°
σc = CONSTANT = 22 7
σc σd VARIABLE

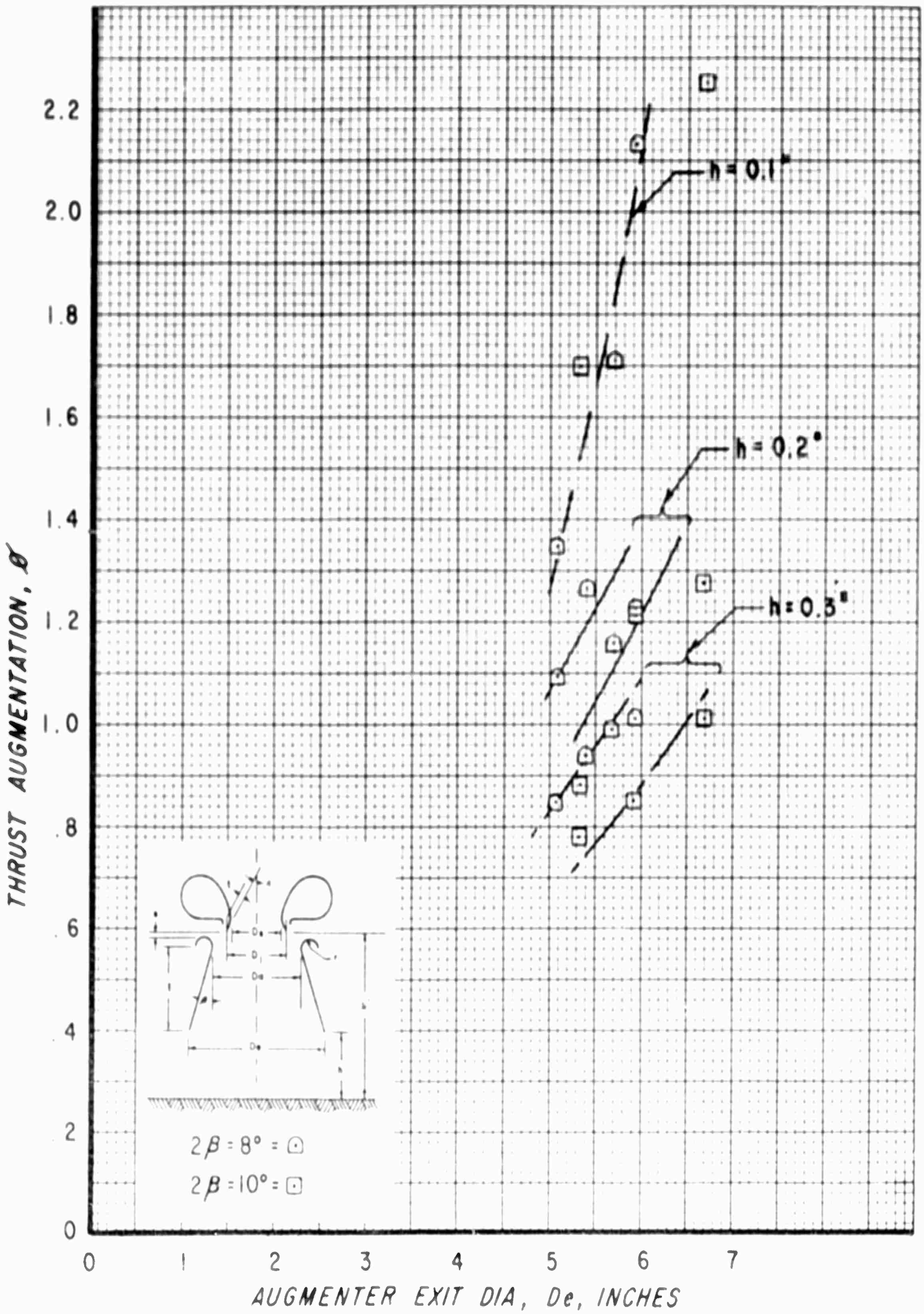

FIGURE   THRUST AUGMENTATION IN GROUND EFFECT AS A FUNCTION OF AUGMENTER EXIT DIAMETER.

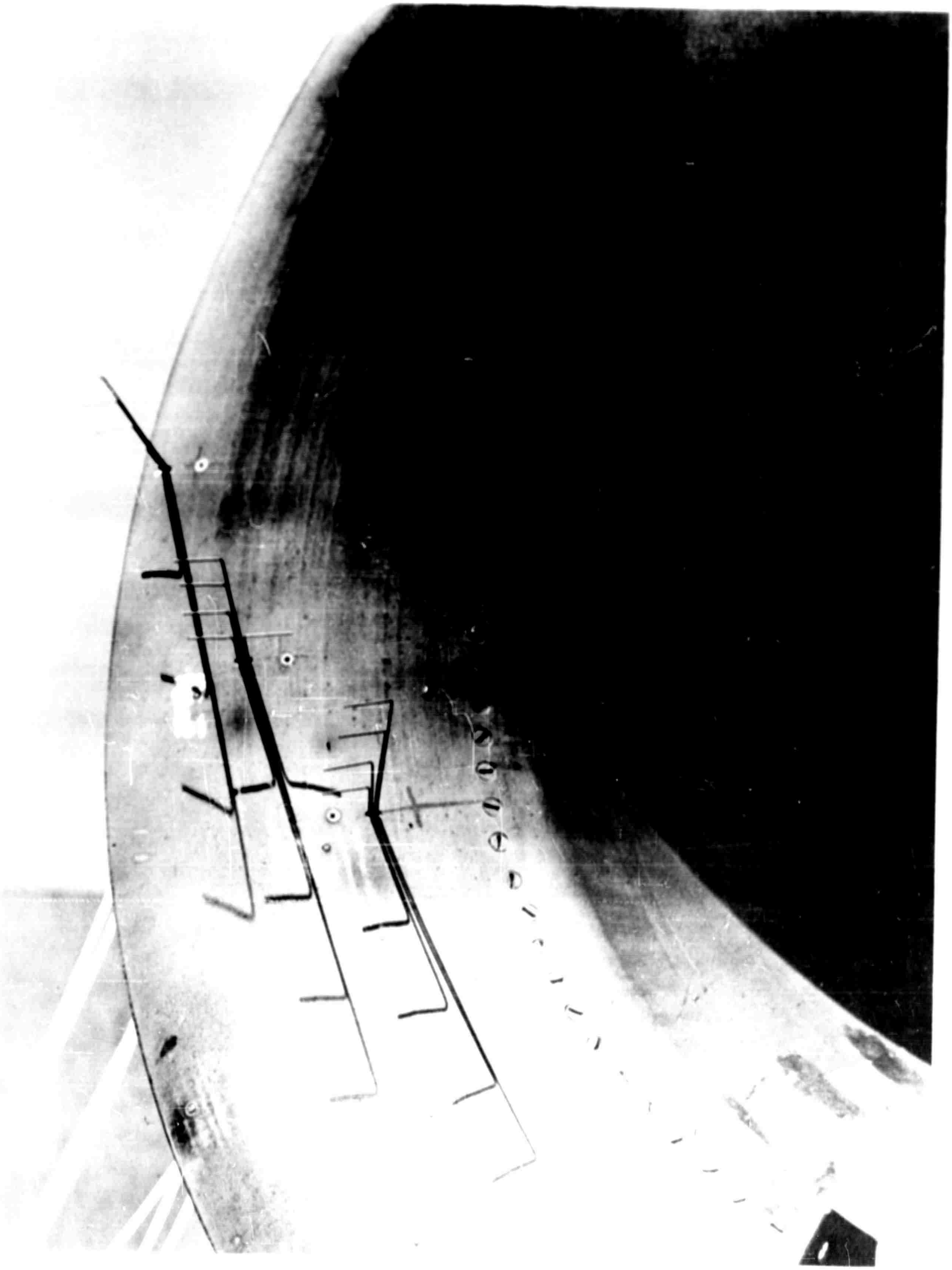

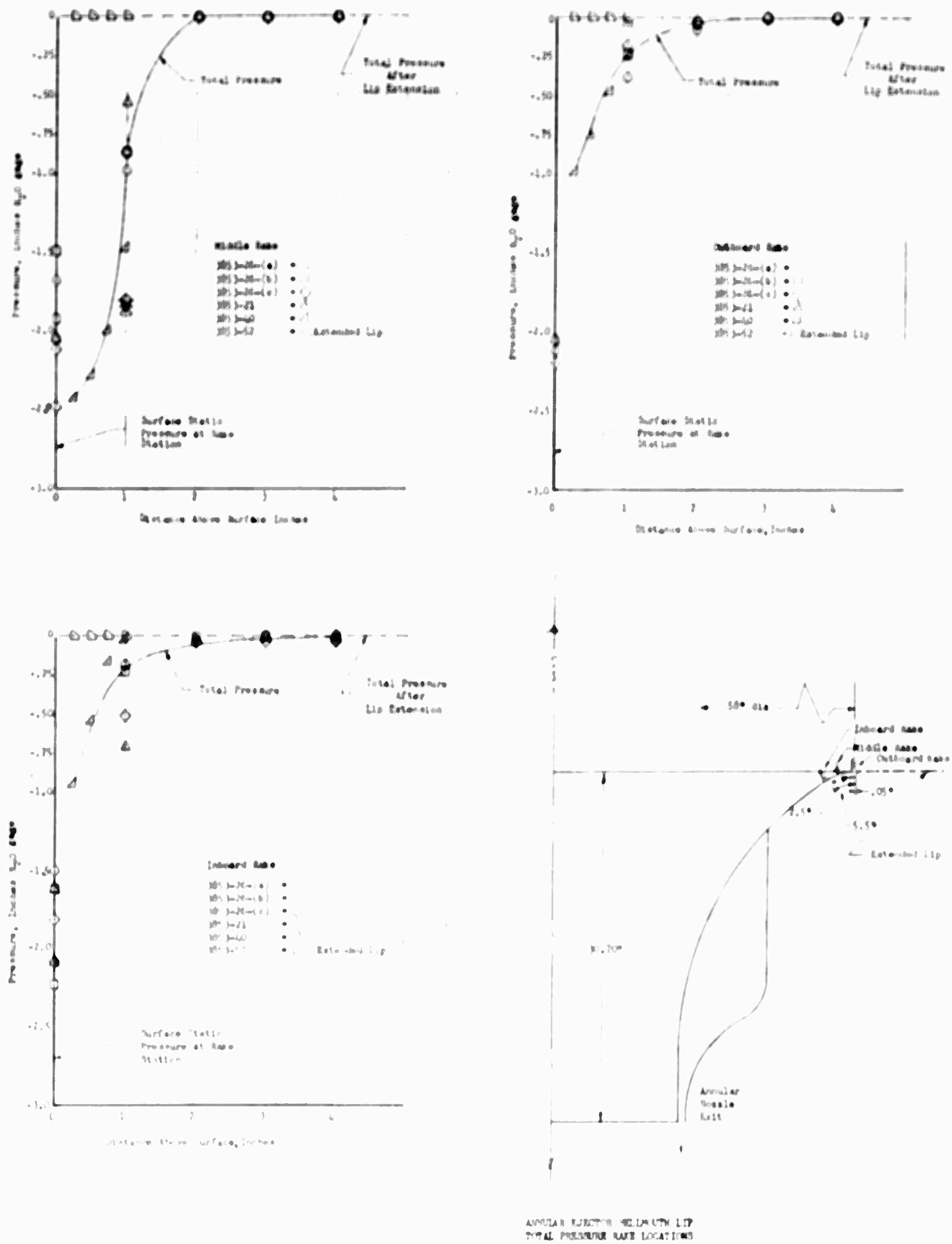

FIGURE 25: BELLMOUTH LIP PRESSURE DISTRIBUTIONS

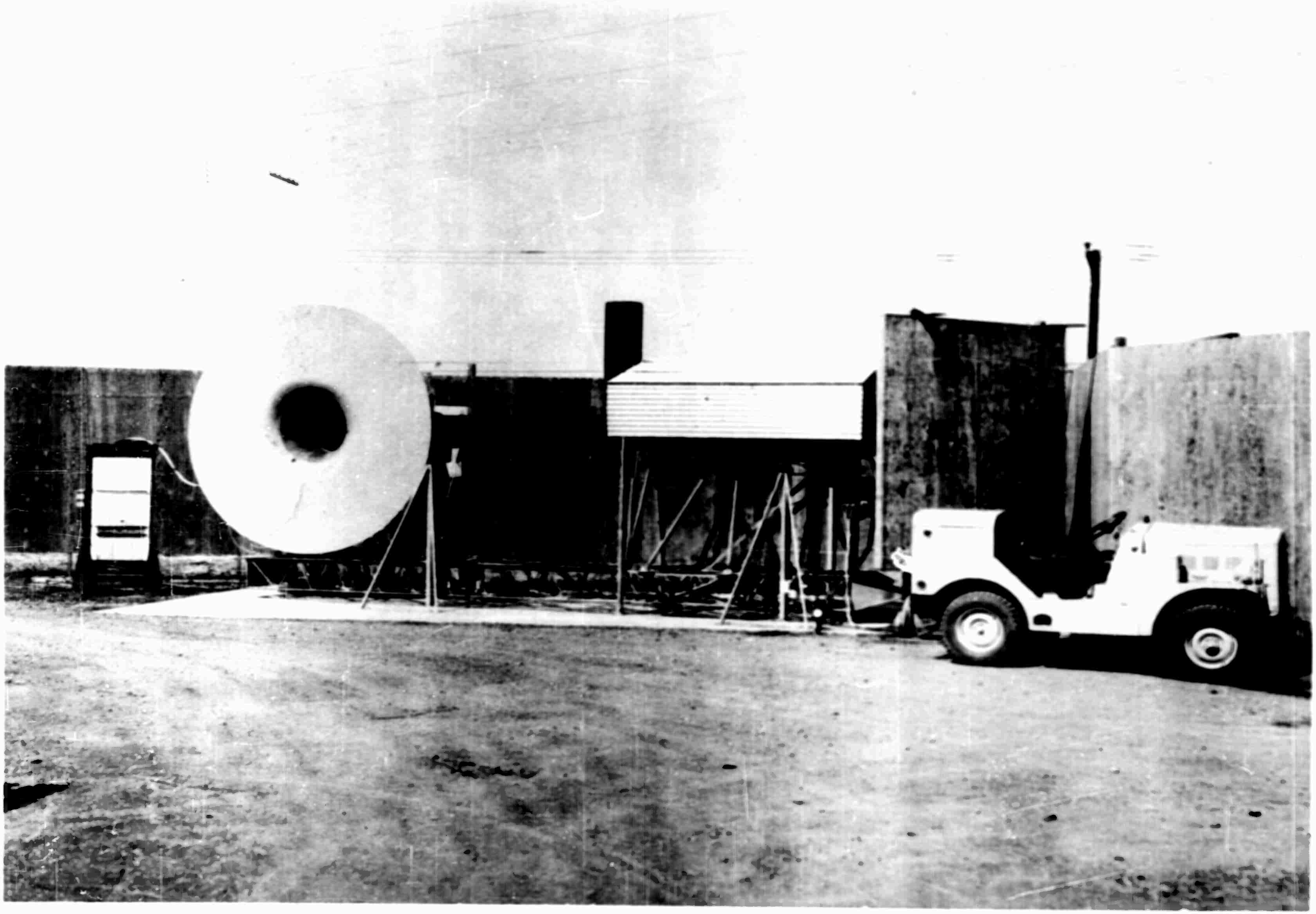

FIGURE 26: ANNULAR EJECTOR - BELLMOUTH LIP MODIFICATION

FIGURE 27: EJECTOR INLET FLOW BEFORE AND AFTER LIP MODIFICATION

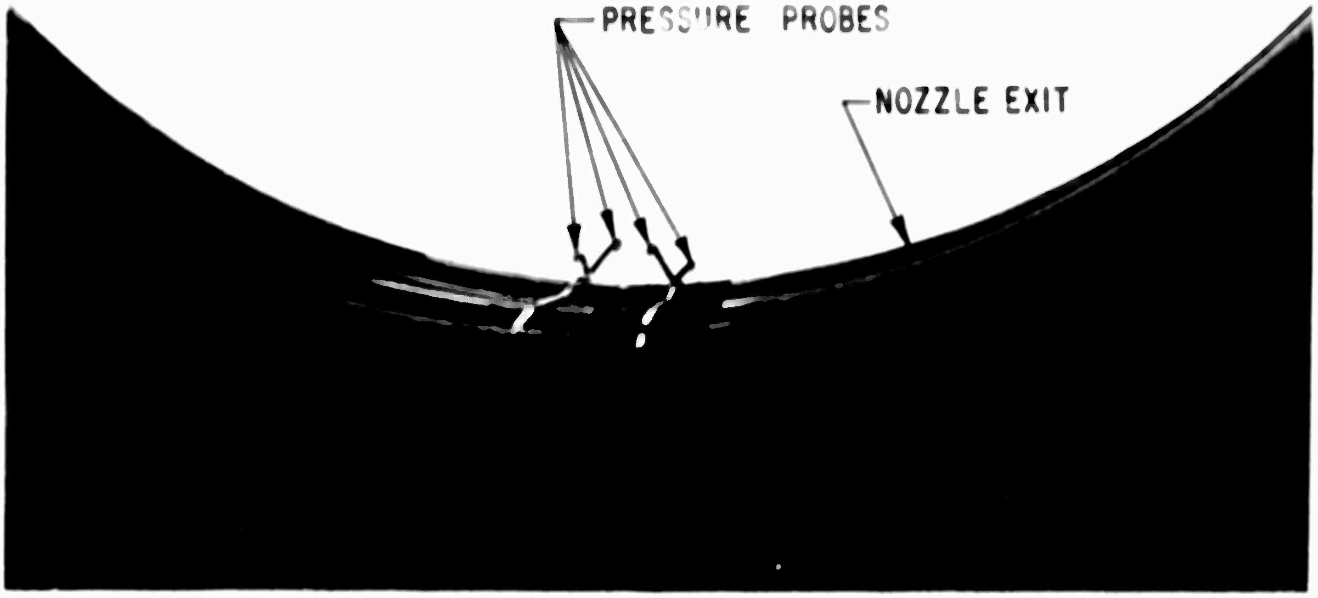

PRESSURE PROBES AS SEEN FROM BELLMOUTH INLET

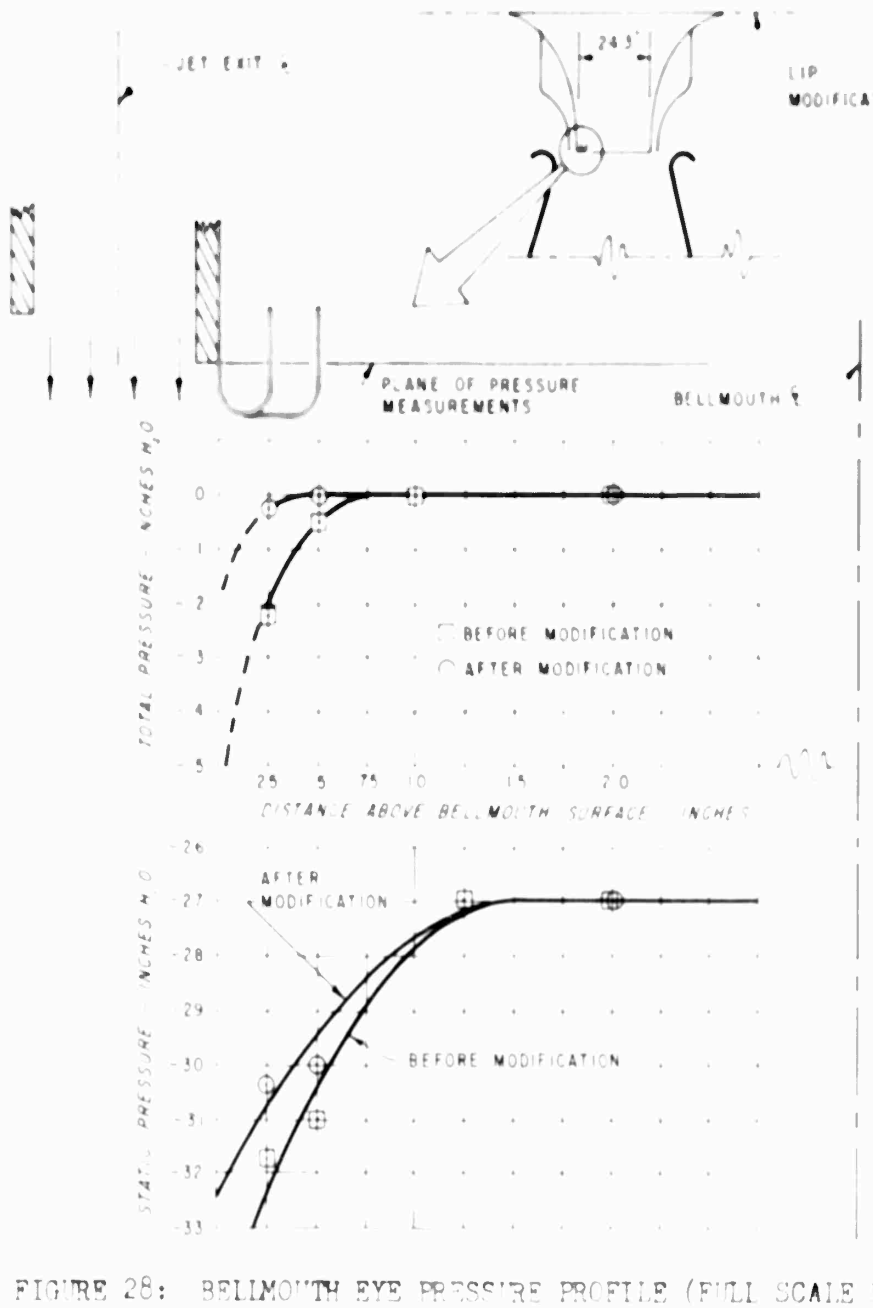

FIGURE 28: BELLMOUTH EYE PRESSURE PROFILE (FULL SCALE EJECTOR)

APPENDIX [illegible]

Report No. ARD-242
Appendix to ARD-243

September 1959

SUMMARY REPORT - MODEL TEST PROGRAM

ANNULAR NOZZLE EJECTOR - CONTRACT NONR 2840(00)

PRELIMINARY DESIGN DEPARTMENT
Z. M. Ciolkosz
Principal Investigator

PROPULSION DEPARTMENT
M. F. Gates
C. L. Cochran

Reproduction in whole or in part
is permitted for any purpose of
the United States Government

ADVANCED RESEARCH
DIVISION OF HILLER AIRCRAFT CORPORATION

1a. SUMMARY

Three basic annular nozzle ejectors have been tested in combination with several mixing tubes in order to determine the variation of thrust augmentation with ejector geometry and to establish the optimum geometry for design of a full scale ejector to be used with a turbojet engine.

The best augmentation ratio* obtained for a mixing tube L/D of 3 was 1.55. Characteristic details of the annular nozzle ejector model were: nozzle aspect ratio, approximately 100; primary nozzle area, 0.758 inches^2. The plenum chamber supply pressure was 21 in. Hg gage. The mixing tube for this combination was divergent (included angle 8°) and the ratio of mixing tube throat area to primary nozzle area was 9.8.

As part of the determination of near optimum ejector geometry the following additional tests were made: (1) evaluation of the addition of swirl to the primary flow, (2) determination of the distribution of thrust between primary nozzle flow, bell-mouth flow and mixing tube, (3) evaluation of the effect of a reduced plenum chamber volume on system efficiency, (4) limited flow visualization studies to define the flow of secondary air into the bell-mouth and mixing tube, and (5) incorporation of the Coanda ejector into the bell-mouth design.

*defined in section 6a

Appendix

TABLE OF CONTENTS

LIST OF FIGURES

LIST OF SYMBOLS

A_A - Area of mixing tube at throat, inches^2

A_B - Base area of wall separating primary jet from secondary jet, inches^2 (See Figure 1)

A_{J_2} - Outlet area of primary jet nozzle, inches^2 (See Figure 1)

A_{s_2} - Outlet area of Bellmouth, inches^2 (See Figure 1)

AR - Aspect Ratio $\dfrac{\text{(Mean Primary Nozzle Circumference)}}{\text{Slot Width}}$

F_J - Thrust due to primary jet alone in presence of Bellmouth flow. (See page 14)

F_m' - Total thrust of annular nozzle without augmenter tube, lbs.

F_m - Total thrust of annular nozzle ejector system, lbs.

F_s - Thrust due to Bellmouth flow, lbs. (See page 14)

n - Ratio of specific heats

P_o - Ambient pressure, psia

$P_{o_{SL}}$ - Standard sea level pressure, 14.7 psia

P_1 - Supply pressure in plenum, in Hg abs (unless otherwise noted)

P_B - Base pressure acting on A_B, assumed equal to P_{s_2}, psia

P_{J_2} - Base pressure acting on A_{J_2}, equal to P_o + 1/2 (P_B - P_o), psia

P_{s_2} - Base pressure acting on A_{s_2}, psia

q - Dynamic pressure, lbs/ft^2

T_1 = Supply temperature in plenum, $^\circ R$

$T_{o_{SL}}$ = Standard sea level temperature, $520^\circ R$

V_{j_2} = Velocity of primary jet, ft/sec

V_s = Average secondary velocity, ft/sec

V_{s_2} = Average secondary velocity of bellmouth flow at outlet (See Fig. 1), ft/sec

$\dot{w}_m$ = Primary weight flow rate in presence of augmenter tube, lbs/sec

$\dot{w}_j$ = Weight flow rate of primary nozzle without augmenter tube, lbs/sec

$\dot{w}_s$ = Secondary weight flow rate without augmenter tube lbs/sec

θ = $\frac{T_1}{T_{o_{SL}}}$

δ = $\frac{P_o}{P_{o_{SL}}}$.

ρ_o = Ambient density, slugs per ft^3

η_n = Primary nozzle efficiency, $\frac{\Delta h\ act}{\Delta h\ theo}$

η_{n_s} = Secondary nozzle efficiency, $\frac{\Delta h\ act}{\Delta h\ theo}$

Δs = Entropy Change

2a. INTRODUCTION

Prior to the award of this contract, Hiller Aircraft Corporation expended considerable effort, using company funds, to explore the benefits that might be obtained from the annular nozzle ejector-mixing tube combination as a thrust augmenting system. The results of more extensive model testing, supported by the Office of Naval Research under contract Nonr 2840(00), are presented in this report.

It is to be emphasized that the primary effort under Contract Nonr 2840(00) is to design, construct, and test a full scale ejector using a turbojet engine as the source of the primary hot jet. Consequently, the purpose of the model testing, for which data are presented in this report, was to establish near optimum geometry for this full scale article. The program was established and performed within this framework.

It is felt that results from testing of the full scale ejector will demonstrate two things: (1) thrust augmentation figures which are large enough to be attractive, and hence which will encourage support for investigation of such devices for VTOL Aircraft and for Ground Effect Machines (GEM) and, (2) a direct correlation, or at least a means for establishing correlation, between future model tests and full scale annular ejectors.

3. DISCUSSION

The basic model test program was established to evaluate annular nozzle ejectors with aspect ratios (average nozzle slot circumference/nozzle slot width) of 60.97, 99.95 and 129.09, all with a constant slot width of 0.086 inch. The primary jet nozzle areas were 0.458 in^2, 0.758 in^2, and 0.959 in^2, which resulted in secondary nozzle area/* primary jet nozzle area ratios of 3.36, 6.84 and 9.28, respectively.

These basic nozzles were tested in combination with mixing tubes at a supply pressure of 21 in. Hg gage. A typical arrangement is shown in Figure 1. Figure 2 presents details of the annular nozzle design. Figure 3 identifies by letter and subscript, throat diameter, and type the basic mixing tubes which were tested. Figure 4 shows typical mixing tubes tested in this program, with one of them mounted in the mixing tube support. Model construction, procedure and data reduction are discussed in Appendix I.

The combinations of mixing tubes and nozzles tested, along with the augmentation ratios, are tabulated and plotted in Figure 5 through 7. Figure 6 shows the effect of area ratio (mixing tube throat area/primary jet nozzle area, A_A/A_{J_2}), on thrust augmentation for constant area mixing tubes at constant L/D (length/diameter) ratios. Figure 7 presents the same information for diffusing mixing tubes.

In general, the nozzle with aspect ratio 100, tested in combination with diffuser type mixing tubes, gave the best performance. When used in

* Secondary nozzle area = area of the bell-mouth throat (eye of the annulus)

combination with mixing tube B_6 at an L/D ratio of 5.1 and an area ratio of 11.9 this nozzle gave the best augmentation ratio obtained in the program, 1.61 (see Fig. 5).

The 61 aspect ratio nozzle also gave better performance when tested in combination with the diffusing mixing tubes than when tested with the constant area mixing tubes. Budgetary limitations and the difficulties in the forming of such large diffusing type mixing tubes prevented the testing of the 129 aspect ratio nozzle with this type of mixing tube.

When tested in combination with constant area mixing tubes, all three basic nozzles gave much the same performance for simillar L/D ratios (Fig. 6). It is noted however, that the dependence of improved performance on area ratio increases with increasing aspect ratio. Another significant factor is that since L/D is based on the throat diameter, the diffusing mixing tube not only provides a better augmentation for the same exit area but has less physical length. For example, the constant area mixing tube B_3 may be compared with the diffusing tube B_4. In each case investigated, an increase in the length/diameter ratio, L/D, gave an increase in augmentation. The area of interest stated in the INTRODUCTION precluded an exhaustive study of this trend.

The spacing between the mixing tube and the primary nozzle was referenced to the ejector nozzle exit plane. Distances above and below this plane (Fig. 1) were designated positive and negative, respectively. As the augmentation performance of all the mixing tubes was very nearly constant for spacing from - 1/4 in. to + 1/2 in., all tests were conducted between these spacing limits, with the majority of the tests at zero spacing.

It will be noted in Figure 2 that a surface was added to simulate the lower surface of an aircraft wing. It was determined that the presence of this surface had no measurable effect on system performance.

Calculation of primary nozzle Reynolds numbers for the three basic nozzles gave values of about 8.5×10^5, based on the hydraulic radius of the annular nozzle.

Two primary nozzle modifications were evaluated as a possible means of improving performance. One modification was the inclusion of the Coanda ejector into the system, the other was introduction of swirl into the primary flow.

The arrangement pictured in Figure 8, a combination of the annular nozzle ejector and the Coanda ejector, was evaluated as a method of possibly increasing the performance of the annular nozzle ejector by the induction of more secondary flow. This model was tested at various nozzle gap spacings between the limits shown in Figure 8.

Figure 9 gives a comparison of augmentation ratios for the basic annular nozzle ejector configuration and this Coanda modification. It was found that the performance of this modification improved as the gap was reduced. With the gap essentially eliminated the performance equals that of the basic annular nozzle ejector. In general, addition of the Coanda ejector did not benefit system performance. The scale of the model prevented further work to optimize performance by better matching of the geometry of the Coanda ejector (which is critical) to the annular nozzle ejector.

The other method evaluated for improving the performance of the basic system by the induction of a greater secondary flow was swirl, or axial rotation, of the primary jet. It had been hypothesized that the swirl motion would cause the primary flow to expand outward due to centrifugal force. This would result in a stronger sink for the secondary flow through the eye of the annulus. In turn this stronger sink would induce a greater secondary flow than would the undeflected primary jet.

An annular nozzle ejector used in previous company sponsored tests, Reference [illegible] was modified as shown in Figure 10 for the swirl tests. (The aspect ratio of this model essentially duplicated that of the smallest of the three fabricated for the basic program.) Vanes were constructed for deflection angles of 0° (to simulate added friction and provide a basis for comparison), 30° and 45°. Figure 11 shows the 30° and 45° deflection "vane rings" and a mixing tube on the model "wing surface" with the 0° deflection vane ring installed in the nozzle.

The swirl tests were conducted at plenum chamber pressures of approximately [illegible] in. Hg gage. The three vane-rings were each tested at the [illegible] with and without the nozzle extension tube. (The nozzle extension tube extends the outer peripheral surface of the annular nozzle as shown in Figure 10.) The nozzle extension tended to decrease performance.

Despite the increased secondary "pumping" caused by axial rotation of the primary jet, there was an overall decrease in ejector performance shown in Figure 12. The decrease of performance below that of the 0° deflection can be accounted for by taking into account a first order loss due to the fact that the primary jet velocity vector is no longer aligned with the thrust axis, thereby reducing the useable primary thrust by the cosine of the deflection angle, and a secondary frictional loss due to turning.

A comparison of the mass flow ratios, $\dot{w}_s/\dot{w}$, for the 0° and 45° jet deflection angles indicates that the addition of swirl resulted in a mass flow ratio increase of 78% (see Appendix I for the calculation of secondary mass flow). Specific values are tabulated below:

deflection angle, degrees	mass flow ratio $\dot{w}_s/\dot{w}$
0°	.766
45°	1.368

Refinement of the secondary flow path (elimination of surface irregularities, etc.) would increase these mass flow ratios over the values quoted above but not sufficiently to result in augmentation.

The annular nozzle ejector with the 45° deflector was also tested with two different mixing tubes. The addition of the mixing tubes, which were not optimized, gave only a slight increase in performance.

In short, rotation of the primary jet flow does not give sufficient increase in performance to overcome the losses inherent in achieving the rotation. Budgetary limitations prevented further investigation of the swirl type system, which might include other means of introducing rotation or of strengthening the secondary sink.

In a further effort to improve the performance of the annular nozzle ejector by increasing the basic nozzle efficiency, the nozzle throat length was shortened from an original length equivalent to 10 nozzle slot widths to a length equivalent to 7.6 slot widths. The nozzle was then retested alone and with mixing tube B_5-3. The test procedures employed were the same as prior to the modification.

The test data indicated a trend towards improved performance, but the net improvement due to a change in nozzle throat length of this magnitude was not significant. It was thought that further reduction of the nozzle throat length, which in turn reduces the clearance between the "wing surface" and the mixing tube inlet, might be deleterious to overall ejector performance, for although the primary nozzle efficiency would be increased, the [illegible] (or tertiary) flow might be restricted enough to reduce the overall performance. The insensitivity of the annular nozzle ejector-mixing tube combination to spacing (performance was constant over spacing equivalent to [illegible] slot widths) would probably permit some "parameter juggling" to achieve a higher overall performance at a reduced nozzle throat length.

Incorporation of the plenum chamber volume of the model as shown [illegible] 2 into the full [illegible] because correlation between the model and full scale test results is one of the objectives of the overall program, it was necessary to maintain a geometric similarity between the two. Consequently the model was altered to the design of the full scale ejector and retested. It should be pointed out that this plenum design modification is not recommended for prototype design and is merely a test expedient for this program. This simple modification of the model, which amounted to converting the plenum chamber to a diffuser, is shown in Figure 13. Test data were obtained by the same procedure used previously and also by direct measurement of pressure loss across the nozzle. These data indicated that an overall loss of 6% in augmentation performance can be expected with this plenum chamber design. A variation in this loss (4.5% to 7.5%) was found between the side adjacent to the supply pipe and the opposite side. The greatest indicated loss was on the adjacent side.

The original model supply system design indicated a loss of approximately 2%. It should be emphasized that this figure can be approached in an aircraft installation by adherence to accepted duct design criteria.

In order to determine the real effect of the mixing tube on ejector nozzle performance, the aspect ratio [illegible] nozzle was tested with mixing tubes B_4-2 and B_5-2 1/2 in position, but supported independently. As data techniques were exactly as before, this allowed a measure of the change in annular nozzle ejector performance due to the presence of the mixing tube. The results of this investigation indicated that approximately 50% of the increase in thrust is due to the net force on the mixing tube; the remaining is due to increased secondary flow through the bell-mouth center of the annular nozzle.

Mixing tube lip size effects were examined briefly using diffusing mixing tube 8_4. The original lip shape (Fig. 3) was cut to 90° from the mixing tube throat plane as shown in Figure 14. Test and data reduction procedures were identical to those used prior to the cut. The effect of this mixing tube lip alteration on the performance of this ejector configuration was negligible.

Limited flow visualization studies were made of the inflow in an attempt to determine a means of improving the performance of this ejector system. Study of the mixing phenomenon associated with this system was beyond the scope of the program. The smoke studies that were made indicated an inflow pattern that would be anticipated from potential flow considerations. No flow discontinuity was noted nor were any new avenues toward improvement discovered.

4. CONCLUSIONS

The primary conclusion resulting from this investigation is that good augmentation can be obtained from an annular nozzle ejector-mixing tube combination with small L/D ratios for the mixing tube.

Divergent mixing tubes were found to augment annular nozzle ejector performance more than did constant area mixing tubes. Neither the rotation of the primary jet flow in the manner described in this report nor the Coanda ejector modification were of value in increasing the augmentation performance of the system.

The geometry of the model with aspect ratio 100 in combination with mixing tube R_5 has been chosen for scale up to full size. The reduction of the plenum chamber cross section shown in Figure 13 is included.

5. REFERENCES

1. Propulsion and Preliminary Design Departments, "Thrust Augmentation of Several Annular Nozzle Ejectors as Determined by Model Tests", Hiller Aircraft Corporation, Advanced Research Division, Report ARD-222 (1959).
2. Gates, M. F., "Static Lift Characteristics of Jet Slots - A Clarifying Study of the External Ejector", Hiller Aircraft Corporation, Advanced Research Division, Report ARD-213 (1958).
3. Ciolkosz, Z. M.; Fan, T. C.; and Spiegelberg, C. H., "Preliminary Proposal for a Method of Thrust Augmentation and Jet Temperature Velocity and Noise Reduction for Ejector Systems as Applied to Jet Supported VTOL Aircraft", Hiller Aircraft Corporation, Advanced Research Division, Report ARD-217 (1958).
4. Reid, Elliott G., "Annular Jet Ejectors", NACA Report TN-1949 (1949).
5. DeLeo, R. V., "An Experimental Investigation of the Use of Hot Gas Ejectors for Boundary Layer Control - Part III", University of Minnesota, Rosemount Aeronautical Laboratories, Research Report No. 122 (1956).
6. Morrisson, R., "Jet Ejectors and Augmentation", NACA Advance Report (1942).
7. DeLeo, R. V., and Wood, R. D., "An Experimental Investigation of the Use of Hot Gas Ejectors for Boundary Layer Control - Part II", University of Minnesota, Rosemount Aeronautical Laboratories, Research Report No. [illegible] (19[illegible]3).
8. Ciolkosz, Z. M., and Spiegelberg, C. H., "Proposal for the Full Scale Investigation of Thrust Augmentation of Ejectors with Annular Nozzles", Hiller Aircraft Corporation, Advanced Research Division, Report ARD-220 (1958).

6a. DESCRIPTION OF TEST EQUIPMENT AND PROCEDURES

The basic test equipment was designed and constructed so that changes in annular nozzle geometry could be made by simply changing nozzles, the other portions of the test equipment remaining the same for all tests.

The test model was installed on the high pressure supply duct as shown in Figure 15 and supported above the scale by a strut incorporating knife edges on both top and bottom ends. The supply duct has a flexible, hinged joint at its axial centerline 93.5 inches upstream of the model centerline. This joint effectively eliminates supply tube static pressure effects from the thrust measuring system and permits thrust measurement with minimum mechanical friction. The flexible, hinged joint, the flow measuring section and the blower system are shown in Figure 16. The blower system is comprised of 2 Allison V1710 superchargers operating in series. Power is supplied by two 150 HP Ford engines. The flow measuring section meets American Gas Association specifications.

In order that the air flow would leave the nozzle uniformly and with low losses, the model was constructed with a plenum chamber proportioned to give a uniform static pressure at the nozzle inlet.

The plenum chamber was probed to determine the degree of uniformity of the internal static pressure. The pressure probe locations are shown in Figures 17 and 18. It was found that there was no measurable variation in static pressure within the plenum chamber. It was also determined that the pressure losses (from plenum total pressure to jet total exit pressure) were of the order of 2% of the plenum total pressure.

Concentric alignment of the annular nozzle and mixing tube was within one slot width. Axial alignment was within 1°. The mixing tube support (Figure 18) was designed to allow small vertical, horizontal, and angular adjustments in the alignment of the annular nozzle and mixing tube.

The support bracket for the mixing tubes was mounted on the manifold ring, as in Figure 18. The mixing tubes were made from hot formed commercial glass tubing. Glass was chosen for the mixing tubes because of its excellent surface smoothness and the relative inexpensiveness of the part.

The length of the mixing tubes was changed by cutting with the conventional hot wire. The tape shown in Figure 4 is at the cuts in the tube length. For the most part, excellent cuts were made and the tube surface smoothness was not affected. Because the forming of the mixing tube inlet was a hand operation, small variations in contour were present from one mixing tube to the next. It is felt that these variations were not significant. For determining the full scale mixing tube geometry, the exact shape was taken from a template cut to the mixing tube B_5.

Prior to ejector evaluation tests the thrust measuring system was calibrated by dead weight loading both while the system was unpressurized and statically pressurized to test level. Appropriate corrections determined by this test were applied to ejector data. The flow section was checked by determining the flow rate of a model at a given set of inlet conditions with three different orifice sizes. In addition to these calibrations and checks the leakage from the system was checked and found to be less than 0.4% of the model rated weight flow.

Measured and recorded for all tests were the pressure upstream from the metering orifice, the pressure drop across the orifice, barometer pressure, the total temperature of the stream in the flow measuring section and the total thrust.

The augmentation ratios presented in this report are on the basis of a constant unit power input. This is achieved by reducing all thrust values to a one pound per second flow rate ($\dot{w}\sqrt{\theta}$) base (via $\frac{F}{\dot{w}\sqrt{\theta}}$) as described in Reference 2. To complete the requirements for a unit power input the test supply pressure $\frac{P_1 - P_0}{\delta}$ is maintained constant

The augmentation ratio is then

$$\frac{\dfrac{F_m}{\dot{w}_m\sqrt{\theta}}}{\dfrac{F_j}{\dot{w}_j\sqrt{\theta}}} \qquad \frac{P_1 - P_0}{\delta} = \text{const.}$$

F_j is defined by the equation $\frac{\dot{w}_j}{g} V_j$, which is the thrust resulting from the primary jet alone when the primary nozzle exit plane is operated in the pressure environment which results from the ejector action inherent with the [illegible] and when the appropriate corrections are applied for secondary flow and base pressure effects. F_j is obtained from the equation:

$$F'_m = F_s + F_j + A_{s_2}(P_{s_2} - P_o) + A_B(P_B - P_o) + A_{J_2}(P_{J_2} - P_o)$$

F'_m = Total thrust of Annular Nozzle alone, i.e., without augmenter duct installed

$$F_s = \frac{\dot{w}_s}{g} V_{s_1} = P_{s_2} A_{s_2} \left(\frac{2n}{n-1}\right) \left[\left(\frac{P_T}{P_{s_2}}\right)^{\frac{n-1}{n}} - 1 \right] \eta_s \qquad \text{Assume } \eta_s = .98$$

and $\frac{\dot{w}_s}{g} V_{s_1} = A_{s_2}(P_T - P_{s_2}) + \int p\,dA$ over the bellmouth

$A_B(P_B - P_o)$ = (Physical Base Area)(Base Pressure - Ambient Pressure)

$A_{J_2}(P_{J_2} - P_o)$ = (Annular Nozzle [illegible])(Nozzle Exit Plane Pressure - Ambient Pressure)

F'_m may [illegible] be thought of as the thrust of the annular nozzle [illegible] augmenter [illegible] that would be measured if there were [illegible] secondary flow effects [illegible] and if it were operated in a [illegible] [illegible]

[illegible] thrust that [illegible] nozzle expanded to ambient [illegible] rather than [illegible]

[illegible]

exhausts to ambient pressure and passes the same weight flow with the same supply pressure.

The following factor is given to permit the augmentation ratios presented in this report to be put in this form for the case where the equivalent primary nozzle is assumed to be 100% efficient ($\Delta s = 0$).

$$\left.\frac{\dfrac{F_j}{\dot{w}_j\sqrt{\theta}}}{\left.\dfrac{F}{\dot{w}\sqrt{\theta}}\right|_{\Delta s = 0}}\right|_{\frac{P_1 - P_0}{\delta} = \text{const}} = 0.98$$

Mass flow ratios for the tests incorporating swirl in the primary air were determined by comparing the measured primary flow rate with a calculated secondary flow rate. Secondary air weight flow was calculated from $\dot{w}_s = g\,\dfrac{F_s}{V_s}$

where, F_s is as above, and $V_s = \left\{\dfrac{2n}{n-1}\,\dfrac{P_o}{\rho_o}\left[1 - \left(\dfrac{P_{s_2}}{P_o}\right)^{\frac{n-1}{n}}\right]\eta_{n_s}\right\}^{1/2}$

The accuracy of the specific thrust values is ± 2%.

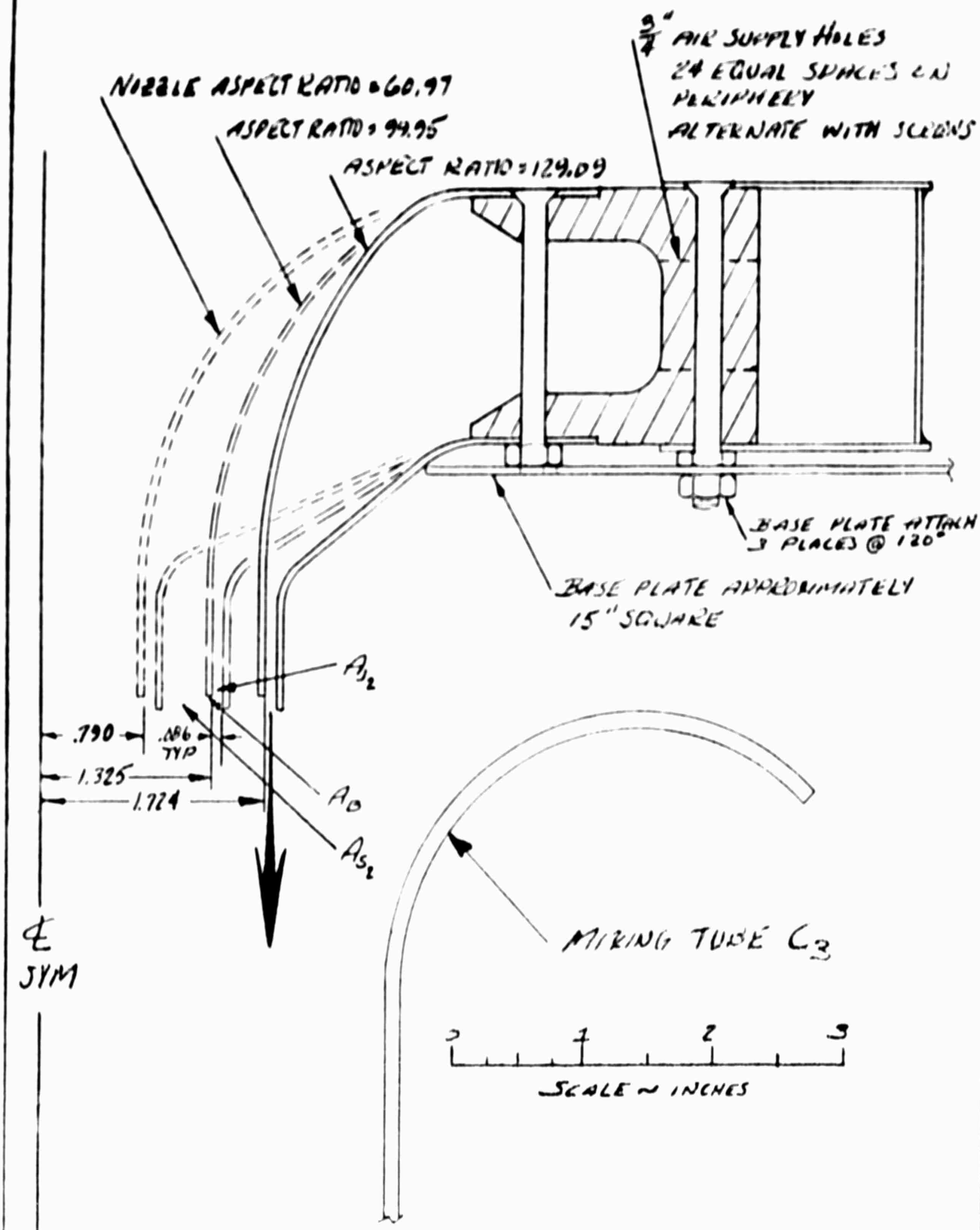

FIGURE 1

TYPICAL ARRANGEMENT OF ANNULAR NOZZLE AND MIXING TUBE COMBINATION

Appendix

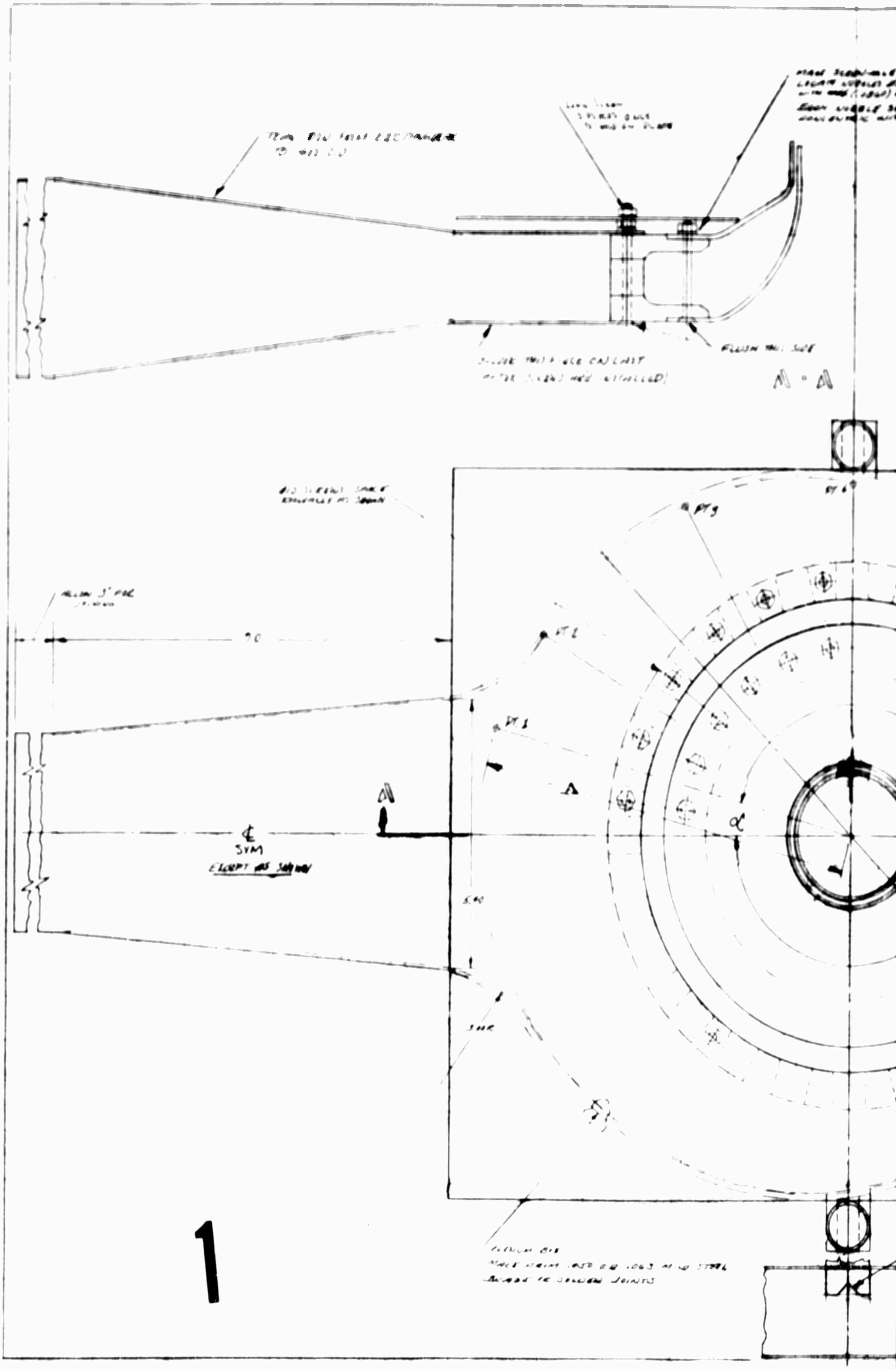

1

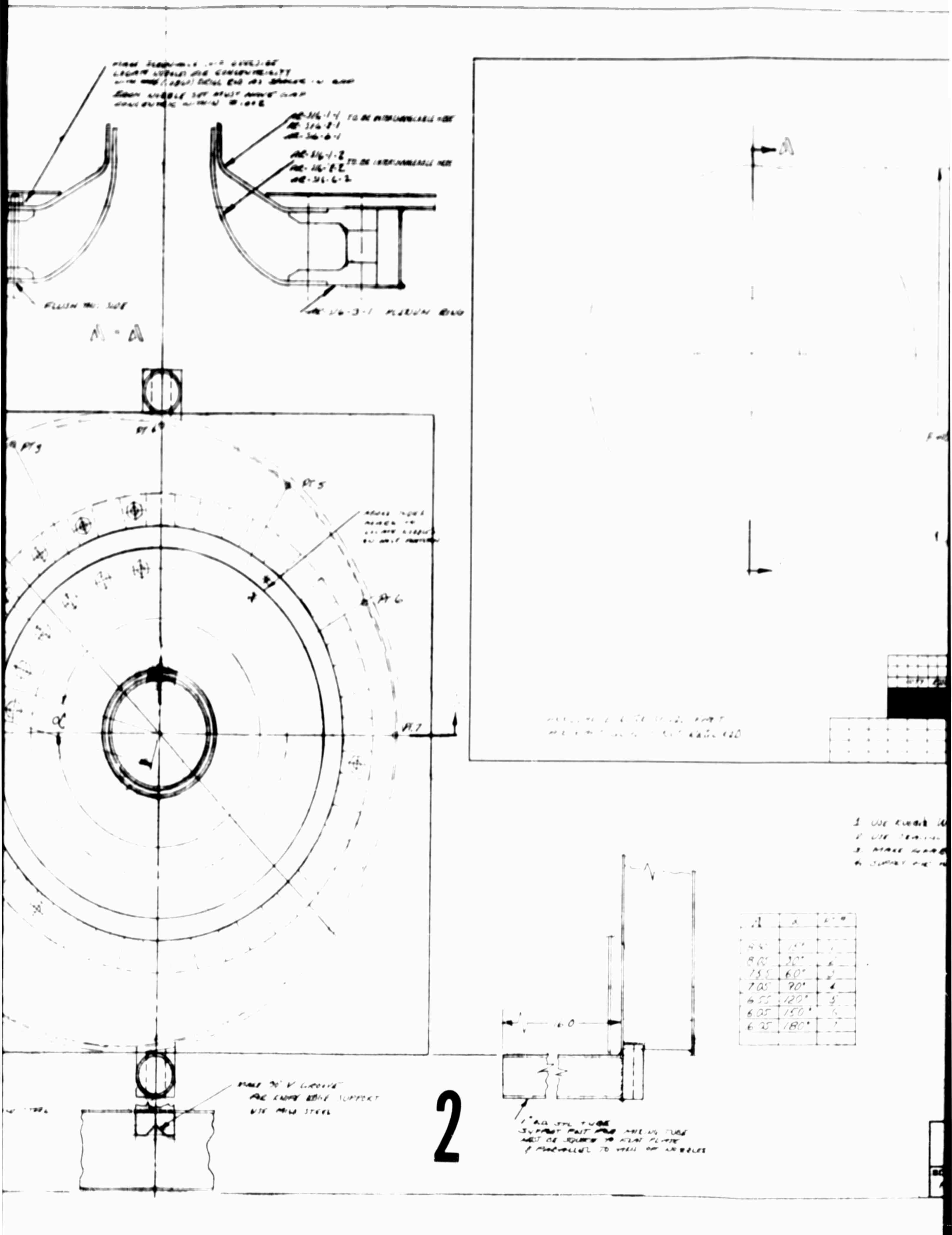

A	α	[illegible]
[illegible]	[illegible]	1
8.05	20°	2
7.55	60°	3
7.05	70°	4
6.55	120°	5
6.05	150°	6
6.25	180°	7

2

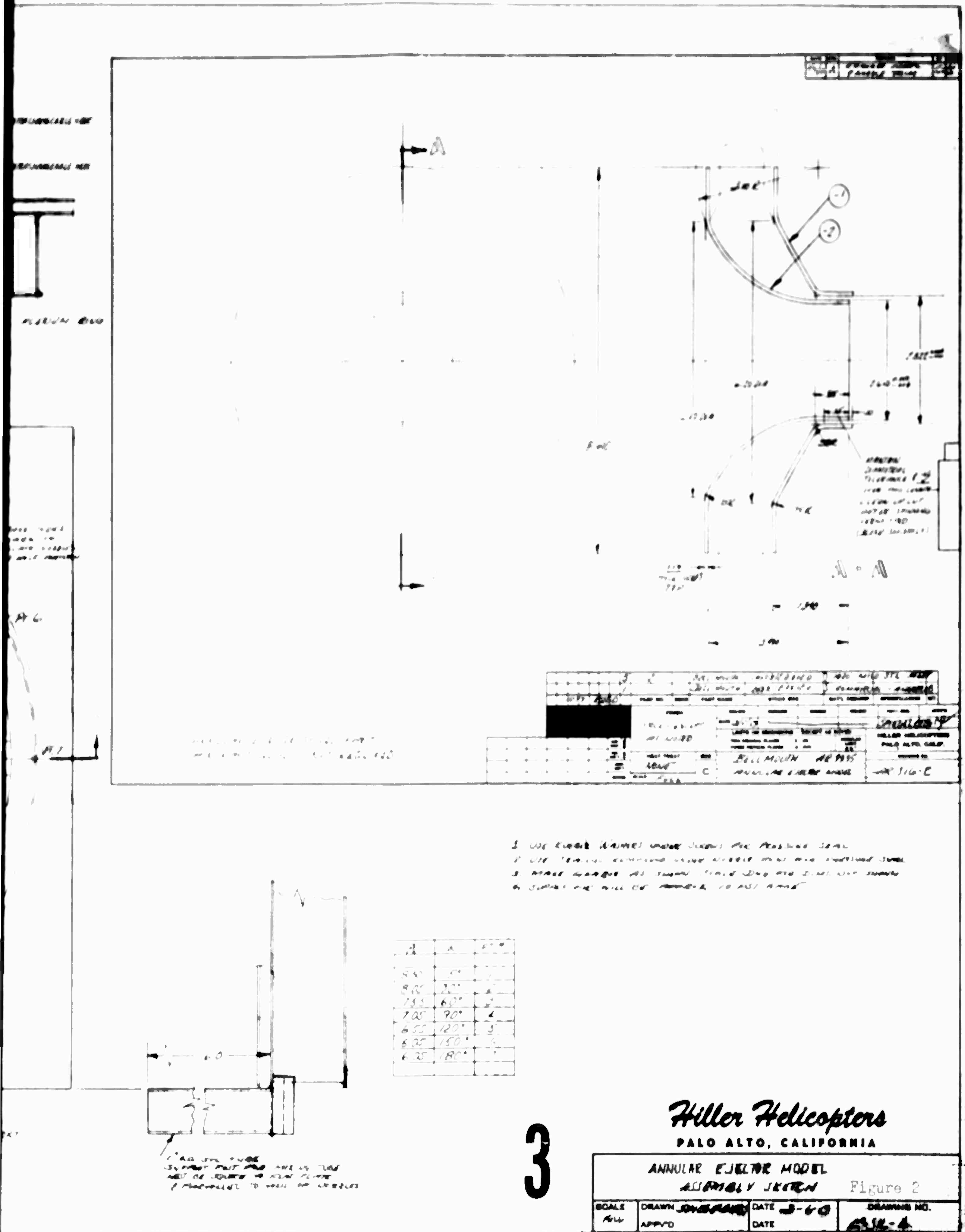

Hiller Helicopters
PALO ALTO, CALIFORNIA
ANNULAR EJECTOR MODEL
ASSEMBLY SKETCH
SCALE
DRAWN
DATE
APP'V'D
DATE
DRAWING NO.

3

Figure 2

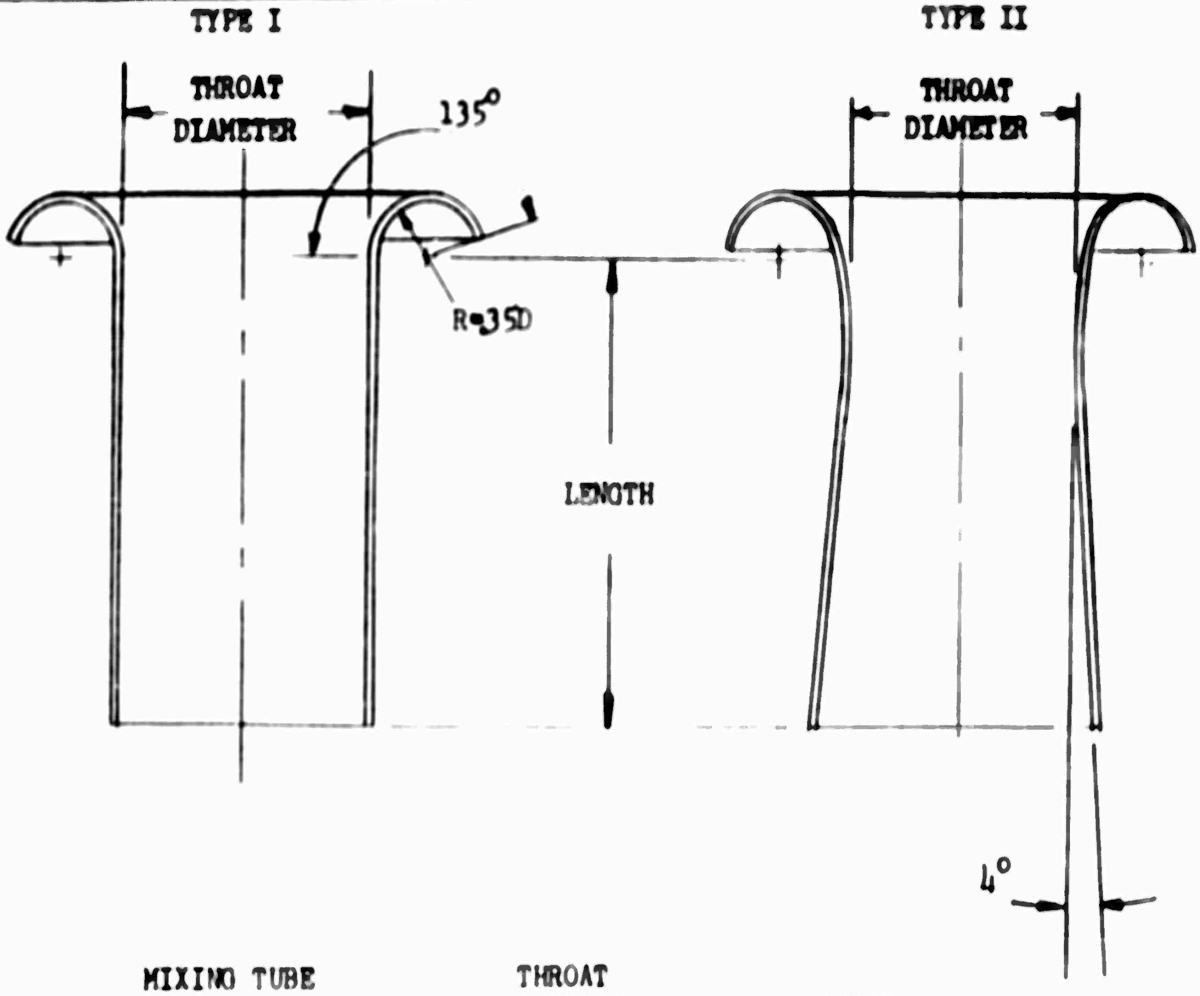

MIXING TUBE IDENTIFICATION	THROAT DIAMETER	TYPE
A_1	2.12	I
A_2	1.93	II
A_3	1.82	II
A_5	2.50	I
B_1	3.20	I
B_2	3.72	I
B_3	4.16	I
B_4	2.90	II
B_5	3.07	II
B_6	3.38	II
C_1	4.16	I
C_2	4.68	I
C_3	5.23	I

FIGURE 3

BASIC IDENTIFICATION OF MIXING TUBES BY LETTER AND SUBSCRIPT, THROAT DIAMETER, AND TYPE

Appendix

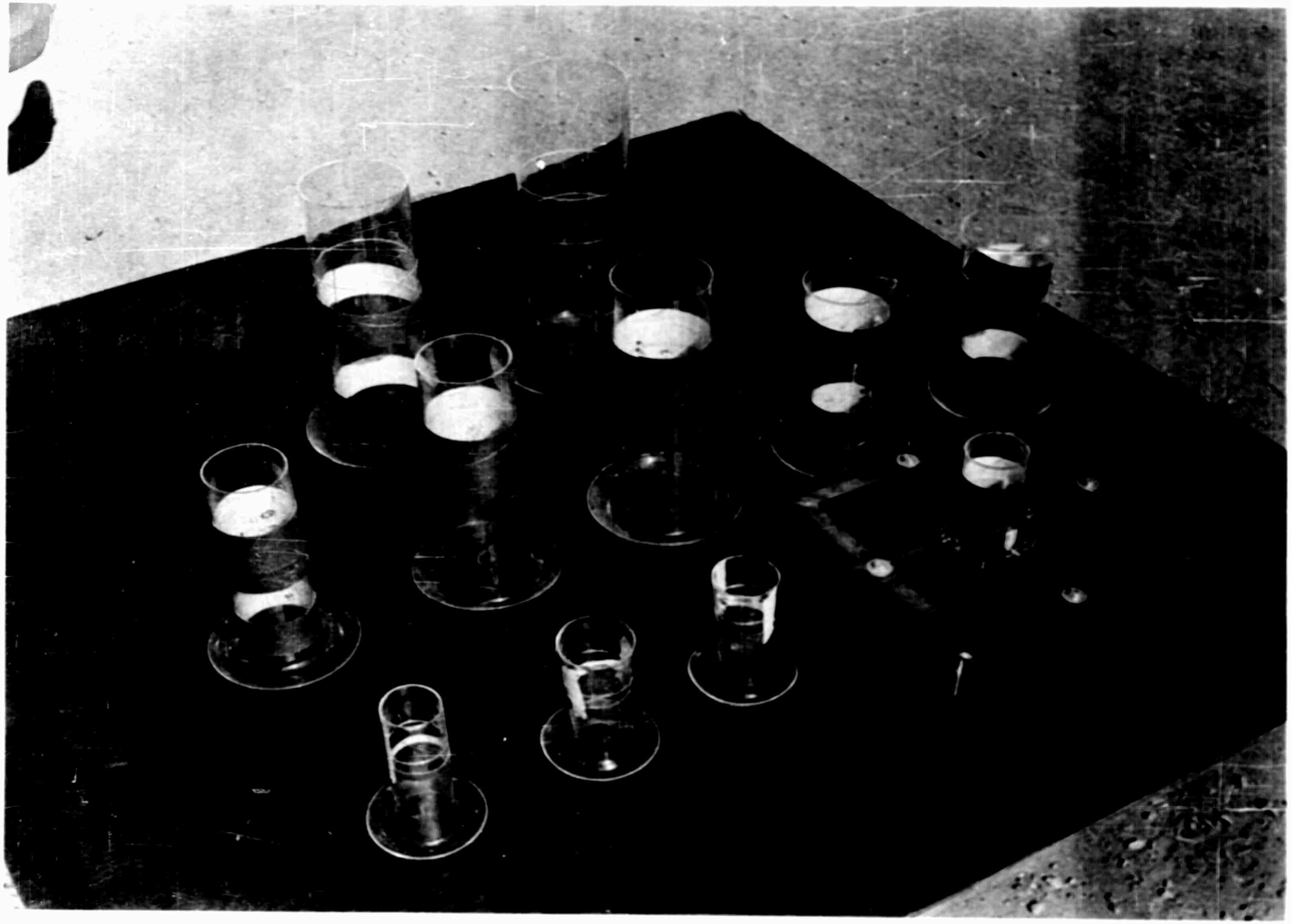

FIGURE 4
TYPICAL MIXING TUBES TESTED IN THIS PROGRAM, WITH ONE OF THEM MOUNTED IN THE MIXING TUBE SUPPORT
Appendix

Nozzle Aspect Ratio	Mixing Tube	Augmentation Ratio	Nozzle Aspect Ratio	Mixing Tube	Augmentation Ratio
60.97	A_1 - 2*[1]	1.22	99.95	B_5 - 2	1.39
	A_1 - 3	1.27		B_5 - 2 ½	1.46
	A_2 - 2	1.33		B_5 - 3	1.55
	A_2 - 3	1.40		B_6 - 1.3	1.33
	A_3 - 2	1.31		B_6 - 1.8	1.42
	A_3 - 3	1.37		B_6 - 2	1.4[illegible] *[2]
	A_5 - 1 ½	1.21		B_6 - 2.8	1.53
	A_5 - 2	1.30		B_6 - 3	1.5[illegible] *[2]
	A_5 - 3	1.31		B_6 - 3.8	1.5[illegible]
	B_1 - 1 ½	1.21	99.95	B_6 - 5.1	1.61
	B_1 - 2	1.24	129.09	C_1 - 1 ½	1.26
	B_1 - 3	1.36		C_1 - 2	1.25
	B_4 - 2	1.22		C_1 - 3	1.29
60.97	B_4 - 3	1.39		C_2 - 1 ½	1.35
99.95	B_1 - 1 ½	1.22		C_2 - 2	1.36
	B_1 - 2	1.23		C_2 - 3	1.38
	B_1 - 3	1.28		C_3 - 1 ½	1.36
	B_2 - 1 ½	1.29		C_3 - 2	1.40
	B_2 - 2	1.33	129.09	C_3 - 3	1.42
	B_2 - 3	1.35			
	B_3 - 1 ½	1.32			
	B_3 - 2	1.37			
	B_3 - 3	1.40			
	B_4 - 2	1.35			
99.95	B_4 - 3	1.47			

*[1] Mixing tube code: A_1 - 2

Basic identification
See Figure 3

L/D = 2

*[2] Interpolated

FIGURE 5
AVERAGE AUGMENTATION RATIOS FOR ALL MIXING TUBE - ANNULAR NOZZLE COMBINATIONS TESTED IN THIS PROGRAM

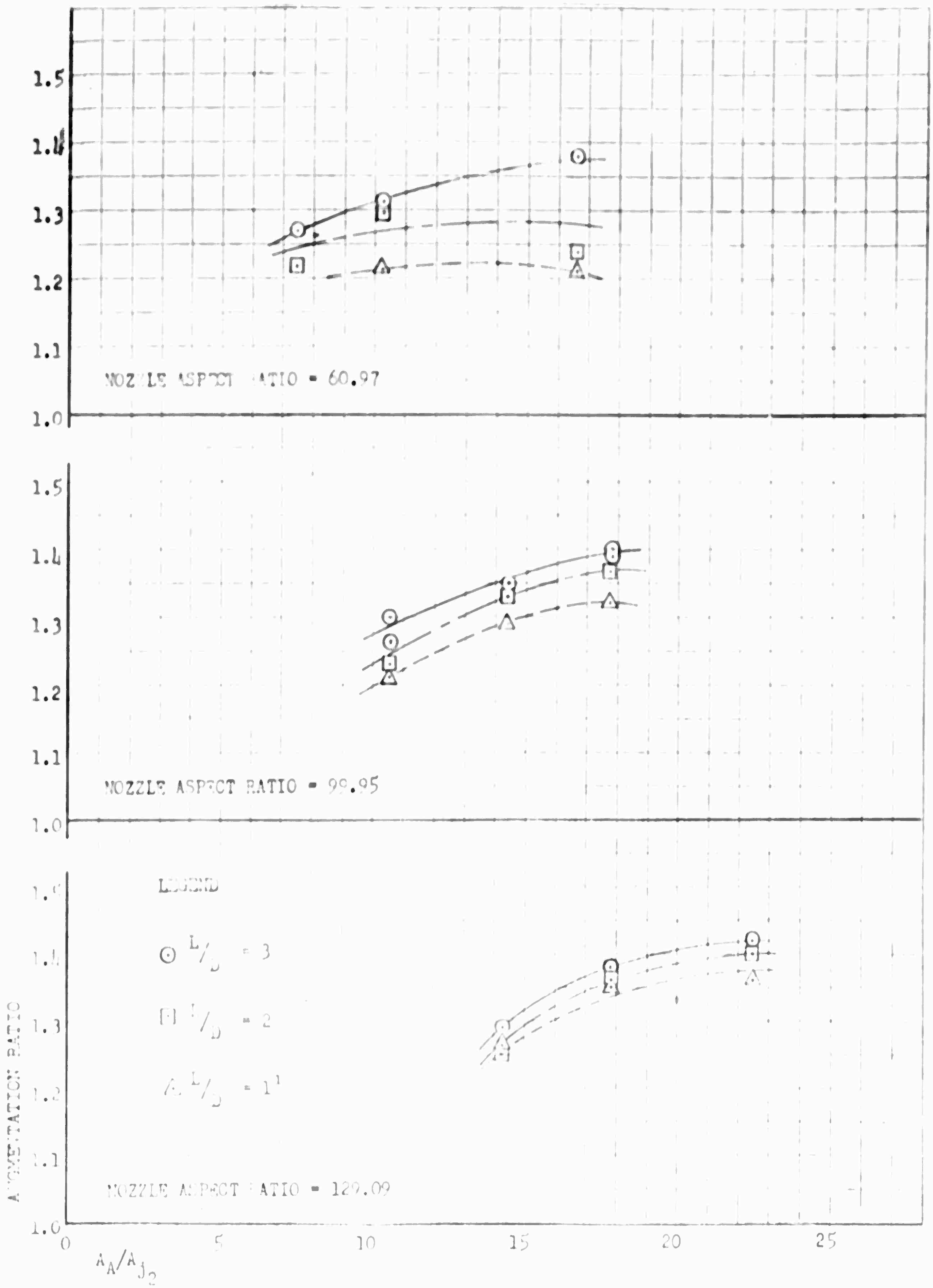

FIGURE 6

EFFECT OF AREA RATIO ON AUGMENTATION PERFORMANCE AT CONSTANT L/D RATIOS FOR CONSTANT AREA MIXING TUBES

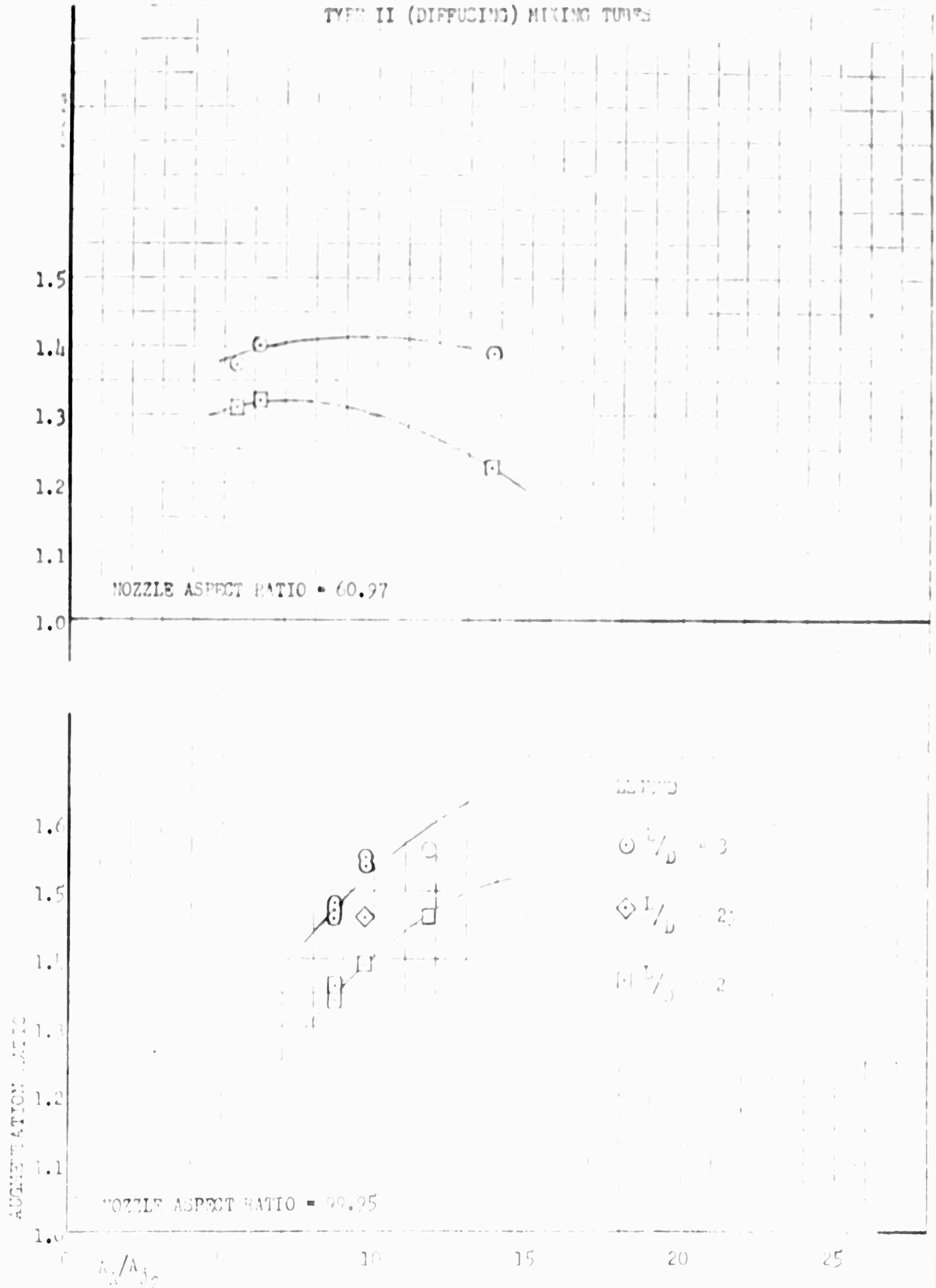

FIGURE 7

EFFECT OF AREA RATIO ON AUGMENTATION PERFORMANCE AT CONSTANT L/D RATIOS FOR DIFFUSING MIXING TUBES

Appendix

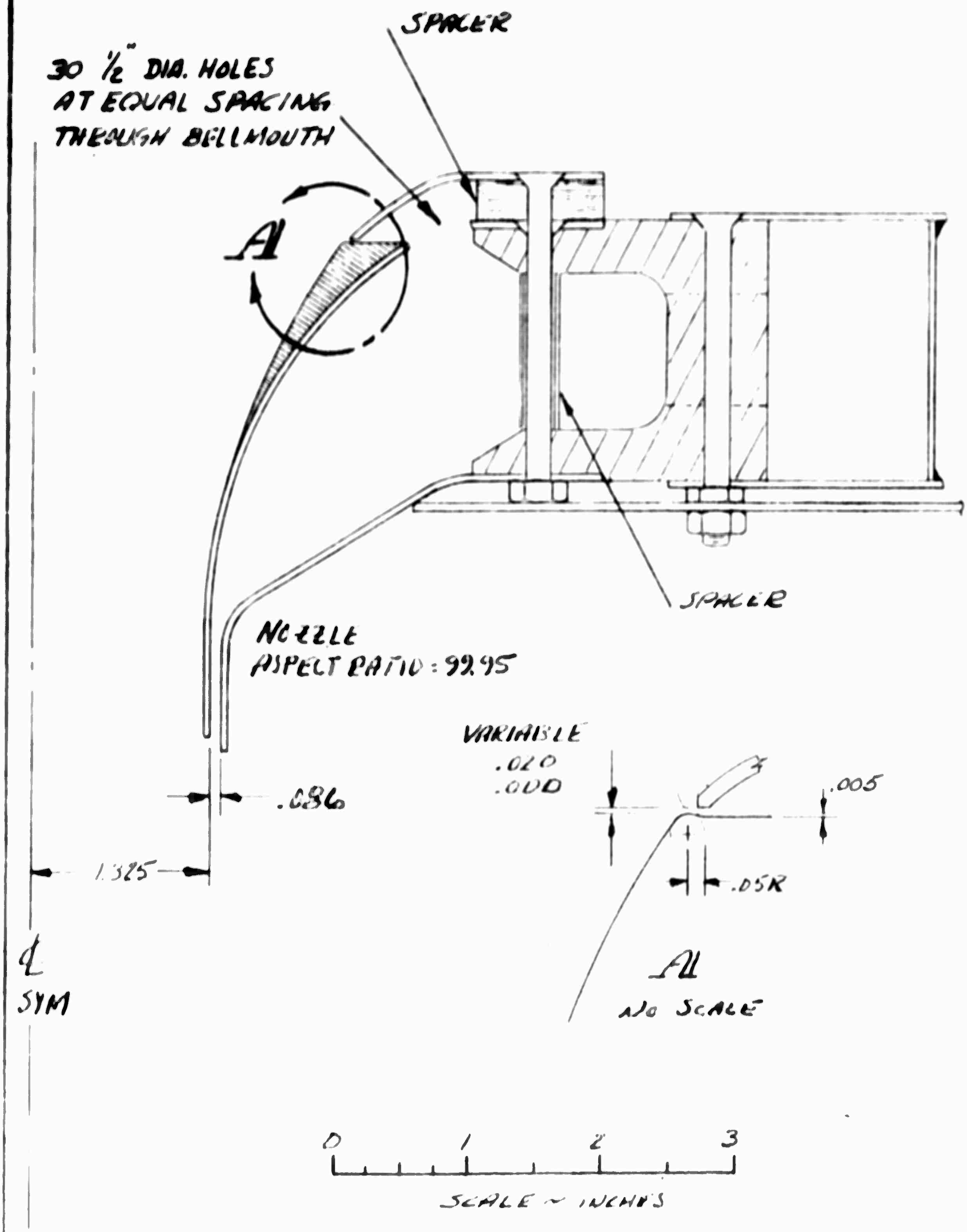

FIGURE 8

ANNULAR NOZZLE EJECTOR AND COANDA EJECTOR COMBINATION

	BASIC ANNULAR NOZZLE EJECTOR AUGMENTATION RATIO	ANNULAR NOZZLE EJECTOR WITH COANDA EJECTOR AUGMENTATION RATIO	
		Gap .000 in. to .005 in.	Gap .005 in. to .010 in.
No Mixing Tube	1.035	1.031	1.009
Mixing Tube B_4			
$\frac{L}{D} = 2$	1.34	1.35	
$\frac{L}{D} = 3$	1.47	1.44	
Mixing Tube B_5			
$\frac{L}{D} = 2$	1.39	1.37	
$\frac{L}{D} = 3$	1.55	1.50	

FIGURE 9

COMPARISON OF AUGMENTATION PERFORMANCE FOR BASIC ANNULAR NOZZLE EJECTOR
AND COANDA EJECTOR MODIFICATION

Appendix

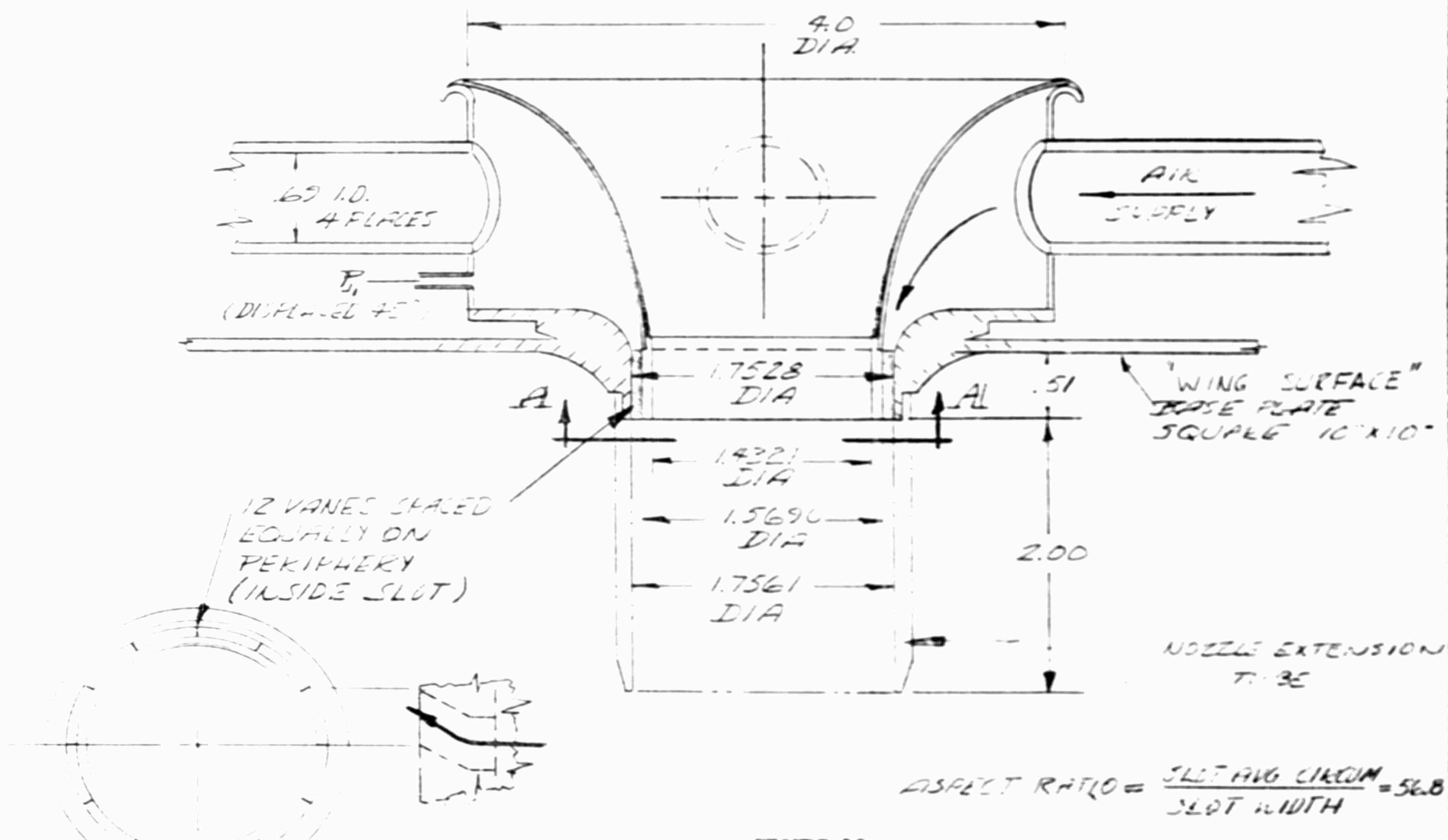

FIGURE 10

DETAILS OF MODIFIED ANNULAR NOZZLE EJECTOR USED FOR SWIRL TESTS

FIGURE 11

THE 30° AND 45° DEFLECTION "VANE-RINGS" AND A MIXING TUBE ON THE MODEL "WING SURFACE". THE 0° "VANE-RING" IS INSTALLED IN THE NOZZLE

Appendix

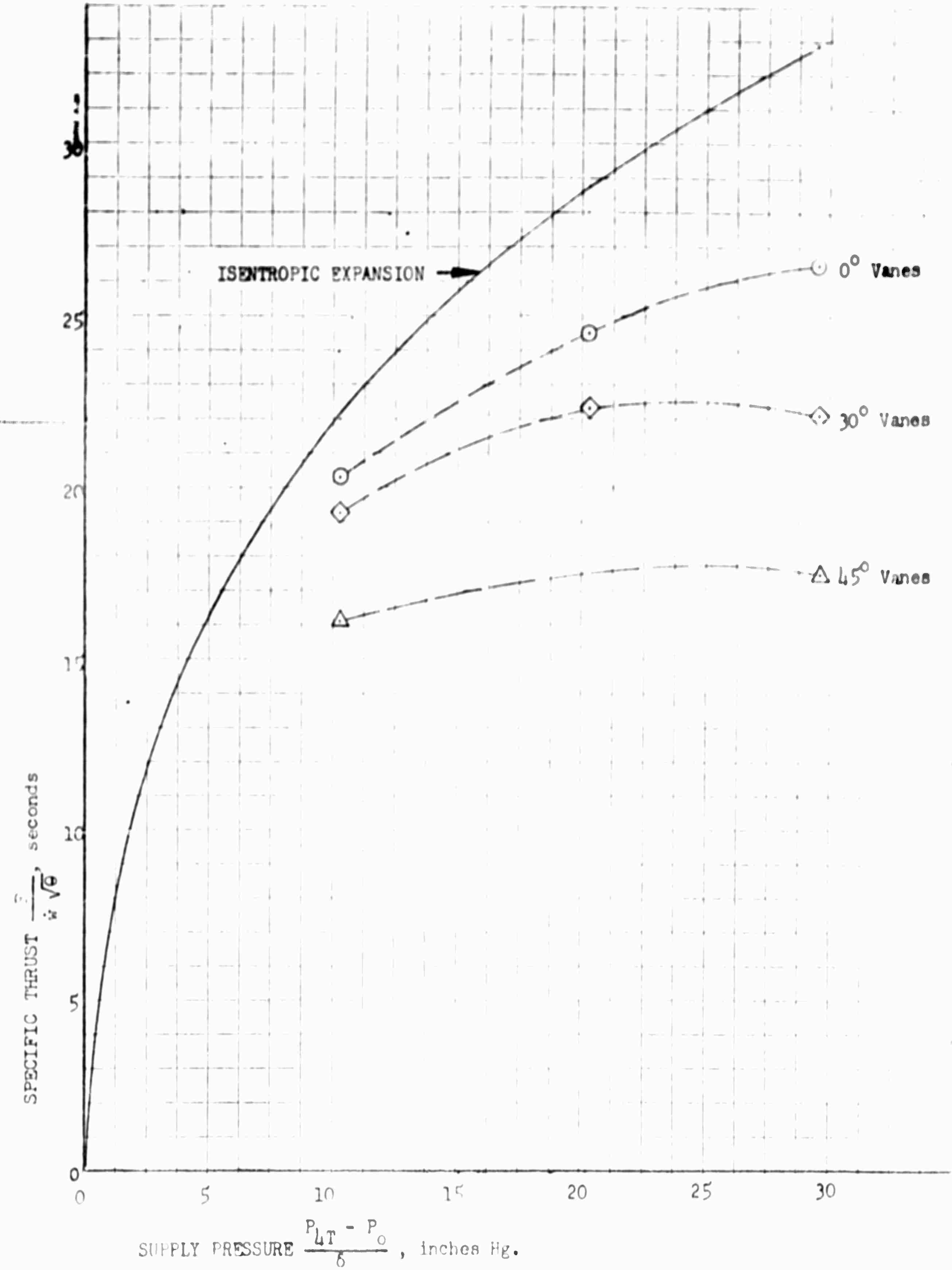

FIGURE 12

EFFECT OF PRIMARY JET ROTATION ON THRUST PERFORMANCE OF AN ANNULAR NOZZLE EJECTOR

Appendix

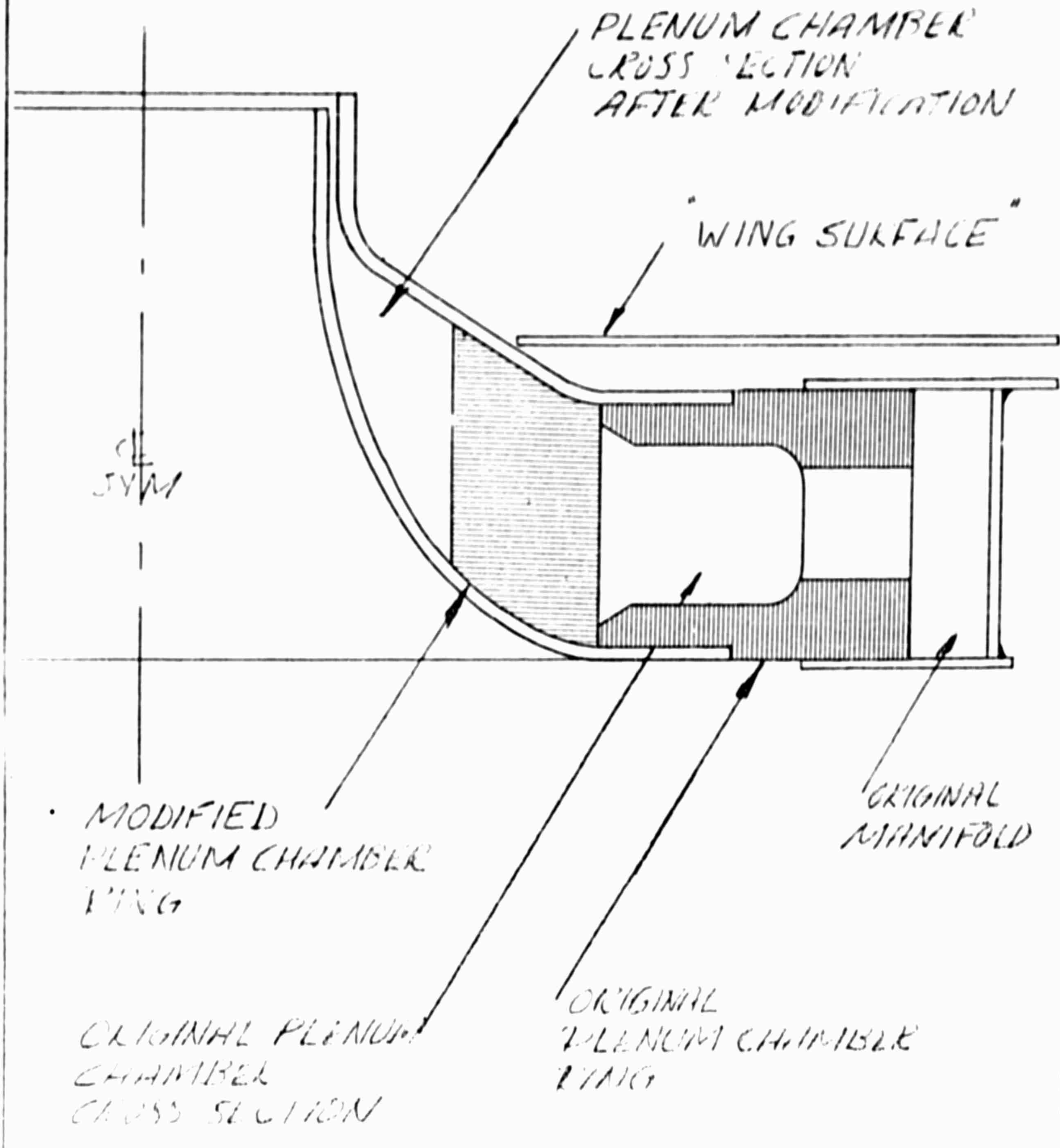

FIGURE 13

CROSS SECTIONAL VIEW OF PLENUM CHAMBER MODIFICATION

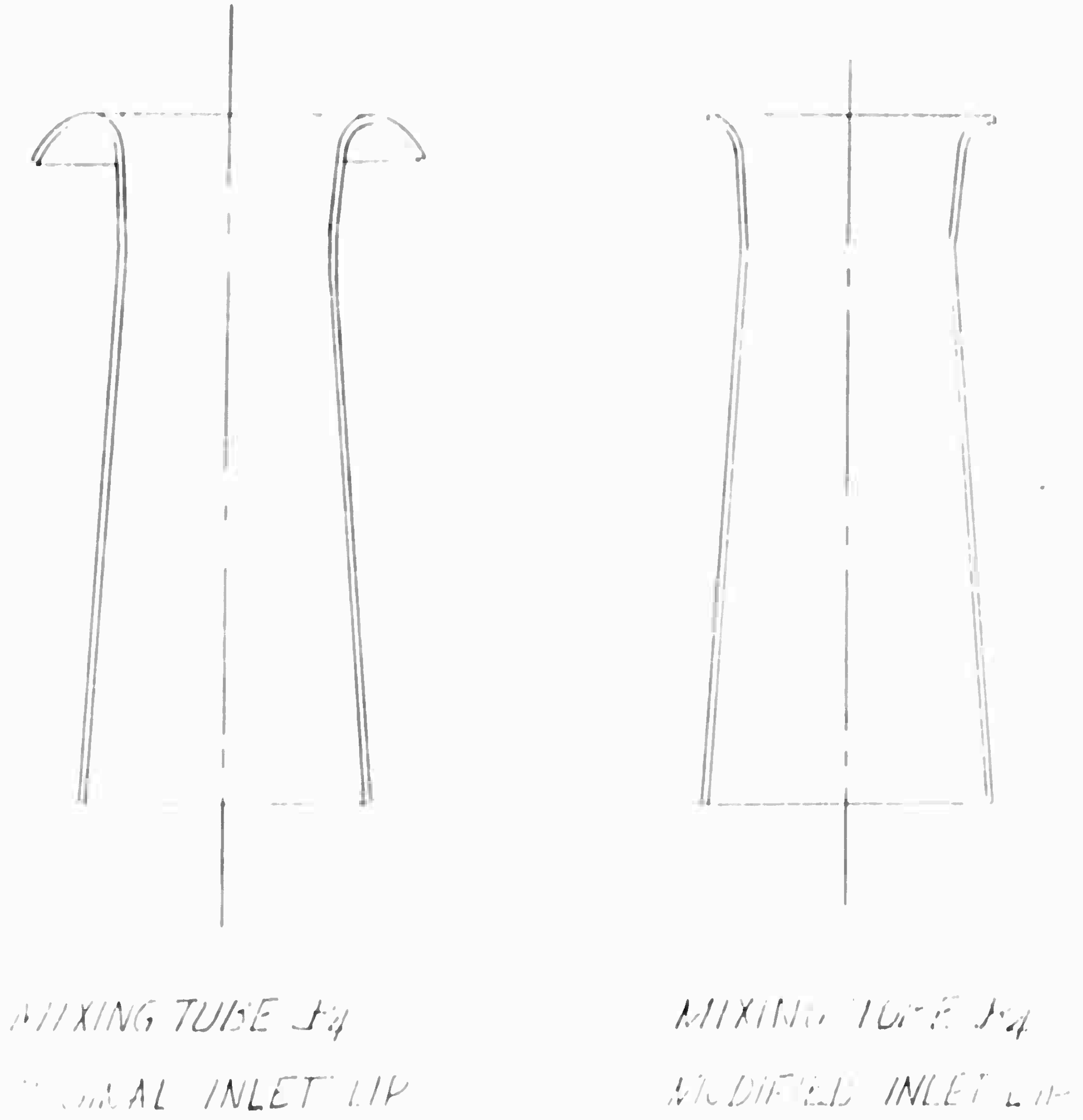

FIGURE 14

LIP SHAPE ALTERATION ON MIXING TUBE B_4

[illegible]

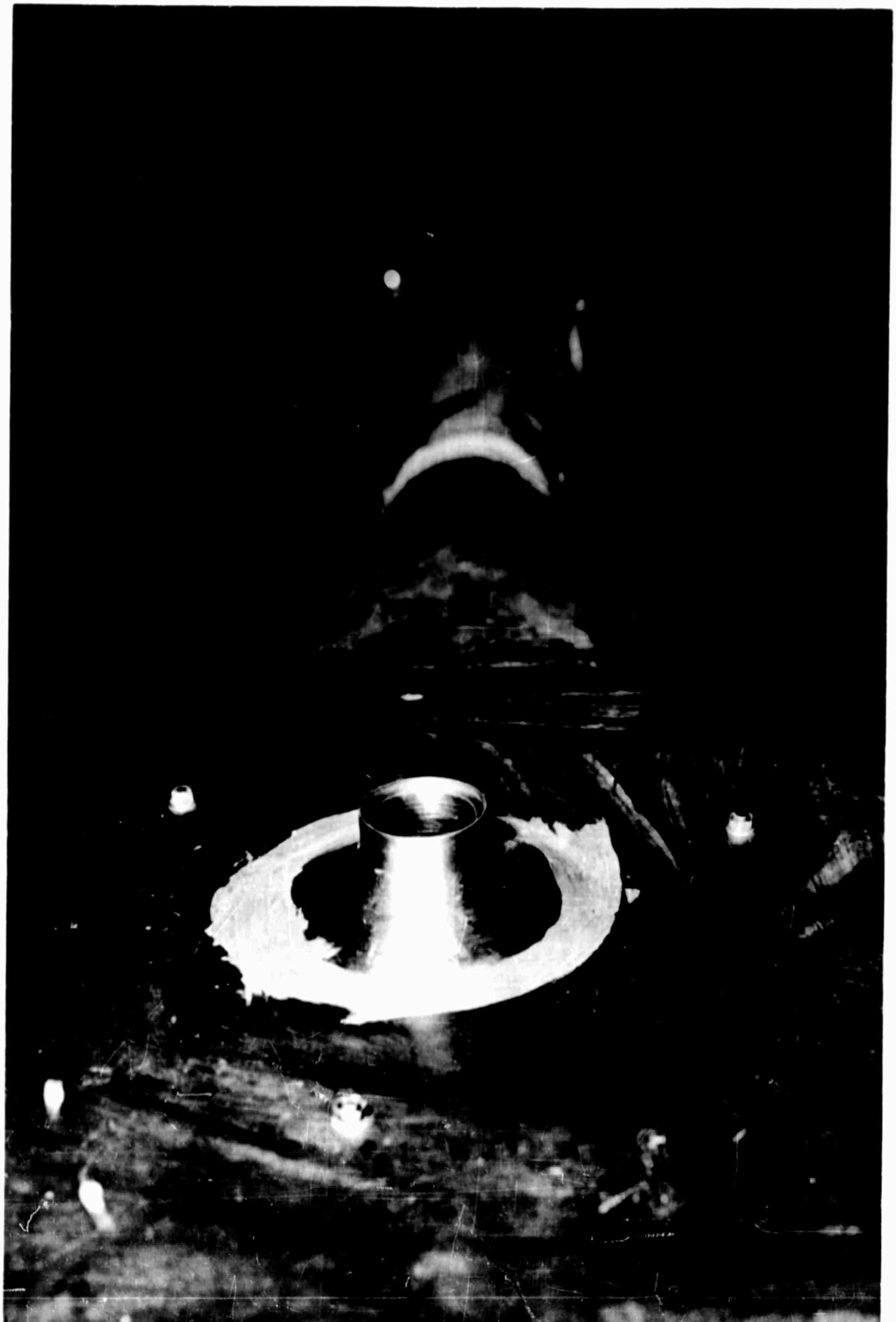

FIGURE 15

INSTALLATION OF ANNULAR NOZZLE EJECTOR AT END OF HIGH PRESSURE SUPPLY DUCT

Appendix

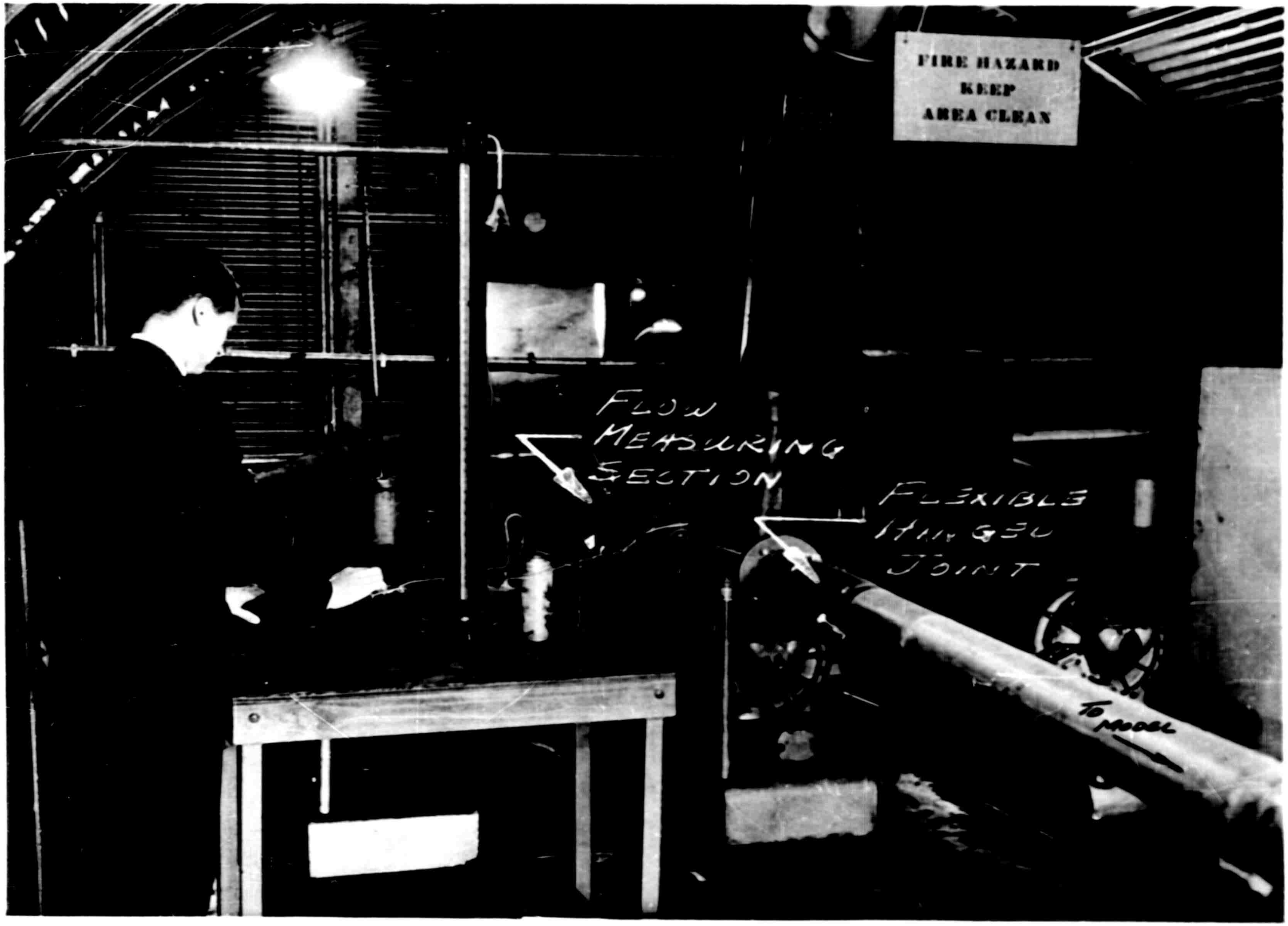

FIGURE 16 HIGH PRESSURE BLOWER SET UP

Appendix

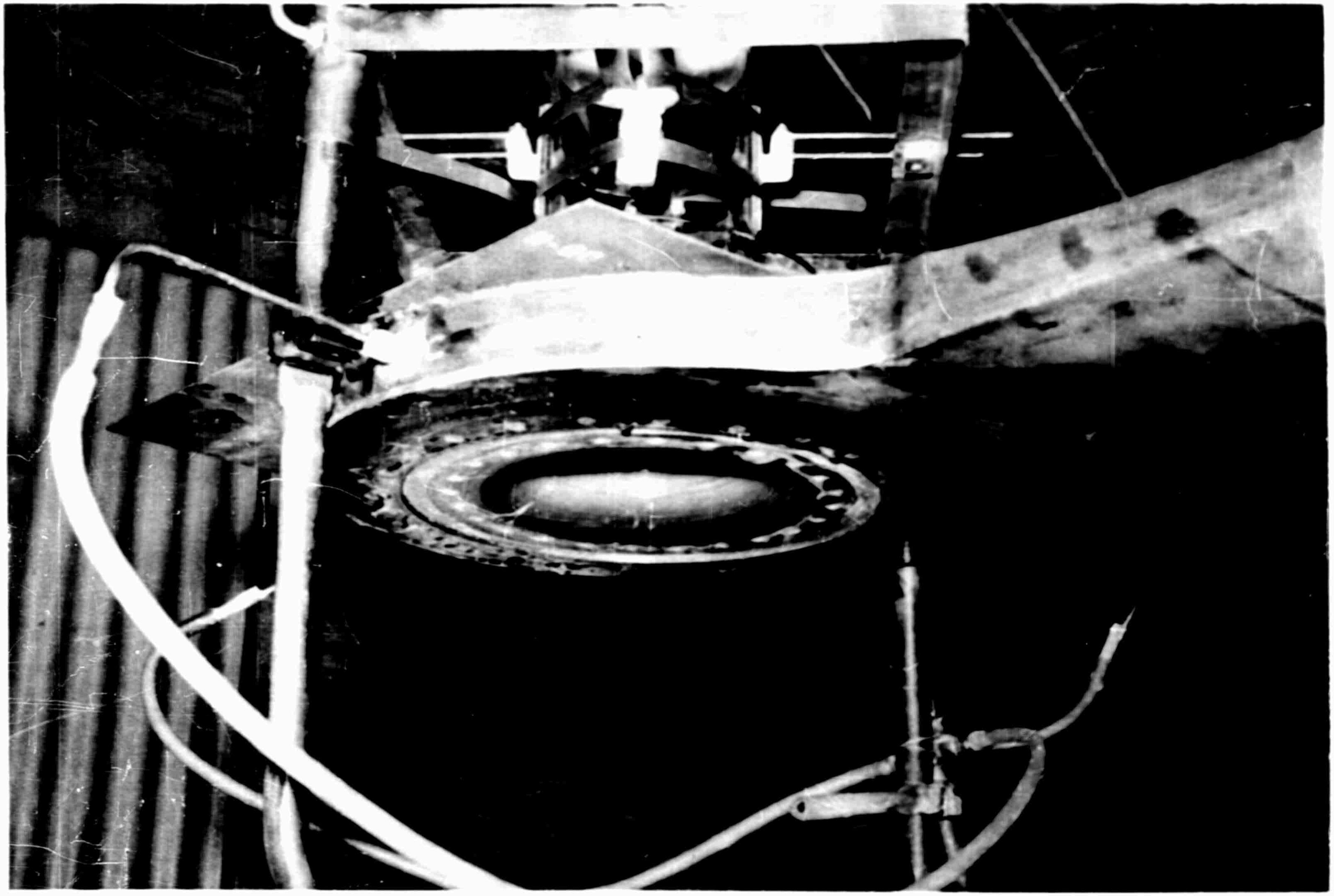

FIGURE 17

SECONDARY NOZZLE INLET, PLENUM CHAMBER PRESSURE PROBES, MIXING TUBE AND SUPPORT FROM BELOW

Appendix

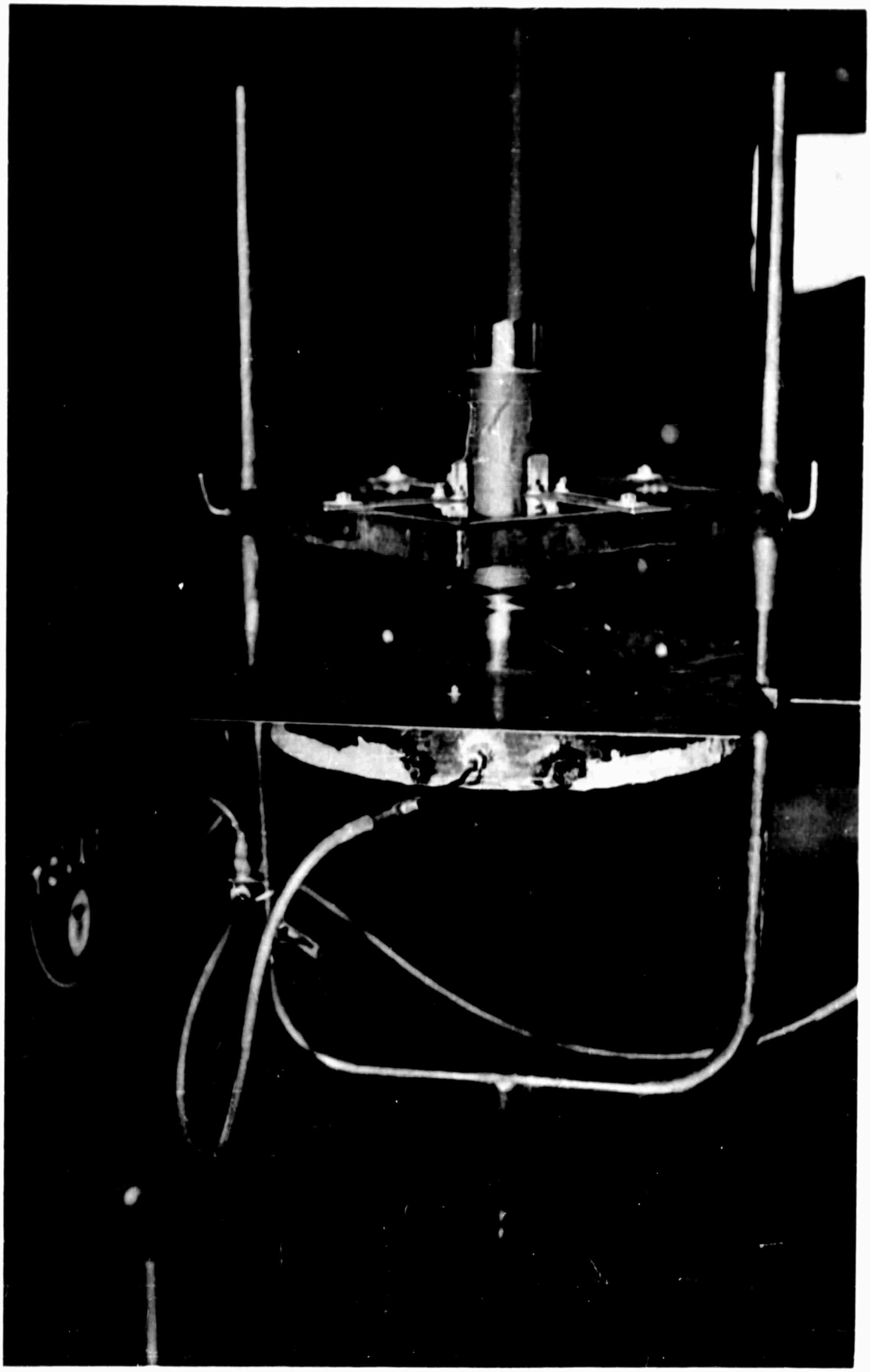

FIGURE 18

ARRANGEMENT OF ANNULAR NOZZLE EJECTOR-MIXING TUBE COMBINATION

Appendix

APPENDIX II

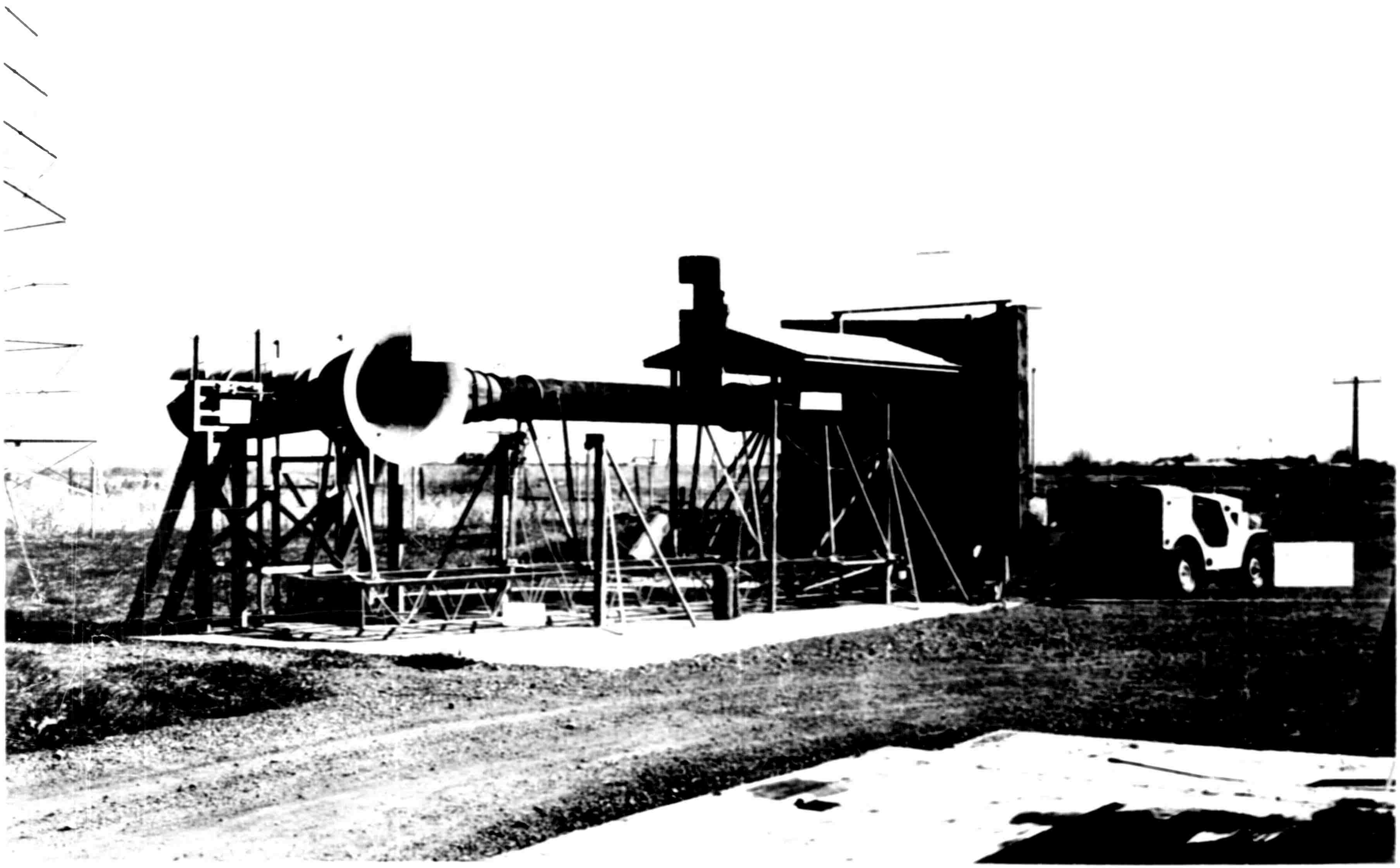

FIGURE 1: COMPLETE EJECTOR ASSEMBLY AND J-34 TURBOJET ENGINE TEST INSTALLATION

APPENDIX II

FIGURE 2: ANNULAR EJECTOR ASSEMBLY

APPENDIX II

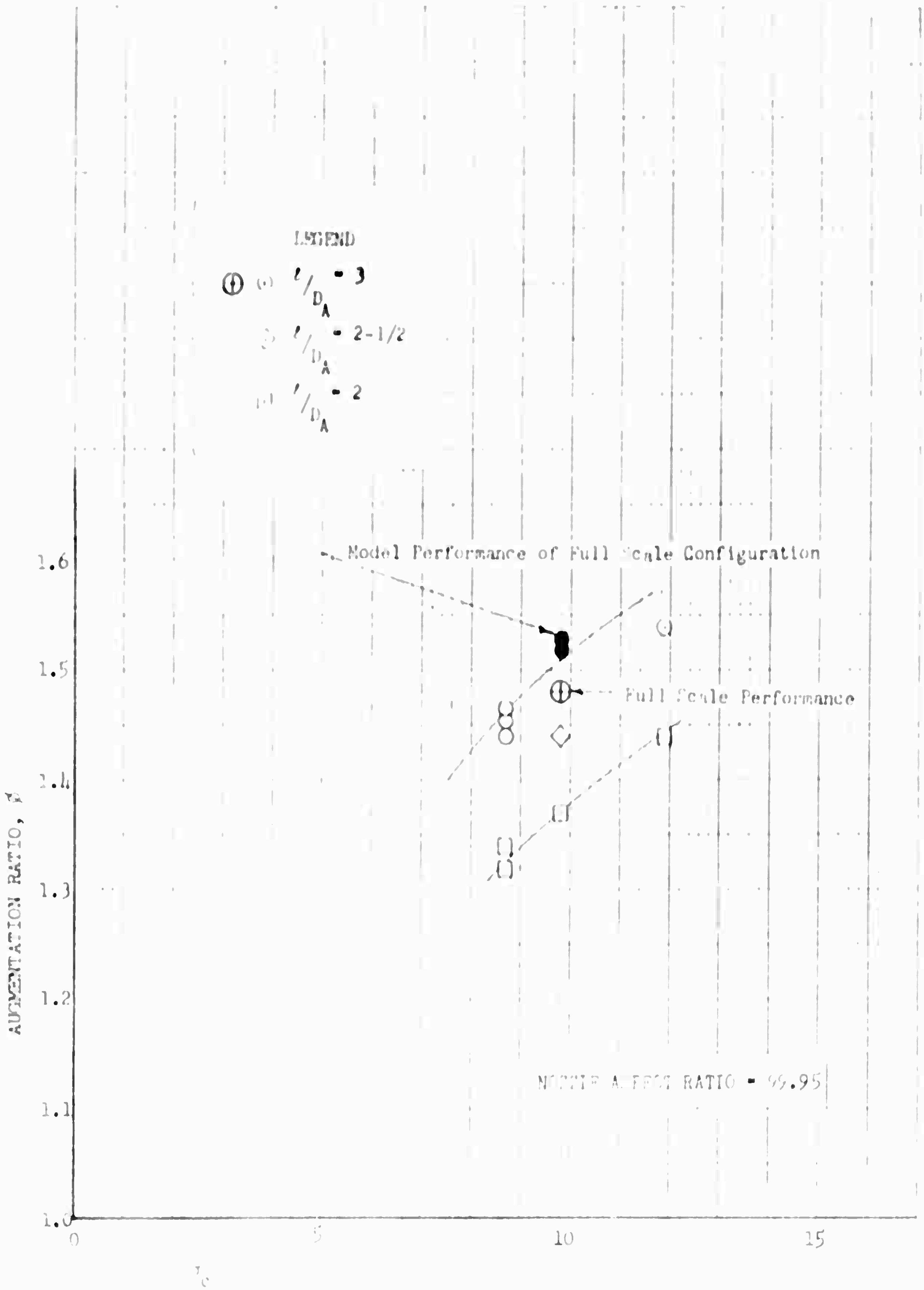

FIGURE 4: COMPARISON OF MODEL AND FULL SCALE TEST RESULTS

APPENDIX II

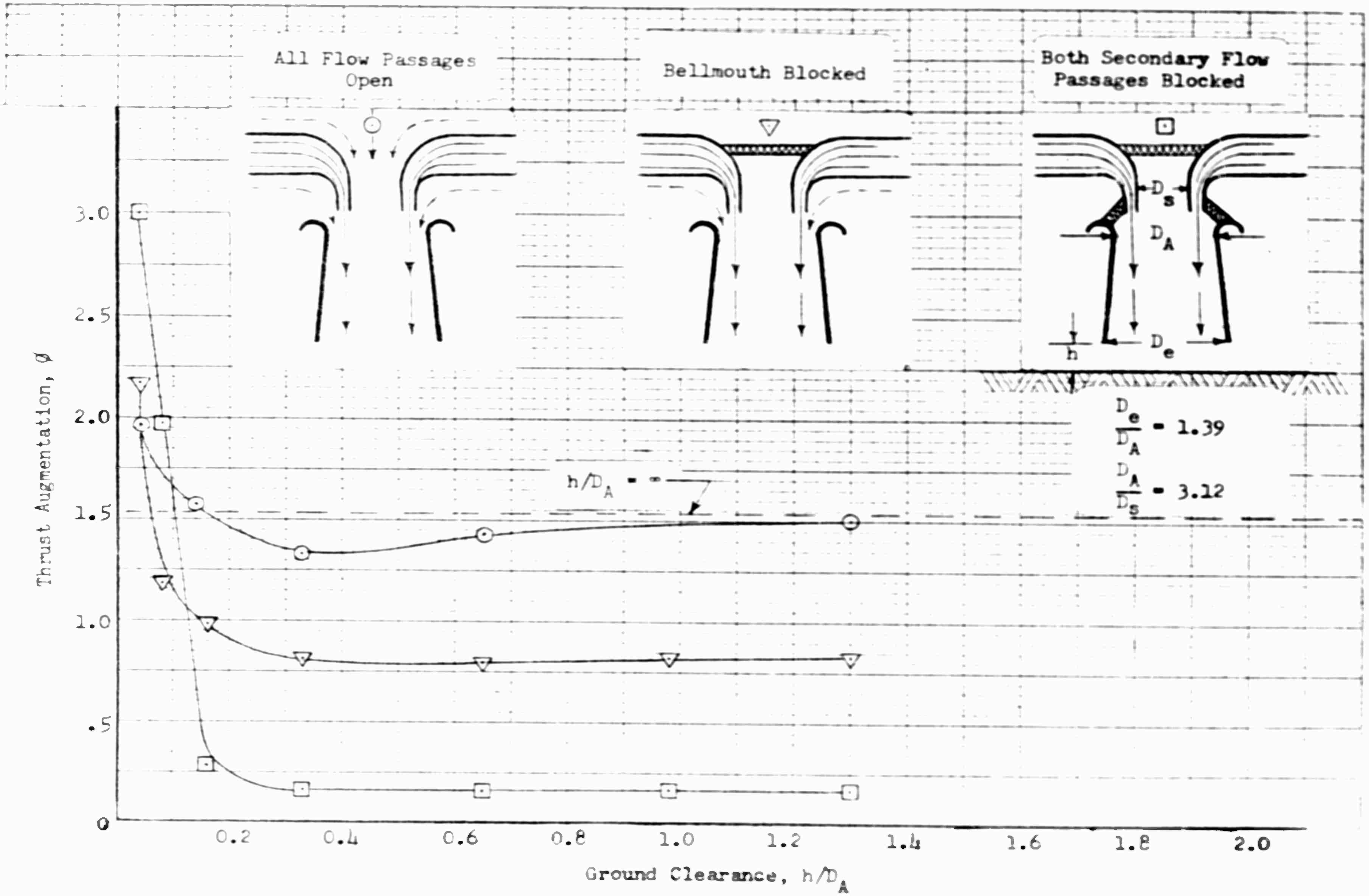

FIGURE 4 : GROUND EFFECT PERFORMANCE OF ANNULAR EJECTOR

APPENDIX II

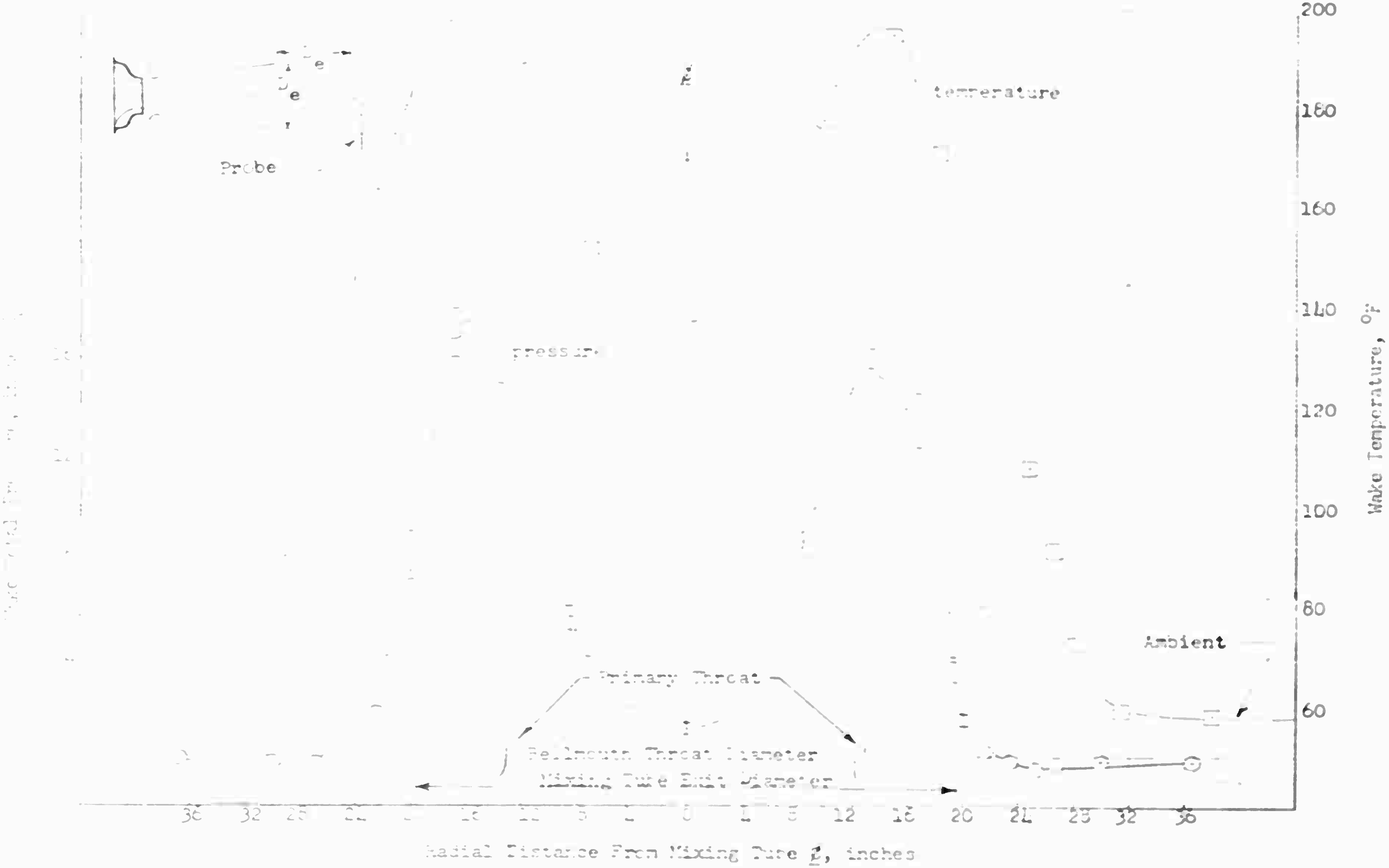

FIGURE 5: WAKE TOTAL PRESSURE AND TEMPERATURE PROFILE - EJECTOR ASSEMBLY
APPENDIX II

AD [illegible] Accession No. [illegible]

[illegible] Advanced Research [illegible], California

FINAL REPORT - PHASE [illegible] ANNULAR EJECTOR PROGRAM

R. [illegible] Gates and J. [illegible] Fairbanks

Report No. [illegible] [illegible]
Contract Nonr [illegible]

UNCLASSIFIED REPORT

A [illegible] was made [illegible] the annular ejector characteristics to determine a configuration [illegible] provide improved performance in and out of ground effect, and eliminate the performance loss encountered in Phase [illegible] during ground effect transition. The Phase [illegible] investigation encompassed the combined possibilities of a [illegible] annular primary jet, wide angle augmentors and flow control vanes. Qualitative [illegible] tests were conducted with two-dimensional [illegible] and three-dimensional [illegible] models. The primary nozzles of the 3-D models incorporated three [illegible] divergence angles of [illegible] and [illegible], but otherwise [illegible] geometry [illegible] The primary nozzle of [illegible] Phase [illegible] geometry with the exception of the primary annular jet divergence angle [illegible] aspect ratio [illegible]. The 2-D and 3-D primary nozzles were [illegible] which represented a comprehensive range of area ratios, [illegible] and positioning parameters. The 3-D investigation [illegible] primary jet thrust of approximately [illegible] thrust was [illegible]. The pressure ratio [illegible] in both instances. Maximum 3-D and [illegible] of ground effect performance produced thrust augmentation of [illegible] and [illegible] respectively. This performance is referred to the isentropic thrust of the primary [illegible] approximated previous results obtained with a full [illegible] annular ejector employing a zero divergence annular jet.

Flow control vanes were installed in the secondary mixed flow passage of the 3-D [illegible]. Proper adjustment of these vanes reduced the ground effect transition [illegible] by approximately [illegible] the loss without vanes. The maximum resulting loss of augmentation during transition was approximately 5% of out of ground effect augmentation.

UNCLASSIFIED

1. Annular Nozzle Ejector
2. Ground Effect
3. Augmentation
4. Nozzles
5. Inlet

I. R. F. Gates
J. W. Fairbanks
II. Contract Nonr [illegible]

AD [illegible] Accession No. [illegible]

[illegible] Advanced Research [illegible], California

FINAL REPORT - PHASE [illegible] ANNULAR EJECTOR PROGRAM

UNCLASSIFIED REPORT

UNCLASSIFIED

1. Annular Nozzle Ejector
2. Ground Effect
3. Augmentation
4. Nozzles
5. Inlet

I. R. F. Gates
J. W. Fairbanks
II. Contract Nonr [illegible]